PARITY-TIME SYMMETRY IN LASERS AND OPTOELECTRONIC OSCILLATORS

Zheng Dai

**Thesis submitted to the University of Ottawa
in partial fulfillment of the requirements for the
Doctor of Philosophy Degree in Electrical and Computer Engineering**

School of Electrical Engineering and Computer Science
Faculty of Engineering
University of Ottawa

uOttawa

ACKNOWLEDGEMENT

I would like to take this opportunity to express my sincere gratitude to those who have provided invaluable support and guidance throughout the course of my doctoral studies.

First and foremost, I am profoundly indebted to my supervisor, Professor Jianping Yao, whose insightful guidance, patient encouragement, and continuous support have been essential in shaping both my academic and my mental growth. From the very beginning, Professor Yao not only directed my research with clarity and precision, but also encouraged me to think independently and critically, shaping my ability to tackle complex scientific problems. Besides, his commitment to scientific rigor has inspired me greatly and will remain a lifelong influence.

Special appreciation is extended to my senior colleagues Weifeng Zhang, Zhiqiang Fan, Jiejun Zhang, Jian Tang, Bin Wang and Peng Li in the Microwave Photonics Research Laboratory, whose generous guidance and thoughtful advice during my early days in the group helped me quickly adapt to the research environment. Their patience in introducing me to experimental techniques, laboratory routines, and the overall culture of scientific inquiry laid a solid foundation for the progress of my doctoral work.

I would like to thank the following people, who are current or former colleagues working with me in the Professor Yao's research group at the School of Electrical Engineering and Computer Science, University of Ottawa: Cheng Li, Yu Huang, Ruoshi Xu, Zhejing Jiao, Long Huang, Zhuoran Wang, Junhan Fu, Yiran Guan, Amir Sardarzadeh, Mahdi Chegini, Shanshan Cheng, Xu Hu, and Zihang Gao, for their contributions to the discussion and assistance in the experiments and for sharing their expertise. I will always cherish the good

memories of working with them.

Finally, I wish to express my heartfelt thanks to my father and my mother. Their unwavering love, patience, material and spiritual support have been a source of strength throughout the challenges of this journey. Without them, this achievement would not have been possible.

ABSTRACT

Parity-time (PT) symmetry, originally proposed in quantum mechanics, has been extended to photonics and microwave photonics, offering a new framework to study the interplay between gain, loss, and coupling coefficients for single-mode selection in lasers and optoelectronic oscillators (OEOs).

This thesis focuses on the use of PT symmetry for mode selection in fiber ring lasers and OEOs. Five PT-symmetric architectures are proposed and experimentally demonstrated in this work to address challenges such as structural complexity, limited stability, poor tunability, and relatively low sidemode suppression ratios (SMSRs) in conventional PT-symmetric lasers and OEOs.

Chapter 1 introduces the background of PT symmetry, tracing its origin in quantum mechanics and its extension into the broad field of physical waves. It further reviews the principles of lasers and OEOs, providing the motivation for employing PT symmetry to simplify architectures and improve performance. Building on this motivation, Chapter 2 establishes the theoretical framework by developing coupled-mode and temporal coupled-mode theory, from which PT-symmetric Hamiltonians and the operation principles of single-longitudinal-mode (SLM) lasers and OEOs are derived.

Guided by this theoretical basis, Chapter 3 demonstrates a PT-symmetric fiber ring laser realized in a single physical loop. By emulating two counter-propagating subloops with balanced gain and loss in a polarization-dependent Sagnac structure, stable SLM lasing with sub-kilohertz linewidths and high SMSR is achieved. Extending the single-loop PT system

concept from optics to microwave photonics, Chapter 4 reports the first PT-symmetric OEO in a single physical loop, enabling frequency-tunable single-mode oscillations from 2 to 12 GHz with excellent phase noise performance, thereby eliminating the need for ultra-narrowband RF filters.

While these single-loop designs prove the feasibility of PT symmetry for mode selection, enhanced performance can be achieved by combining PT symmetry with the Vernier effect. Chapter 5 introduces a dual-loop PT-symmetric fiber laser with a rational loop-length ratio, which drastically reduces mode density and improves mode selectivity. Experiments confirm single-mode lasing with a record SMSR of 53.2 dB and sub-kilohertz linewidths. Building on the same principle, Chapter 6 presents a dual-loop PT-symmetric OEO with a rational loop-length ratio, where the joint action of PT symmetry and the Vernier effect results in stable single-mode oscillations tunable from 2 to 12 GHz, with an SMSR of 40.7 dB and superior phase noise characteristics.

In general, PT-symmetric mode selection enables stable single-frequency oscillation, but inherently limits the generation of multiple frequencies. However, as demonstrated in Chapter 7, the combination of PT symmetry and injection locking enables stable dual-frequency single-mode oscillation in an OEO. The two output frequencies are 8.15 GHz and 9.35 GHz, with corresponding SMSRs of 17.2 dB and 22.3 dB, respectively.

Finally, Chapter 8 summarizes the research findings and highlights future directions, including the integration of PT symmetry into photonic circuits, and exceptional point (EP)-enhanced sensing technologies.

TABLE OF CONTENTS

LIST OF FIGURES

LIST OF ACRONYMS

ASE: Amplified spontaneous emission, 19

BPF: Bandpass filter, 12

CCW: Counter-clockwise, 50

CMT: Coupled-mode theory, 22

CO_2: Carbon dioxide, 9

CW: Clockwise, 50

DBR: Distributed Bragg reflector, 10

DC: Direct current, 55

DFB: Distributed feedback, 10

EA: Electrical amplifier, 12

EDFA: Erbium-doped fiber amplifier, 49

EOM: Electro-optic modulator, 12

EP: Exceptional point, 1

ESA: Electrical spectrum analyzer, 56

F-P: Fabry-Pérot, 10

FSR: Free spectral range, 7

FWHM: Full-width at half maximum, 37

He–Ne: Helium–neon, 9

InP: Indium phosphide, 11

MDR: Microdisk resonator, 41

MPF: Microwave photonic filter, 14

MZM: Mach-Zehnder modulator, 39

OC: Optical coupler, 50

OEO: Optoelectronic oscillator, 7

OSA: Optical spectrum analyzer, 54

OSNR: Optical signal-to-noise ratio, 54

OVA: Optical vector analyzer, 76

PBC: Polarization beam combiner, 84

PBS: Polarization beam splitter, 49

PC: Polarization controller, 49

PD: Photodetector, 12

PM: Phase modulator, 41

PM–IM: Phase-modulation to intensity-modulation, 41

PS-FBG: Phase-shifted fiber Bragg grating, 10

PT: Parity-time, 1

RBW: Resolution bandwidth, 66

RF: Radio frequency, 7

SiN: Silicon nitride, 6

SLM: Single-longitudinal-mode, 10

SMF: Single-mode fiber, 49

SMSR: Sidemode suppression ratio, 15

SSB: Single-sideband, 39

SSB+C: Single-sideband-with-carrier, 41

TCMT: Temporal coupled-mode theory, 24

TLS: Tunable laser source, 62

TOBF: Tunable optical bandpass filter, 49

UFBG: Uniform fiber Bragg grating, 72

WGM: Whispering gallery mode, 4

CHAPTER 1 INTRODUCTION

1.1 Parity-time symmetry

In standard quantum mechanics, operators representing physical observables are required to be Hermitian, ensuring real eigenvalues and physical measurability. This mathematical framework provides a fundamentally accurate description of microscopic phenomena [1]. However, in 1998, Bender and Böttcher introduced a groundbreaking concept by demonstrating that a broader class of non-Hermitian Hamiltonians can also exhibit real eigenvalues, provided that the system satisfies parity-time (PT) symmetry [2].

A Hamiltonian $\hat{H}$ is said to be PT-symmetric if it commutes with the combined parity (P) and time-reversal (T) operators, i.e., $\left[\widehat{H}, PT\right] = 0$. In this case, the eigenfunctions are simultaneous eigenstates of the PT operator, and even though the Hamiltonian itself is non-Hermitian, all eigenvalues are completely real in the unbroken PT-symmetric phase. By contrast, in the broken PT-symmetric phase, PT symmetry is spontaneously broken, and the complex-conjugate eigenvalue pairs give rise to exponential growth or decay. The transition point between these two regions is called an exceptional point (EP), and is characterized by both eigenvalues and eigenvectors coalescing as well as non-trivial degeneracies.

The introduction of PT symmetry significantly broadened the conceptual boundary of physical theories. Before Bender's work, the prevailing belief held that only Hermitian operators could guarantee real eigenvalues and unitary dynamics. PT symmetry overturned this orthodoxy by showing that spectral reality can arise from a more general condition:

invariance under the combined P and T operations. This insight not only expanded the mathematical tools available to quantum theory but also established a new paradigm for describing open systems in which energy exchange with the environment cannot be neglected. The possibility of accessing real spectra in such systems stimulated tremendous theoretical interest, leading to extension studies on PT-symmetric quantum mechanics, perturbation theory in non-Hermitian operators, and the classification of phase transitions at EPs [3,4,5,6]. However, the experimental realization of PT symmetry in genuine quantum systems proved elusive, as it required exquisite control over balanced gain and loss at the atomic scale, something that remains technologically challenging even today.

Despite these difficulties, researchers soon recognized that PT symmetry could be realized in alternative physical platforms, where the constraints of decoherence and many-body interactions no longer exist [7]. Among these, photonic systems have emerged as the most natural and versatile candidate. The paraxial wave equation governing light propagation in weakly guiding media is mathematically equivalent to the Schrödinger equation. In this analogy, the position z plays the role of time, while the complex refractive index distribution acts as the potential. The real part of the refractive index is the normal refractive index and indicates the phase velocity, and the imaginary part corresponds to gain and loss. By engineering a refractive-index profile whose real part is an even function and imaginary part is an odd function, one can effectively implement a PT-symmetric Hamiltonian in an optical system.

This mapping between optics and quantum mechanics provided the first practical pathway toward the experimental demonstration of PT symmetry. Around 2010, a series of landmark

experiments used coupled optical waveguides to implement balanced gain and loss channels. These systems revealed several iconic PT phenomena, including symmetry-breaking phase transitions, loss-induced transparency, and asymmetric power oscillations [8,9,10]. The coupled-waveguide geometry was particularly well suited because it allowed direct observation of mode evolution, offered controllable gain and loss through optical pumping or absorption, and provided a compact platform where PT transitions could be induced by tuning experimental parameters. These early results established optics as the experimental origin of PT symmetry, marking the inception of the broader field now known as non-Hermitian photonics.

Following these demonstrations, PT symmetry rapidly expanded to optical resonators and microcavities, which offer higher quality factors and stronger mode confinement than simple waveguides. Microring resonators became an especially powerful platform. In 2014, two independent studies published in Science [11,12] showed that single-mode lasing could be achieved by operating in the PT-symmetry-broken region. When the balanced gain/loss exceeds the inter-resonator coupling coefficient, one super mode acquires amplification while the other is suppressed, leading to stable single-mode emission without the need for ultra-narrowband filters. Together, these works represented a major breakthrough, demonstrating that non-Hermitian physics could be harnessed not merely to explain exotic mathematical features but to solve practical engineering challenges, such as mode competition in lasers. This marked the moment when PT symmetry transitioned from mathematical abstraction to a design principle for photonic devices.

One of the most transformative directions in PT photonics has been its application to sensing,

particularly through the use of EPs. At an EP, not only do eigenvalues coalesce, but eigenvectors also become identical, producing a spectral degeneracy of nontrivial order. This degeneracy fundamentally alters the system's response to perturbations. While Hermitian systems exhibit linear eigenvalue splitting proportional to perturbation strength, PT-symmetric systems at a second-order EP show a square-root response, and higher-order EPs yield even stronger nonlinear dependencies. For instance, higher-order EPs can yield an $\epsilon^{1/N}$ dependence for an N-th order degeneracy, meaning that arbitrarily small perturbations can be detected with greatly enhanced sensitivity. This principle was experimentally validated in two 2017 Nature reports, where EP-enhanced whispering-gallery-mode (WGM) microcavities were used to detect single nanoparticles with sensitivities surpassing those of conventional cavity-based sensors [13,14]. The significance of these demonstrations extended beyond proof-of-concept; they established EP physics as a viable route to ultra-sensitive metrology. Subsequent studies expanded this concept to optofluidic sensors, rotation sensors, and biosensors, demonstrating that PT-based EP platforms offer superior sensitivity under small perturbations [15,16,17,18].

Another frontier of PT photonics involves nonlinear optical processes. In conventional Hermitian photonic systems, nonlinear processes such as the Kerr effect and four-wave mixing typically require high optical intensities to produce observable responses. In PT-symmetric systems operating near exceptional points, the localization of optical energy enhances the effective nonlinear interaction, enabling nonlinear effects to occur at significantly reduced power levels. Experimental observations have confirmed PT solitons, where the combination of Kerr nonlinearity and PT-symmetry yields self-localized nonlinear

states [19]. Theoretical predictions further suggest that in PT lattices, four-wave mixing and second-harmonic generation efficiencies can be significantly boosted due to the anomalous scaling of perturbations at EPs [20,21]. This nonlinear dimension of PT photonics links the field to nonlinear signal processing, expanding its technological relevance beyond mode control and sensing.

PT-symmetric concepts have also been actively explored in conjunction with other non-Hermitian phenomena, most notably in topological photonics and nonreciprocal transparency [22,23,24,25]. In topological photonics, non-Hermitian Hamiltonians augmented with PT-symmetric potentials can host topologically protected edge states that remain robust against certain classes of fabrication imperfections and disorder, though not entirely immune to all forms of scattering. In parallel, PT-symmetric photonic structures have been shown to realize unidirectional invisibility. This effect is most prominently predicted and observed in PT-symmetric Bragg gratings operated near the EP. In such systems, the refractive index modulation consists of an even real part that enables conventional Bragg scattering and an odd imaginary part corresponding to spatially balanced gain and loss. When the modulation amplitudes are precisely tuned to satisfy the PT-symmetric condition, destructive interference between the gain/loss profile and the periodic scattering potential eliminates back-reflection from one side, while maintaining nearly unity forward transmission with negligible phase distortion. From the opposite direction, however, the interference no longer compensates the scattering, resulting in strong reflection.

The integration of PT symmetry into photonic circuits marks another major step forward. After the initial demonstrations in fiber and bulk-optic platforms, researchers turned to silicon

and III–V photonic platforms to pursue miniaturized PT devices. In 2017, an integrated PT symmetric microring laser was reported in Nature Communications, combining III–V gain materials with silicon passive components to realize electrically pumped, wavelength-tunable, and single-mode emission [26]. This demonstration proved that PT symmetry could be embedded into CMOS-compatible platforms, accelerating the path toward large-scale integration. Besides, integrated PT devices have included isolators, EP-enhanced sensors, and tunable filters [14,15,27,28,29]. These devices exploit PT symmetry not as a theoretical novelty but as a practical design rule. Furthermore, the use of low-loss silicon nitride (SiN) platforms has enabled fast thermo-optic PT-symmetric switch, demonstrating that PT symmetry can coexist with state-of-the-art integrated photonic circuit technologies [30].

In addition to optical implementations, PT symmetry has been successfully extended to a variety of other wave-based systems, further highlighting its universality across physics. Acoustic realizations of PT symmetry exploit the balance between amplification and absorption of sound. In conventional sensing, detecting an incoming acoustic signal inevitably requires absorbing part of its energy, which disturbs the measurement process and introduces reflections and shadowing effects. These limitations are overcome through two coupled acoustic cavities, one designed to provide active gain through a loudspeaker and the other incorporating absorptive materials, enabling the realization of a transparent, shadow-free sensor for audible airborne waves that completely absorbs the incoming signal while neither disturbing its detection process nor producing a scattering trace. These results confirm that PT symmetry, can be directly extended to acoustics and leveraged for advanced sound engineering applications [31].

The influence of PT symmetry has also expanded into the microwave domains, particularly through the development of optoelectronic oscillators (OEOs). Traditional OEOs rely on long optical fiber delay lines to achieve ultrahigh quality factors and low phase noise. However, the dense mode spectrum of these long cavities makes stable single-mode oscillation difficult, requiring ultra-narrowband filters or multi-loop Vernier configurations, in which multiple loops with slightly mismatched lengths generate different free spectral ranges (FSRs), and only the modes that satisfy the resonance condition in all loops simultaneously are reinforced, effectively increasing the mode spacing and enabling improved mode selection. PT symmetry provides a fundamentally different approach: by balancing gain and loss between coupled loops, one oscillation mode with highest gain can be selectively amplified while others remain neutral. Early theoretical proposals of PT-OEOs suggested that this could suppress sidemodes without ultranarrow passband radio frequency (RF) filtering [32,33]. The extension of PT symmetry into OEOs indicates a broader message: non-Hermitian physics is not confined to optics but represents a general principle for controlling oscillatory and wave systems. In this context, PT-OEOs serve not only as practical devices for generating spectrally pure microwaves but also as physical laboratories for exploring non-Hermitian dynamics. Their operation at or near EPs makes them attractive for studying perturbation responses, stability landscapes, and nonlinear interactions in systems where both photonic and electronic domains are involved. This combinatorial function makes PT-OEOs a microcosm of the development path of this discipline: from abstract quantum mechanics to practical photonic devices and further into hybrid electronic-photonic architectures.

Taken together, the evolution of PT symmetry over the last twenty-five years illustrates a

remarkable trajectory: from a mathematical conjecture in non-Hermitian quantum mechanics to a powerful framework for practical device engineering across optics, microwaves, and hybrid photonic-electronic systems. Its central features—spectral reality under balanced gain and loss, the existence of EPs with anomalous scaling, and single-mode selection capabilities—constitute a powerful tool for controlling wave phenomena. In this thesis, PT symmetry provides not only theoretical inspiration but also the design foundation for developing lasers and OEOs with simplified architectures, enhanced stability, and superior spectral performance. The following sections will first review the fundamental principles of lasers and OEOs before turning to the novel PT-based architectures introduced in this work.

1.2 Laser

The word laser, an acronym for Light Amplification by Stimulated Emission of Radiation, encapsulates the core physical mechanism underlying all laser systems: the process of stimulated emission, which was first predicted by Einstein in 1917 [34]. In this process, a photon interacting with an excited atomic or molecular system can induce the emission of a second photon identical in phase, frequency, polarization, and direction, resulting in coherent amplification. When combined with an optical resonator that provides feedback, this mechanism produces self-sustained oscillations of coherent light. Since the first demonstration of the laser in 1960 by Maiman, lasers have revolutionized science, technology, and industry by providing coherent, monochromatic, and highly directional light sources [35].

The operation of a laser relies on three essential components: a gain medium, an energy pump source, and an optical resonator. The gain medium provides population inversion, the pump

source supplies the necessary excitation energy, and the resonator establishes feedback and mode selection. The interplay of these elements gives rise to distinct characteristic features such as high temporal coherence, narrow linewidth, and high brightness. Depending on the type of gain medium, lasers are broadly classified into gas lasers, solid-state lasers, semiconductor lasers, dye lasers, and fiber lasers. The historical development of lasers can be divided into several stages. In the 1960s and 1970s, gas lasers such as the helium–neon (He–Ne) and carbon dioxide (CO_2) lasers became dominant sources in both research and industrial applications. He–Ne lasers provided stable, narrow-linewidth emission for spectroscopy and metrology, whereas CO_2 lasers enabled high-power materials processing and machining [36,37,38]. The 1980s and 1990s witnessed the rapid rise of semiconductor lasers, which became indispensable for optical communications, data storage, and consumer electronics. During the same period, solid-state and fiber lasers evolved into robust platforms for high-power and ultrafast applications. The development of mode-locking techniques enabled femtosecond pulse generation, while the appearance of optical frequency combs around 2000 revolutionized precision metrology and spectroscopy [39,40,41,42,43,44]. Over the past six decades, advances in materials, cavity designs, and photonic integration technologies have extended the laser family across the electromagnetic spectrum, from ultraviolet to terahertz regime. Today, lasers span nearly every wavelength range and application domain, reflecting the continued synergy of materials science, physics, and photonic engineering.

Beyond their fundamental role in optical physics, lasers have become indispensable tools across a broad range of scientific and technological fields. They underpin modern spectroscopy, quantum optics, ultrafast science, and nonlinear optics, while driving advances

in optical communications, precision manufacturing, remote sensing, medical diagnostics, and defense applications [45,46,47,48,49,50]. The development of semiconductor lasers and fiber lasers has accelerated the widespread availability of compact, energy-efficient, and scalable light sources, laying the foundation for the information age. In recent years, the emergence of ultrashort-pulse mode-locked lasers, optical frequency combs, and PT-symmetric lasers that exploit non-Hermitian physics for stable single-mode operation and enhanced perturbation sensitivity have further expanded the scope of laser science and applications [11,12,13,14,45,46].

As laser technologies continue to advance, maintaining high spectral purity becomes increasingly important for many applications ranging from high-resolution spectroscopy to coherent communication and frequency metrology. This requirement places strong emphasis on the ability to suppress unwanted longitudinal modes, motivating the need for reliable single-longitudinal-mode (SLM) operation.

A particularly critical challenge in laser development is the realization of SLM operation. In a Fabry-Pérot (F-P) resonator, longitudinal modes are separated by the FSR, which decreases as cavity length increases. In many practical lasers, the gain bandwidth spans several FSRs, resulting in multiple longitudinal modes that compete for inversion. Such mode competition broadens the laser linewidth, destabilizes the output, and degrades coherence. Various approaches have therefore been developed to enforce SLM operation. Distributed feedback (DFB) and distributed Bragg reflector (DBR) structures, introduced in the 1970s, rely on periodic index modulation to create wavelength-selective reflection, thereby suppress undesired modes [51,52]. Phase-shifted fiber Bragg gratings (PS-FBGs) extend this concept

to fiber lasers, enabling narrow-bandwidth spectral filtering suitable for long cavities [53]. The Vernier effect, produced by combining cavities of unequal lengths, further enhances mode discrimination by creating a much larger effective FSR [54]. Another strategy involves injection locking or self-injection feedback, in which an external seed or a delayed replica of the laser output stabilizes the oscillation frequency and suppresses sidemodes [55,56].

Integrated photonics combined with PT symmetry has opened a new frontier for SLM laser development. Silicon photonics and indium phosphide (InP) platforms offer compact, electrically pumped devices with high output power and tunability [57]. One of the landmark results was the demonstration of integrated PT microring lasers in 2014, where balanced gain/loss engineering in the PT broken region enforced stable SLM lasing without narrowband filters [12]. Later, in 2017, electrically pumped PT-symmetric integrated microring lasers were realized in hybrid III–V/Si structures, offering wavelength tunability and robustness against fabrication imperfections [26]. The key advantage of PT symmetry in these devices lies in its intrinsic single-mode selection mechanism. Unlike conventional SLM techniques that rely on narrowband reflectors, external filters, or multiple cavities, PT-symmetric structures exploit the asymmetric mode evolution near the EP. When the gain/loss contrast exceeds the inter-resonator coupling, the PT-broken phase ensures that only one super mode acquires net amplification while all other competing modes experience remain neutral. This selective mechanism provides a built-in, filter-free pathway to SLM operation, enabling compact, integrated lasers to maintain stable single-frequency emission even in the presence of fabrication imperfections. These devices combine ultra-low loss passive cavities with integrated gain sections, achieving levels of coherence once thought possible only in

laboratory-scale fiber systems. Such integrated narrow-linewidth sources are now being pursued for coherent LiDAR, quantum key distribution, and frequency metrology [58].

Today, lasers not only represent a cornerstone of modern photonics but also a versatile platform for exploring frontier physics, including PT symmetry, topological photonics, and quantum technologies. Their continuous evolution reflects the synergy between fundamental science and technological innovation, ensuring that lasers remain at the forefront of both fundamental and applied research.

1.3 Optoelectronic oscillator

OEOs are hybrid systems of photonics and electronics that exploit the high-quality factor of optical delay lines or resonators to generate spectrally pure microwave signals. First proposed by Yao and Maleki in 1996, the OEO concept has since become a cornerstone of microwave photonics, offering frequency stability and phase noise performance superior to most purely electronic oscillators [59]. As shown in Fig. 1.1, a typical OEO consists of a continuous-wave laser source, an electro-optic modulator (EOM), a long length of optical fiber, a photodetector (PD), a bandpass filter (BPF) and an electrical amplifier (EA) forming a closed feedback loop. Light from the laser is modulated by an RF signal, propagates through the optical fiber, and is converted back to the electrical domain by the PD. The resulting delayed RF signal is then amplified and fed back to the modulator, forming a closed loop that sustains microwave oscillations. The long optical fiber acts as a low-loss delay element, effectively providing a very high-quality resonance. This unique feature allows OEOs to generate microwave signals with ultralow single-sideband phase noise.

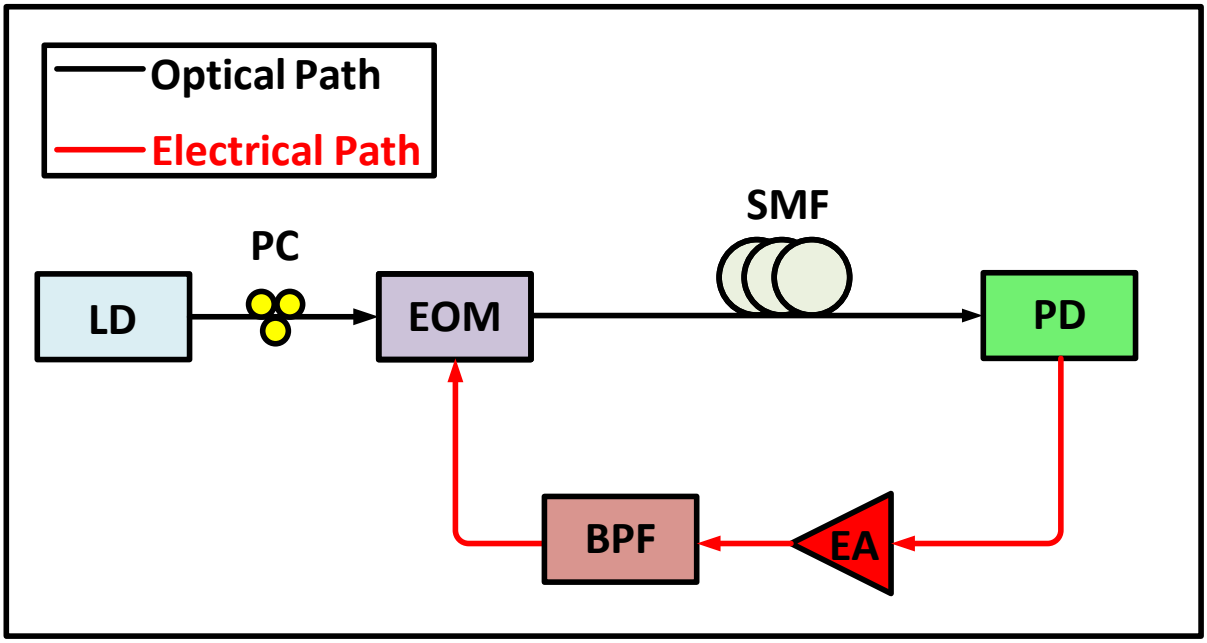

Fig. 1.1 Schematic of an optoelectronic oscillator (OEO). LD: laser diode, PC: polarization controller, EOM: electro-optic modulator; SMF: single mode fiber, PD: photodetector; EA: electronic amplifier, BPF: bandpass filter.

The original OEO design demonstrated the possibility of generating microwave signals with phase noise an order of magnitude lower than that of electronic oscillators at the time [60]. This breakthrough attracted significant interest from radar, satellite communication, and wireless industries, where low-phase-noise is essential [47,61,62]. Over the following decades, OEOs have evolved into a diverse family of architectures optimized for different metrics such as phase noise, tunability, environmental robustness, and integration. Among these, single-loop OEOs remain the simplest and most widely studied configuration. However, the long fiber delay required to achieve low phase noise introduces an ultra-dense mode spectrum, as the FSR of the cavity decreases inversely with fiber length. This mode density gives rise to mode competition, which can destabilize oscillation and generate spurious signals. Addressing this mode-selection problem has therefore been a central research

challenge in OEO development.

A widely adopted solution is the dual-loop OEO, where two fiber loops of different lengths are combined [63]. The Vernier effect arising from their mismatched FSRs produces a significantly larger effective FSR, thereby reducing the number of oscillation modes within the gain bandwidth. Dual-loop OEOs can achieve stable single-mode oscillation across wide frequency ranges, though at the cost of increased system complexity and environmental sensitivity. Another major approach relies on microwave photonic filters (MPFs) applied to the OEO loop. By tailoring the optical or RF spectrum with elements such as fiber Bragg gratings, F-P interferometers, or micro resonators, the loop response can be engineered to select a single oscillation frequency [64,65,66,67]. While MPF-based OEOs provide effective mode control, they often suffer from insertion loss and limited bandwidth, constraining their practical performance.

Beyond mode selection, substantial efforts have focused on improving the phase-noise performance of OEOs. The fundamental phase noise is limited by the thermal and shot noise of the photodetector and amplifier, but environmental perturbations such as temperature drift and mechanical vibrations also play major roles. To address these issues, stabilization strategies such as vibration-isolated packaging, temperature-controlled enclosures, and active feedback loops have been implemented. Moreover, the development of compact resonator-based OEOs has offered alternatives to long fiber delay lines. High-quality WGM resonators, for instance, provide short delay equivalents with FSRs on the order of tens of GHz, enabling compact OEOs with competitive phase noise performance. Similarly, low-loss integrated microring resonators on SiN platforms have been investigated as chip-scale delay elements,

bringing OEO technology closer to photonic integration [67,68,69].

The push toward integration has accelerated over the past decade, driven by the demand for compact, low-power, and scalable OEO solutions. Hybrid integration of III–V lasers with silicon photonics has enabled on-chip OEO prototypes where the optical source, modulator, and filter are monolithically or heterogeneously integrated. Recent reports have demonstrated fully integrated OEOs operating at microwave and millimeter-wave frequencies with phase noise competitive to fiber-based systems [70,71]. These integrated OEOs not only reduce footprint and power consumption but also offer new opportunities for reconfigurability and mass production, aligning with the broader trend toward silicon photonic integration in communication and sensing systems.

Despite these advances, mode selection remains a critical challenge, especially in long-delay OEOs where ultra-dense mode spectra persist. Traditional solutions, such as dual-loop designs, Vernier architectures, and high-quality filters, often involve trade-offs in complexity, loss, and tunability. Thus, the emergence of PT symmetry provides a novel solution to these problems. By balancing the gain and loss in coupled loops to reach the PT symmetry broken region, single-mode oscillation can be achieved. In such systems, the oscillation mode with highest gain experiencing amplification while all competing modes are suppressed, eliminating the need for ultra-narrowband RF filters. Theoretical studies have predicted that PT-OEOs can achieve pure single-mode oscillation with high sidemode suppression ratios (SMSRs) [32,33]. These designs confirm that PT symmetry provides an alternative mechanism for stabilizing OEOs, directly addressing the fundamental bottleneck of dense mode competition.

In modern communication systems, multi-band radar and wireless systems increasingly require carriers at widely separated frequencies for frequency-diverse sensing, joint radar–communication, and instantaneous bandwidth enhancement [72,73,74,75,76,77]. Multi-frequency OEOs offer several inherent advantages arising from their ability to simultaneously generate multiple, mutually coherent microwave tones within a single compact platform. One key benefit is the capability to support multi-band microwave signal generation without requiring multiple independent oscillators, thereby reducing hardware complexity, footprint, and power consumption. Since the generated tones share the same optical path and electronic feedback loop, they typically exhibit high mutual coherence, low relative phase noise, and excellent frequency stability, allowing multi-band systems such as radar, communication links, and sensing architectures to operate with intrinsically synchronized channels. This contrasts with architectures relying on separate oscillators, where channel-to-channel drift, de-synchronization, and phase mismatches are problematic.

In addition, multi-frequency OEOs enable flexible spectral engineering. By carefully designing loop filters, mode-selection mechanisms, or injection-locking structures, the spectral distribution—such as the spacing, number, and relative power of the microwave tones—can be precisely controlled. This is particularly advantageous in applications requiring frequency-agile microwave sources, multi-tone testing, linearization of RF components, and photonics-assisted arbitrary waveform generation.

Today, OEOs are at the forefront of microwave photonics, bridging the gap between photonics and high-frequency electronics. Their ability to generate low-phase noise microwave signals not only underpins applications in next-generation wireless networks,

radar, and satellite navigation, but also provides a versatile platform for fundamental research in non-Hermitian physics, PT symmetry, and sensing at EPs.

1.4 Major contributions of this research

This thesis focuses on the application of PT symmetry in lasers and OEOs, aiming to address the challenges commonly encountered in conventional PT-symmetric lasers and OEOs, including structural complexity, low stability, and difficulty in mode selection. In this work, four novel PT-symmetric laser and OEO architectures are proposed, each of which is subjected to rigorous theoretical analysis and experimental performance evaluation. The results demonstrate significant improvements over traditional PT-symmetric systems, effectively mitigating the limitations and enhancing overall system performance.

1）A PT-symmetric fiber laser based on a single physical loop architecture is proposed and experimentally demonstrated. Unlike conventional PT-symmetric lasers that rely on two physically separated loops with identical geometries, the single-loop configuration incorporates balanced gain and loss into one Sagnac loop, significantly simplifying the system design while enhancing stability. Through theoretical analysis of PT-symmetry phase transitions and EP dynamics, the feasibility of mode selection within a single-loop structure is analytically established. Experimental demonstrations further confirm stable single-longitudinal-mode lasing with improved spectral purity, thus introducing a compact and practical PT-symmetric laser design that paves the way for broader applications.

2) A widely frequency-tunable PT-symmetric OEO using a polarization-dependent Sagnac loop is implemented. This design represents the first demonstration of PT symmetry in an

OEO based on a single physical feedback loop. By exploiting the bidirectional propagation in the Sagnac loop, two equivalent loops with identical geometries are formed, thereby overcoming the critical challenge of mismatch between physically separated loops. By carefully balancing the gain and loss to exceed the coupling coefficient, PT symmetry breaking is achieved, enabling stable single-mode microwave oscillation over a broad frequency range from 2 to 12 GHz. The oscillator exhibits excellent phase noise performance of –128 dBc/Hz at a 10 kHz offset, showing that PT symmetry provides an effective alternative to ultra-narrow BPFs for single-mode selection in frequency-tunable OEOs.

3) A dual-loop PT-symmetric fiber laser with a rational loop-length ratio is proposed and demonstrated. Traditional PT-symmetric systems typically require identical loop lengths to ensure resonant wavelength matching, whereas this work demonstrates that PT symmetry can also be established in non-identical loops when their lengths follow a rational ratio. By combining PT symmetry with the Vernier effect, the number of competing resonant modes is significantly reduced, leading to enhanced mode selection. A proof-of-concept experiment is carried out in which a fiber ring laser with a length ratio of 200/3 between the two loops is implemented. The laser achieved single-longitudinal-mode operation at 1555.88 nm with a record-high SMSR of 53.2 dB and a sub-kHz linewidth. This study not only introduces a novel PT-symmetric architecture but also expands the theoretical framework of PT symmetry to systems with rational length mismatches, providing a new design principle for lasers with superior performance.

4) A frequency-tunable PT-symmetric OEO employing two coupled loops with a rational loop-length ratio is realized. In this design, PT symmetry and the Vernier effect are jointly

utilized to enable efficient mode selection and enhanced operational stability. The system is theoretically analyzed and experimentally verified, demonstrating stable single-mode oscillation with a frequency tuning range from 2 to 12 GHz. The SMSR is improved to 40.7 dB, corresponding to a 3.9 dB enhancement compared with a dual-loop OEO using only the Vernier effect. Moreover, the generated microwave signal exhibits a phase noise of –114 dBc/Hz at a 10 kHz offset, highlighting the improved spectral purity and reduced mode competition. This work establishes a new framework for dual-loop PT-symmetric OEOs, offering practical solutions for next-generation high-performance microwave photonic oscillators with both tunability and stability.

5) A dual-frequency PT-symmetric OEO is proposed and experimentally demonstrated. In this design, a spectrally sliced amplified spontaneous emission (ASE) source is transmitted through a large dispersion optical component and detected by a PD to implement a dual-channel MPF. The PT symmetry enforces single-mode dominance within each channel, effectively suppressing delay-line-induced multimode competition. Subsequently, injection locking with an external electrical signal stabilizes the relative phase and frequency spacing between the two oscillation channels, yielding a mutually phase-locked dual-frequency output. The combined effect of PT symmetry and injection locking results in spectral purity in each channel, robust dual-frequency stability, and immunity to mode hopping, establishing a new mechanism for generating highly stable multi-frequency microwave signals in OEOs.

Overall, the contributions of this thesis collectively establish a coherent research trajectory that advances PT-symmetric photonics and microwave photonics from fundamental concepts to practical implementations. Starting with the simplification of PT-symmetric architectures

in single-loop fiber lasers and OEOs, and progressing to advanced dual-loop configurations incorporating rational length ratios and the Vernier effect, this work systematically addresses long-standing challenges of structural complexity, mode competition, and stability. Theoretical modeling and experimental validations not only confirm the feasibility of these designs but also deepen the understanding of EP physics in resonant systems. Together, these innovations form a comprehensive framework for realizing compact, stable, and frequency-tunable PT-symmetric lasers and OEOs, thereby bridging fundamental non-Hermitian physics with practical applications in high-performance signal generation.

1.5 Organization of this thesis

This thesis is organized into eight chapters as follows:

Chapter 1 provides an introduction to PT symmetry, lasers, and OEOs, together with the motivation of this research. The major contributions of the thesis are summarized at the end of this chapter.

Chapter 2 establishes the theoretical background necessary for the subsequent chapters. Coupled-mode theory and temporal coupled-mode theory are introduced, followed by the fundamentals of PT-symmetric Hamiltonians. The principles of SLM lasers and single/multi-frequency OEOs are also discussed, forming the theoretical foundation of this work.

Chapter 3 demonstrates a PT-symmetric SLM fiber ring laser implemented using a single physical loop. Both theoretical analysis and experimental verification are provided, showing that PT symmetry can enforce single-mode operation in long fiber cavities without need for ultra-narrowband optical filters, thereby the conventional dual-loop PT-symmetric

configurations are optimized.

Chapter 4 reports the first realization of a PT-symmetric optoelectronic oscillator using a single physical loop. By introducing a polarization-dependent Sagnac loop, two counter-propagating feedback paths with balanced gain and loss are formed, enabling simplified single-mode microwave oscillation.

Chapter 5 proposes and experimentally demonstrates a dual-loop PT-symmetric fiber laser with a rational loop-length ratio. The design leverages both the Vernier effect and PT symmetry to significantly improve sidemode suppression and linewidth performance.

Chapter 6 introduces a dual-loop PT-symmetric OEO employing a rational loop-length ratio. The joint use of the Vernier effect and PT symmetry ensures efficient mode selection, and improved stability.

Chapter 7 shows a dual-frequency PT-symmetric OEO. By combining PT symmetry and injection locking, the system simultaneously generates two mutually stable microwave tones, which means the expansion of the PT-symmetric OEO from generating a single frequency signal to multi-frequency signals.

Chapter 8 summarizes the main findings of this thesis and outlines potential research directions for future work.

CHAPTER 2 THEORETICAL OVERVIEW

2.1 Coupled mode theory

Coupled-mode theory (CMT) is a widely used analytical framework for describing the interaction and energy exchange between modes in optical waveguides, resonators, and other electromagnetic structures [78,79]. It is particularly useful in systems where weak perturbations or couplings occur, such as in directional couplers, fiber Bragg gratings, and coupled cavities. The core idea of CMT is that the total field of a system can be expressed as a superposition of unperturbed eigenmodes, and their amplitudes evolve according to a set of first-order differential equations determined by the coupling mechanism.

Consider two optical waveguides or resonators that support modes with field distribution $E_1(r)$ and $E_2(r)$, and complex amplitudes $a_1(z)$ and $a_2(z)$ along the propagation direction z. In the absence of interaction, each mode propagates independently with a propagation constant β_i. When the two structures are brought into proximity, their evanescent fields overlap, and coupling occurs. Under the complex field representation, the total electric field can be expressed as

$$E(r,z) = a_1(z)E_1(r)e^{i\beta_1 z} + a_2(z)E_2(r)e^{i\beta_2 z} \tag{2.1}$$

where the physical electric field is given by the real part of the above expression. By applying Maxwell's equations under the weak coupling approximation, the following coupled differential equations for the mode amplitudes are obtained:

$$\begin{aligned} \frac{da_1(z)}{dz} &= -i\beta_1 a_1(z) - i\kappa_{12} a_2(z) \\ \frac{da_2(z)}{dz} &= -i\beta_2 a_2(z) - i\kappa_{21} a_1(z) \end{aligned} \tag{2.2}$$

where κ_{12} and κ_{21} are the coupling coefficients determined by the overlap integrals of the modes and the perturbation in the refractive index distribution. In the special case of two identical waveguides with symmetric coupling structures, $\beta_1 = \beta_2 = \beta$, $\kappa_{12} = \kappa_{21} = \kappa$, the equations reduce to

$$\begin{aligned} \frac{da_1(z)}{dz} &= -i\beta a_1(z) - i\kappa a_2(z) \\ \frac{da_2(z)}{dz} &= -i\beta a_2(z) - i\kappa a_1(z) \end{aligned} \tag{2.3}$$

Solving this system yields periodic power exchange between the two waveguides, with a coupling length $L_c = \pi/(2\kappa)$, over which complete power transfer from one waveguide to the other occurs. This result explains the fundamental operation of directional couplers and serves as the theoretical basis for many integrated photonic devices.

More generally, CMT can be extended to multiple modes or multiple resonators, leading to a matrix form

$$\frac{da(z)}{dz} = -iMa(z) \tag{2.4}$$

where $a(z) = [a_1(z), a_2(z), \dots, a_m(z)]^T$ represents the mode amplitudes, and M is the coupling matrix containing propagation constants and coupling coefficients. The eigenvalues of M give the effective propagation constants of the super modes, and the eigenvectors describe their field distributions.

However, resonant systems—cavities, coupled resonator optical waveguides, fiber rings,

lasers, and oscillators—are inherently dynamical: energy accumulates, leaks to ports, experiences material gain and saturation, and interacts with external channels. For these, the natural independent variable is time, and the appropriate framework is temporal coupled-mode theory (TCMT) [80]. The passage from CMT to TCMT is most transparent when one exploits the formal equivalence between the paraxial wave equation and the Schrödinger equation, but fixes space and lets the dynamics unfold in time. A narrowband physical field can be expanded as $E(r,t) = \sum_m a_m(t)u_m(r)e^{-i\omega_0 t}$ with slowly varying envelopes $a_m(t)$ from the vector Helmholtz equation, where $u_m(r)$ are the resonant mode profiles and ω_m denotes the resonant frequency of the m-th mode. Substitution into Maxwell's equations and projection onto the eigenmodes using reciprocity reduces the wave equation to ordinary differential equations for the amplitudes.

$$\dot{a} = (i\Omega - \Gamma)a + Ks_+, s_- = Cs_+ + Da \tag{2.5}$$

where $a = [a_1, a_2, \dots, a_m]^T$, and $\Omega = diag(\omega_m - \omega_0)$ is a diagonal matrix containing the detunings of each mode from the reference frequency ω_0, $\Gamma = \Gamma_i + \Gamma_e$ gathers intrinsic and external decay rates, K is the port excitation matrix, $s_\pm$ represents the input/output wave through the port, C is the direct scattering matrix between ports, and D is the radiation matrix from resonant modes to ports.

For two weakly coupled modes (or two resonators) with real coupling κ (from a real-index perturbation), Eq. (2.3) becomes:

$$\frac{d}{dt}\begin{bmatrix} a_1 \\ a_2 \end{bmatrix} = \begin{bmatrix} -i\omega_1 - \gamma_1 & i\kappa \\ i\kappa & -i\omega_2 - \gamma_2 \end{bmatrix}\begin{bmatrix} a_1 \\ a_2 \end{bmatrix} + \begin{bmatrix} k_{11} & k_{12} \\ k_{21} & k_{22} \end{bmatrix}\begin{bmatrix} s_{1,+} \\ s_{2,+} \end{bmatrix} \tag{2.6}$$

In this mapping, the spatial CMT quantities of propagation constant changes correspond

naturally to TCMT quantities of resonant frequency detunings, while distributed losses become time-domain decay rates; intuitively, spatial CMT "transfers amplitude along transmission direction," whereas TCMT "charges and discharges mode energy in the time domain."

Beyond classical optics, CMT and TCMT have been extended to non-Hermitian and PT-symmetric systems, where gain and loss are balanced to realize non-reciprocal wave propagation, single-mode selection, enhancement sensitivity, and EP dynamics. As a result, non-Hermitian CMT and TCMT models have become indispensable tools in guiding the design of next-generation photonics devices, lasers, sensors, and microwave photonic devices, bridging fundamental theory with practical applications.

2.2 Fundamentals of parity-time symmetry

The concept of PT symmetry in physics originates from the discovery that certain non-Hermitian Hamiltonians can exhibit entirely real eigenvalues, provided they commute with the combined P and T operators [2]. In quantum mechanics, Hermiticity of the Hamiltonian is traditionally required to ensure real eigenvalues, energy conservation, and unitary time evolution. PT-symmetric Hamiltonians, however, relax this constraint by allowing controlled non-Hermiticity while still supporting real spectra within specific parameters. This insight broadens the conventional understanding of quantum systems and establishes the foundation of modern non-Hermitian physics. In optics, PT symmetry is naturally mapped to the complex refractive index. A refractive index distribution $n(x)$ satisfies the PT condition when $n(x) = n^*(-x)$, where the spatial origin $x = 0$ is chosen as the center of symmetry. This

implies that the real part of the refractive index is an even function, while the imaginary part (representing gain and loss) is an odd function. The real index controls phase velocity and mode confinement, whereas the imaginary index dictates amplification or absorption. This correspondence allows optical waveguides, resonators, and coupled cavities to directly emulate PT-symmetric Hamiltonians and enter regimes where symmetry breaking and EPs strongly influence wave dynamics.

From a theoretical perspective, PT symmetry provides two major advantages. First, it offers an expanded mathematical framework for describing the spectral properties of non-Hermitian systems, enabling controlled spectral behavior in systems with balanced gain and loss. Second, PT symmetry introduces a powerful physical mechanism for mode selection, sensitivity enhancement, and dynamical control in photonic and microwave systems. For the purposes of this thesis, PT symmetry serves as a theoretical foundation for the design of novel fiber lasers and OEOs that exploit EPs for mode selection and stability enhancement. In the following sections, we focus on how PT symmetry concepts integrate into the theory of SLM lasers and OEOs, providing the basis for the experimental demonstrations presented in later chapters.

2.2.1 Parity-time-symmetric Hamiltonians

In conventional quantum mechanics, the Hermiticity of the Hamiltonian operator is a fundamental requirement, ensuring real eigenvalues and unitary time evolution. A one-dimensional closed quantum system is governed by the stationary Schrödinger equation [81]:

$$\widehat{H}\psi(x) = E\psi(x), \widehat{H} = -\frac{\hbar^2}{2m}\frac{d^2}{dx^2} + V(x) \tag{2.7}$$

where E denotes the eigenenergy, $\psi(x)$ is the wave function, $\widehat{H}$ is a Hamiltonian, $\hbar$ is the reduced Planck's constant, m represents the particle mass, x is the position, and $V(x)$ is a real function that describes the potential of the conservative force acting on the corresponding particle. Hermiticity requires $\widehat{H} = \widehat{H}^{\dagger}$, which in turn enforces $V(x) = V^{*}(x)$. This condition guarantees that the spectrum of $\widehat{H}$ is real, thereby providing the foundation of standard quantum theory. In an open quantum system, energy interaction between the system and the environment must be taken into consideration, the non-Hermitian Hamiltonian is used to simplify the analysis, that is, $\widehat{H} \neq \widehat{H}^{\dagger}$, and the dynamics of the system still formally satisfy the Schrödinger equation. Under these conditions, $V(x)$ becomes a complex function, and the real energy eigenvalues cannot be guaranteed because of the energy flux in and out of the system.

However, Bender and Böttcher demonstrated that Hermiticity is not a necessary condition for the reality of eigenvalues. Instead, it suffices for a Hamiltonian to respect PT symmetry. A Hamiltonian $\widehat{H}$ is said to be PT-symmetric if it satisfies:

$$\left[\widehat{H}, PT\right] = 0 \tag{2.8}$$

or equivalently,

$$PT\widehat{H}(PT)^{-1} = \widehat{H} \tag{2.9}$$

where the parity operator P performs spatial inversion, transforming the position and momentum operators as $x \to -x$ and $p \to -p$, and the time-reversal operator T reverses the direction of time and complex conjugates the imaginary unit: $t \to -t$ and $i \to -i$.

For a PT-symmetric system, this requires that:

$$V(x) = V^*(-x) \tag{2.10}$$

which implies that the real part of the potential is an even function, while the imaginary part is an odd function. The spectral properties of a PT-symmetric Hamiltonian are categorized into two distinct phases: unbroken PT-symmetric phase (all eigenvalues of $\widehat{H}$ are real, leading to a purely real spectrum), and broken PT-symmetric phase (eigenvalues emerge in complex conjugate pairs, signifying exponential growth or decay in physical observables). The transition between these regimes occurs at an EP, where not only the eigenvalues but also the corresponding eigenvectors coalesce.

2.2.2 Parity-time symmetry in photonics and microwave photonics

While the concept of PT-symmetric Hamiltonians originated in the context of quantum mechanics, the direct verification of such non-Hermitian systems in quantum domains remains extremely challenging due to decoherence, uncontrollable many-body interactions, and the practical difficulty of engineering balanced gain and loss at the microscopic level. In contrast, optics offers a uniquely suitable platform for realizing and experimentally exploring PT symmetry.

The paraxial wave equation governing light propagation in optical waveguides is mathematically equivalent to the Schrödinger equation. In this analogy, the spatial coordinate along the waveguide corresponds to time in quantum mechanics, and the refractive index profile acts as the potential. Thus, PT-symmetric Hamiltonians can be mapped directly onto optical systems by engineering the complex refractive index distribution [82]:

$$i\frac{d\varphi(x,z)}{dz}+\left[\frac{1}{2n_0k_0}\frac{d^2}{dx^2}+k_0\left(n_{\mathrm{R}}(x)+in_{\mathrm{I}}(x)\right)\right]\varphi(x,z)=0 \tag{2.11}$$

where $E(x,z)$ is the electric field envelope, $n(x)=n_{\mathrm{R}}(x)+in_{\mathrm{I}}(x)$ is the complex refractive index, and k_0 is the free-space wave vector. Thus, the PT condition becomes:

$$n_{\mathrm{R}}(x)=n_{\mathrm{R}}(-x), n_{\mathrm{I}}(x)=-n_{\mathrm{I}}(-x) \tag{2.12}$$

According to the definition of the refractive index, the real part of $n(x)$ determines the index profile whereas its imaginary part determines the gain/loss profile, which means a PT symmetric system has a symmetric index but a contrary gain and loss. In optics, unlike in quantum mechanics, it is straightforward to realize balanced gain and loss by combining amplifying media (e.g., doped fibers, semiconductor optical amplifiers) with absorbing regions. This provides a direct physical realization of the imaginary part of a PT-symmetric potential.

PT symmetry in optics can be simply achieved by two coupled waveguides with identical geometries with a balanced gain and loss profile. In [9], Rüter et al. have designed a coupled-ridge waveguide, with only one of the two parallel channels being optically pumped to provide a gain for the guided light, whereas the neighbor arm experiences a loss. The optical field in the two coupled waveguides can be expressed by

$$i\frac{dE_1}{dz}+i\gamma_{\mathrm{G}}E_1+\kappa E_2=0, i\frac{dE_2}{dz}+i\gamma_{\mathrm{L}}E_2+\kappa E_1=0 \tag{2.13}$$

where $E_{1,2}$ represent the field amplitudes in channels 1 and 2, $\kappa=\pi/(2L_{\mathrm{C}})$ is the coupling constant with a coupling length L_{C}, γ_{G} is the effective gain coefficient of channel 1, and γ_{L} is the loss of channel 2. To meet the PT symmetric condition, $\gamma=\gamma_{\mathrm{G}}=-\gamma_{\mathrm{L}}$. The eigenvalues

of Eq. (2.13) represent the propagation constants of the coupled super-modes in the two waveguides, that is, $\beta_{\pm} = \beta_0 \pm \sqrt{\kappa^2 - \gamma^2}$, where β_0 is the separate waveguide propagation constant. In this case, the EP of the system becomes $\gamma/\kappa = 1$. When $\gamma/\kappa < 1$, the real eigen propagation constants indicate that even in the presence of gain and loss, the light wave can propagate with conserved energy. However, once $\gamma/\kappa > 1$, the system is in the PT-broken phase, and the propagation constants become a pair of conjugate complex numbers, which means the electric fields are strongly confined either in the gain channel with light amplification or in the loss channel with exponential light decay, leading to nonreciprocal light propagation.

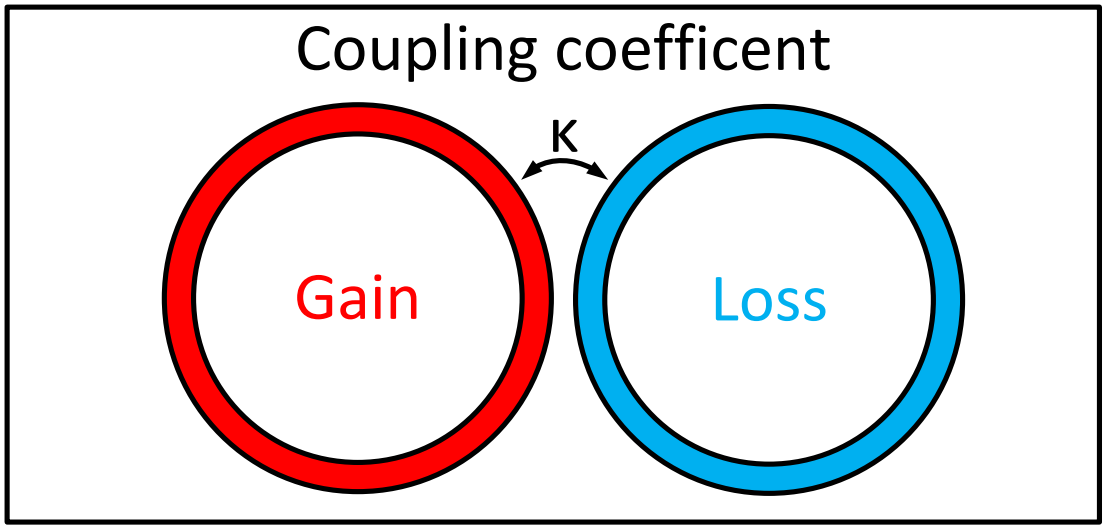

Fig. 2.1 Schematic of the two coupled ring resonators configuration

Moreover, optical platforms provide unparalleled flexibility in tuning coupling coefficients and gain/loss parameters, thereby enabling the observation of non-Hermitian phase transitions and EPs under controlled conditions. This tunability directly enables a PT-symmetric mode-selection mechanism in lasers and OEOs. The principle can be formalized by considering two identical coupled resonant cavities, one with gain and the other with an

equal amount of loss, as shown in Fig. 2.1. According to the TCMT, the effective non-Hermitian Hamiltonian is:

$$H = \begin{bmatrix} -i\omega_n + \gamma_n & i\kappa \\ i\kappa & -i\omega_n - \gamma_n \end{bmatrix} \tag{2.14}$$

where ω_n is the frequency of n-th resonant mode without PT symmetry, γ_n represents the gain/loss coefficient of the n-th mode, and κ denotes the coupling coefficient. The eigenvalues of this Hamiltonian are given by

$$\omega_{\pm} = \omega_n \pm \sqrt{\kappa^2 - {\gamma_n}^2} \tag{2.15}$$

As shown in Fig. 2.2, when $|\gamma_n| < \kappa$, the system is in the unbroken PT phase, with two real eigenvalues corresponding to resonant frequency splitting. At the critical point $|\gamma_n| = \kappa$, the system reaches EP where both eigenvalues and eigenvectors coalesce. For $|\gamma_n| > \kappa$, the system enters the broken PT phase, in which one eigenmode experiences amplification while the other experiences attenuation.

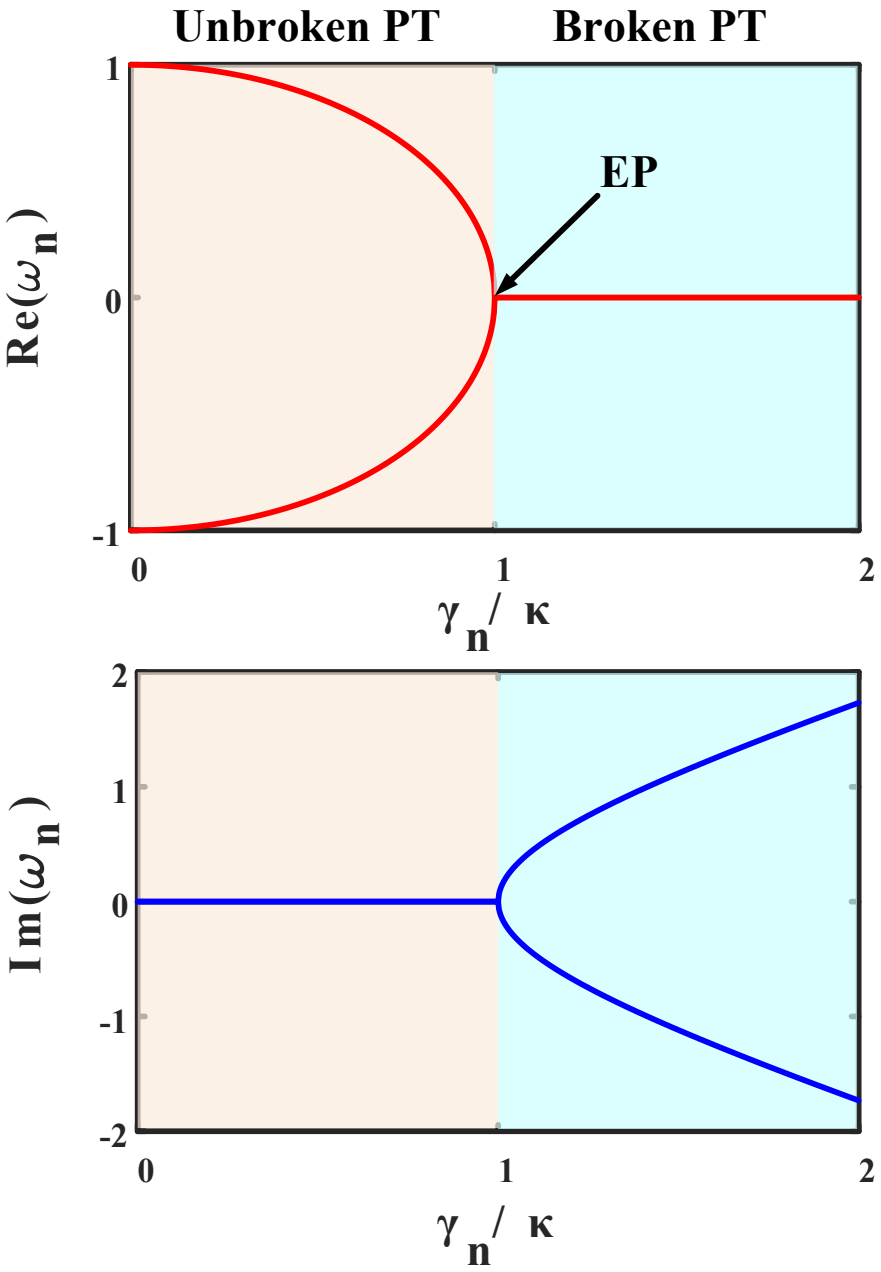

Fig. 2.2 Real and imaginary parts of eigenfrequencies versus coupling strength κ in a PT-symmetric system with gain–loss balance. The transition point corresponds to the exceptional point (EP), where both eigenvalues and eigenvectors coalesce.

In the analysis, we call the mode with the highest gain the primary mode, or the 0-th mode. Once the pair of 0-th modes is located in the broken PT phase, while others are still in the unbroken PT phase, only the primary mode can be amplified, and other modes will remain

neutral. This is how PT symmetry works for single-mode selection.

Besides, PT-symmetric photonic sensors exploit the non-Hermitian spectral characteristics that emerge in systems with balanced gain and loss. In particular, they leverage the presence of EPs to achieve ultra-sensitive response to external perturbations. An EP occurs when $|\gamma_n| = \kappa$, at which the eigenvalues and eigenvectors simultaneously coalesce. This non-Hermitian degeneracy is fundamentally different from Hermitian degeneracies: instead of having two orthogonal eigenmodes, the system possesses a single defective eigenstate with non-orthogonal mode geometry. This collapse of mode orthogonality is responsible for the anomalous sensitivity enhancement that PT-symmetric sensors display.

When the system is perturbed, such as by a nanoparticle binding to a microcavity or by a refractive-index change in the environment, the perturbation ϵ typically introduces a small frequency shift $\Delta\omega$ into one of the two coupled subsystems. In conventional Hermitian resonators, this yields a linear response $\Delta\omega \propto \epsilon$. In contrast, near an EP, the eigenvalue splitting follows a square-root dependence $\Delta\omega \propto \sqrt{\epsilon}$, where ϵ can be interpreted as the deviation of a system parameter (such as the coupling strength or effective refractive index) from its value at the EP. This behavior is illustrated in Fig. 2.2, where the eigenfrequency branches exhibit a characteristic square-root bifurcation as the system parameter is tuned across the EP, reflecting the non-Hermitian degeneracy and enhanced response of the system.

From a broader perspective, PT-symmetric sensors offer a fundamentally new way of detecting weak perturbations by harnessing non-Hermitian physics rather than relying solely on high-quality cavities or resonant enhancement. The mechanism is universal and extends

across platforms including WGM resonators, optofluidic cavities, Bragg gratings, integrated photonic chips, and even microwave and acoustic systems.

As a result, photonics and microwave photonics not only serve as an accessible testbed for verifying the fundamental predictions of PT-symmetric quantum theory but also pave the way for exploiting PT symmetry as a powerful tool in practical device engineering, such as nonreciprocal light propagation, single-mode lasers and OEOs, and sensitivity-enhanced sensors.

2.3 Fundamentals of single-longitudinal-mode lasers

An SLM laser operates at a single frequency within its gain bandwidth, producing a highly coherent and stable optical output. Unlike multimode lasers, where multiple longitudinal modes oscillate simultaneously, an SLM laser ensures that only one resonant wavelength within the cavity reaches the lasing threshold. This property is essential for applications requiring high spectral purity, such as optical communication, interferometry, and precision metrology.

The fundamental principle of a laser lies in the interaction between the laser cavity and the gain medium. In a conventional F-P resonator, the longitudinal modes are determined by the cavity length, satisfying the resonance condition $2nL = m\lambda$, where n is the refractive index, L is the cavity length, m is the mode number, and λ is the optical wavelength. The longitudinal resonances occur at $f_m = mc/2nL$, with an adjacent mode spacing known as the FSR, $\Delta f = c/2nL$. Since the gain medium typically provides a bandwidth much broader than the FSR, many longitudinal modes can lie within the gain profile and, in principle, oscillate.

To achieve single-longitudinal-mode operation, the laser must enforce a condition where only one longitudinal mode dominates, while all others remain suppressed. The condition can be expressed as

$$g(f_m) - \alpha_m > 0, \text{ for only one mode } m \tag{2.16}$$

where $g(f_m)$ is the mode gain, and α_m is the cavity loss.

To achieve SLM lasing, various strategies have been developed, broadly classified into cavity-length engineering, spectral filtering, injection locking, and non-Hermitian mode control.

Cavity-length engineering is the simplest approach, relying on short cavities with large FSRs to ensure that only one longitudinal mode falls within the gain bandwidth. This method is effective in microcavity lasers and certain semiconductor devices, but it is impractical for fiber lasers, where long cavities are desirable for narrow linewidths. Spectral filtering is therefore the dominant strategy in fiber-based systems. DBR and DFB lasers employ periodic index gratings to provide wavelength-selective reflection, enforcing SLM operation. In fiber lasers, PS-FBGs create narrow transmission windows that act as effective mode selectors, often achieving linewidths below a few kilohertz. Dual-loop Vernier cavities provide another filtering method, where the interference between loops produces an enlarged effective FSR, reducing mode density and facilitating single-mode operation.

Injection locking represents a different theoretical framework, in which an external seed or a delayed version of the laser output stabilizes the oscillation frequency. The Adler equation describes the locking dynamics, predicting that the locked frequency range depends on the

seed strength and detuning [83]:

$$\frac{d\varphi(t)}{dt} = \frac{\alpha}{2}\{g[N(t) - N_{\text{th}}]\} - \kappa\frac{A_{\text{inj}}}{A(t)}\sin\varphi(t) - \Delta\omega \tag{2.17}$$

where $A(t)$ is the field amplitude of the slave laser, A_{inj} is the field amplitude of the injected light, $\varphi(t)$ denotes the phase difference between the internal and injected field, α is the linewidth enhancement factor, g represents the laser gain coefficient, $N(t)$ is the number of carriers in the slave laser, while N_{th} is the threshold carrier number, κ is the coupling coefficient, and $\Delta\omega = \omega_{\text{s}} - \omega_{\text{inj}}$ denotes the angular frequency offset between the free-running slave lasers (ω_{s}) and the injected light (ω_{inj}). This method has been successfully applied to semiconductor and fiber lasers, enabling stable SLM operation over extended ranges. However, injection-locking schemes often require external sources or precise timing, limiting their practicality in certain applications. More recently, self-injection mechanisms, in which part of the laser output is fed back after a delay, have been investigated. These configurations can achieve sub-kilohertz linewidths and SLM operation, though they are sensitive to environmental perturbations [84].

PT symmetry introduces a fundamentally new mode-control mechanism for SLM lasers. Instead of relying solely on narrowband filters or external seeding, PT lasers achieve single-mode operation intrinsically through gain/loss engineering. By operating beyond the PT symmetry-breaking threshold, one super mode acquires net gain while the other is suppressed, resulting in single-mode emission. Theoretical analyses based on coupled-mode equations have shown that PT lasers can maintain SLM operation even under conditions where conventional designs fail, such as in long cavities or multimode waveguides. Experimental

studies in both integrated photonic and fiber-based platforms have validated these theoretical predictions, making PT symmetry a promising design principle for SLM lasers [11,12,26,85].

The performance of an SLM laser is fundamentally characterized by two key parameters: the SMSR and the spectral linewidth. These quantities provide direct measures of the mode purity and coherence, respectively, and together determine the suitability of an SLM laser for high-precision applications.

The SMSR quantifies the ability of the laser cavity to discriminate against undesired longitudinal modes. It is defined as [86]:

$$\text{SMSR} = 10\log_{10}\left(\frac{P_{\text{main}}}{P_{\text{side}}}\right)\ [dB] \tag{2.18}$$

where P_{main} is the output power of the dominant lasing mode and P_{side} is the power of the strongest suppressed side mode. A high SMSR implies that mode competition and cross-saturation have been effectively resolved in favor of a single longitudinal resonance. From a theoretical perspective, SMSR is determined by the difference between the net mode gain and cavity loss for the main mode compared with competing modes.

The linewidth of an SLM laser reflects its temporal coherence and is ultimately limited by quantum fluctuations of the intracavity field. According to the Schawlow–Townes relation, the fundamental linewidth is given by [87]:

$$\Delta\nu_L = \frac{2\pi h\nu_L(\Delta\nu_c)^2}{P_{\text{out}}} = \frac{2\pi h\nu_L}{P_{\text{out}}}\left(\frac{\nu_L}{Q}\right)^2 \tag{2.19}$$

where $h\nu_L$ represents the photon energy, $\Delta\nu_c$ is the full-width at half maximum (FWHM) intensity of the resonance related to the quality factor Q, and P_{out} is the output power. The

quality factor Q is directly linked to the photon lifetime τ_P through $Q = 2\pi\nu_L\tau_P$. According to the Eq. (2.19), the laser linewidth scales inversely with the square of the quality factor, or equivalently with the square of the photon lifetime. Therefore, an increase in cavity length, which enhances the photon lifetime, leads to a significant reduction in the laser linewidth. However, a long cavity provides a small FSR, which makes mode competition fierce, resulting in single-mode operation more challenging to achieve.

Therefore, cavity length plays a dual role in SLM lasers: it improves linewidth performance through an increased quality factor, while simultaneously influencing mode competition via the FSR. The design of SLM lasers thus requires a careful balance, where sufficient cavity length is maintained to achieve narrow linewidths without compromising single-mode stability.

2.4 Optoelectronic oscillators

2.4.1 Fundamentals of optoelectronic oscillators

An OEO is a type of oscillator that generates ultra-low phase noise and high-frequency microwave signals by using optical and electronic components in a feedback loop. Unlike traditional electronic oscillators that rely solely on electronic components, an OEO exploits the stability and high spectral purity of optical components to generate highly coherent microwave signals. These OEOs are widely used in applications such as radar systems, telecommunications, microwave photonic sensors, and precision frequency synthesis.

The fundamental working principle of an OEO is based on the conversion of optical energy into an electronic microwave signal through a feedback mechanism. The system consists of

several key components: an optical source (laser), an EOM, a long optical fiber delay line, a PD, an RF amplifier, and a BPF. The oscillator starts with a continuous-wave laser, which provides a stable optical carrier. This optical signal is modulated by an RF signal via an EOM, typically a Mach-Zehnder modulator (MZM). The modulated optical signal then propagates through a long optical fiber, which acts as a high-quality delay element, significantly enhancing the oscillator's spectral purity and phase noise performance. After traversing the fiber delay line, the optical signal is converted back into an electrical RF signal by a high-speed PD. The photo-detected signal, which contains multiple frequency components due to optical modulation, is passed through an RF BPF that selects the desired microwave frequency mode. This filtered signal is then amplified and fed back to drive the EOM, closing the feedback loop. The oscillation condition is satisfied when the loop gain exceeds unity and the total phase shift is a multiple of 2π, leading to the generation of a stable microwave oscillation.

The oscillation frequency of an OEO is determined by the fiber delay length and the BPF characteristics. The frequency spacing between adjacent oscillation modes (FSR) is given by:

$$\Delta f = \frac{c}{nL} \tag{2.20}$$

where c is the speed of light, n is the refractive index of the fiber, and L is the fiber length.

The performance of an OEO is fundamentally determined by its spectral purity, and frequency stability. Among these, the single-sideband (SSB) phase noise is the most critical figure of merit, as it directly reflects the short-term frequency stability and coherence of the generated microwave signal. The phase noise is closely linked to the effective quality factor

of the delay line, $Q_{\text{eff}} \approx \pi f_0 \tau$, indicating that longer optical delays significantly suppress close-to-carrier noise and lead to ultra-narrow linewidths [59]. Another important parameter is the SMSR, since the presence of multiple resonant modes separated by the FSR can lead to multimode oscillations if not adequately suppressed; a high SMSR ensures that a single oscillation mode dominates, thereby guaranteeing spectral purity. Collectively, these factors define the theoretical framework for evaluating OEO performance, with phase noise, frequency stability, and SMSR serving as the core benchmarks that distinguish OEOs from conventional electronic oscillators.

2.4.2 Mode selection techniques of optoelectronic oscillators

A fundamental challenge in OEOs arises from the extremely long cavity length, which leads to a dense spectrum of oscillating modes separated by the FSR. Without additional mode-selection mechanisms, multiple oscillation modes can simultaneously exist, resulting in degraded spectral purity, increased phase noise, and instability. To ensure stable single- mode operation, a variety of mode-selection techniques have been developed.

One widely adopted method is the use of narrowband RF BPFs in the electrical domain. By placing a high-quality filter within the OEO feedback loop, only one oscillation frequency that lies within the passband is reinforced, while other modes are strongly attenuated. This approach is conceptually straightforward and highly effective; however, the filter's bandwidth and center frequency tunability often limit the overall frequency agility of the OEO.

Another common approach employs multi-loop configurations, where several fiber loops of unequal lengths are coupled to generate a Vernier effect. The overlap condition of their

respective longitudinal modes leads to a much larger effective FSR, thereby facilitating single-mode oscillation. This technique provides improved sidemode suppression and has been extensively used in practical high-performance OEO designs. A major drawback of this approach lies in the limited frequency tunability, since the lengths of the loops must be adjustable when the frequency is being tuned, making the implementation very complicated.

To realize a large frequency tunable range, an MPF can be employed for mode selection. The principle relies on a phase modulator (PM) followed by an optical notch filter-such as a PS-FBG, or a microdisk resonator (MDR), and a PD, as shown in Fig. 2.3. The MPF is realized by phase-modulation to intensity-modulation (PM–IM) conversion. If the phase-modulated optical signal is directly detected by the PD, no microwave signal appears at the output, since the beat between the carrier and the upper sideband is equal in magnitude but opposite in phase to that between the carrier and the lower sideband, leading to complete cancellation. The PS-FBG is employed to suppress one of the optical sidebands generated by the PM, thereby producing a single-sideband-with-carrier (SSB+C) optical signal. When this SSB+C signal is sent to the PD, the beating between the optical carrier and the remaining sideband generates a microwave signal, which effectively equivalent to a narrowband MWP. If the spectral notch of the PS-FBG is sufficiently narrow, the filter provides strong frequency selectivity, enabling the OEO to generate a single-frequency microwave signal. Furthermore, the frequency tunability can be achieved by shifting the optical carrier wavelength of the laser diode or by thermally or mechanically tuning the Bragg wavelength of the PS-FBG, thus allowing the microwave frequency to be continuously controlled. However, the single-mode oscillator cannot be guaranteed when the loop length exceeds the kilometer scale due to the

limitation of the bandwidth of the PS-FBG.

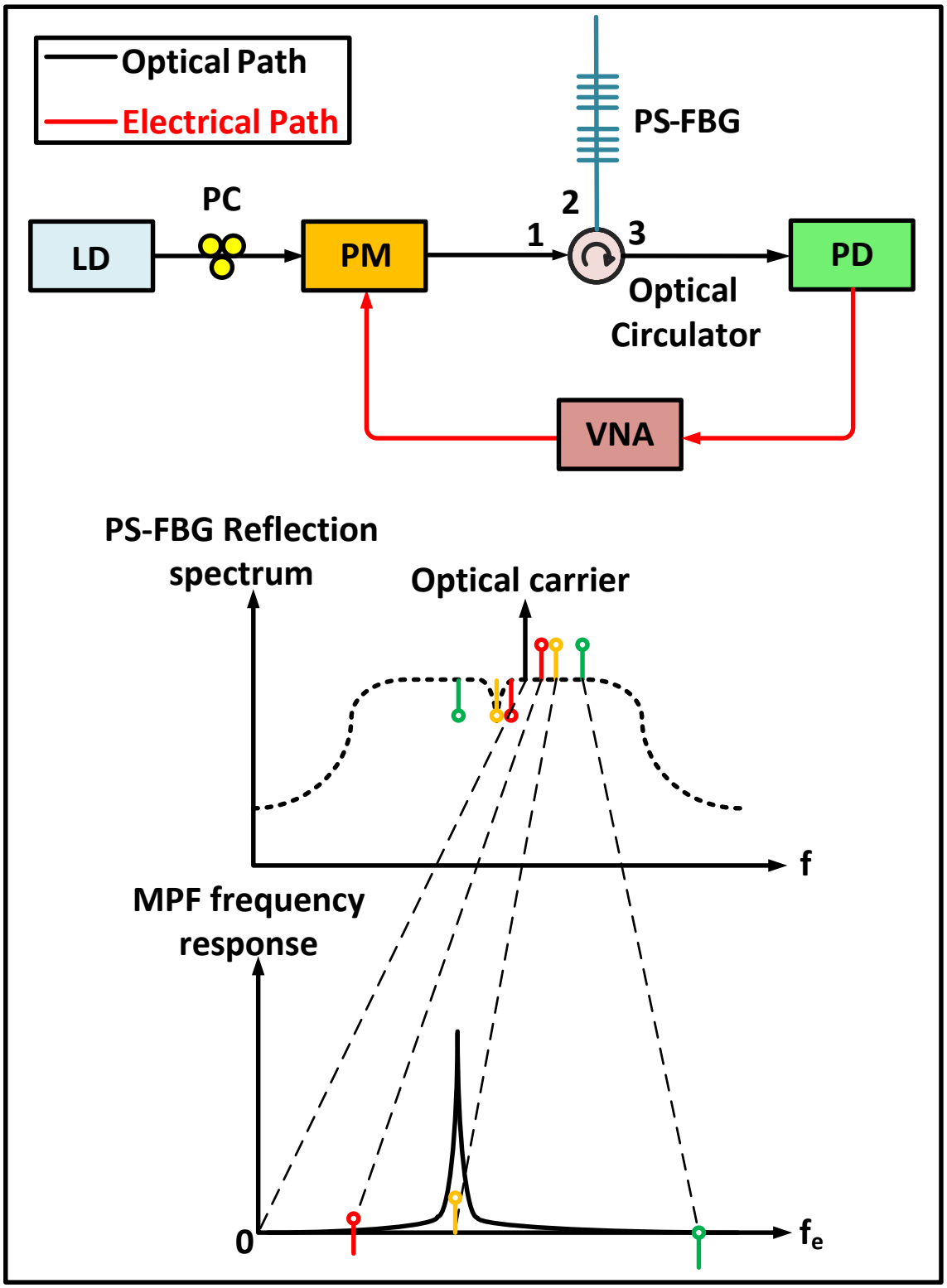

Fig. 2.3 Schematic of the microwave photonic filter (MPF) configuration. LD: laser diode, PC: polarization controller, PM: phase modulator; PS-FBG: phase-shifted fiber Bragg grating; PD: photodetector; VNA: vector

network analyzer.

More recently, non-Hermitian and PT symmetric schemes have emerged as a novel mode-selection mechanism. By adjusting the gain/loss coefficient for a specific mode exceeds the coupling coefficient, PT symmetry is broken, the specific mode will start to oscillate, while the other modes will remain neutral. The PT-symmetric OEO enables single-mode operation without relying on ultra-high-quality filters or complex dual-loop configurations, offering a compact and robust alternative for next-generation oscillators.

2.4.3 Multi-frequency signal generation in optoelectronic oscillators

Multi-frequency OEOs, despite their functional advantages and potential applications in multi-band microwave photonics, face several intrinsic challenges that make their realization significantly more complex than conventional single-frequency OEOs. The most fundamental difficulty arises from severe mode competition within the shared optoelectronic feedback loop. Because all oscillation frequencies experience the same optical path, electronic gain, and nonlinear saturation dynamics, the loop can typically support only a limited amount of net gain. As a result, one oscillation mode often dominates and suppresses the others, leading the system to collapse into single-mode operation unless additional mechanisms—such as injection locking, coupled-loop architectures, or PT-symmetric mode partitioning—are deliberately introduced. This strong mode competition becomes even more pronounced when long fiber delays are employed to achieve low phase noise, because the large effective quality factor enhances sensitivity to small gain differences among the oscillation modes.

Another major difficulty lies in the stringent requirements placed on the loop filter and

frequency-selection architecture. Generating multiple stable oscillation frequencies simultaneously demands a filter response that either permits multiple longitudinal modes to satisfy the oscillation condition or supports structured multi-passband transmission. This necessitates careful control of bandwidth, insertion loss, group delay, and FSR. Even slight mismatches in these parameters can lead to unequal oscillation thresholds, unstable power distribution among the generated tones, or the complete disappearance of certain modes. Moreover, multi-frequency oscillation is highly sensitive to variations in fiber length, temperature, and refractive index, since each oscillation frequency must satisfy the loop phase condition simultaneously—a requirement far more fragile than in single-frequency OEOs.

Maintaining low phase noise and high frequency stability across all oscillation tones introduces additional complications. While single-frequency OEOs rely on long optical delays to achieve exceptionally low phase noise, multi-frequency OEOs must ensure not only that each individual frequency maintains a low noise floor, but also that the mutual phase relationships among the tones remain stable. Without such mutual coherence, multi-band radar, photonic vector analysis, and microwave photonic processing cannot benefit from the multi-tone output. The coexistence of multiple oscillation frequencies also makes the system more susceptible to beating-induced noise, thermal drifts, and dynamic gain fluctuations, which jointly deteriorate stability and spectral purity.

To overcome these challenges, several approaches are proposed and studied [88,89,90,91,92,93]. Decoupling the competing modes in an additional degree of freedom—such as polarization or cavity topology—is an effective way to stabilize multi-frequency

operation. In polarization-division schemes, a dual-polarization modulator or polarization-sensitive filter is used so that different microwave tones oscillate in orthogonal polarization states of the same optical carrier. Gao *et al.* demonstrated a frequency-tunable two-tone RF signal generator using a dual-polarization-modulator-based OEO, where two microwave tones are generated in two orthogonal polarizations and tuned independently by separate electrical filters; polarization isolation suppresses optical interference between the tones and strongly mitigates nonlinear intermodulation in the multi-frequency regime.

A complementary strategy is to employ tailored optical filtering to deliberately shape the loop's spectral response. Multi-passband optical filters, superimposed FBG responses, stimulated Brillouin scattering gain profiles, or micro resonator-based multi-window filters can generate multiple discrete resonance conditions within the loop, allowing several longitudinal modes to meet the oscillation threshold simultaneously. The key lies in engineering comparable net gain for all targeted modes so that no single frequency dominates.

One of the most effective approaches is to introduce controlled mode partitioning through external injection. Assuming that a dual-tone oscillation occurs in an OEO, the microwave signal injected into the RF port of the MZM is written as

$$V_{\text{in}}(t) = V_1 \cos(2\pi f_1 t + \varphi_1) + V_2 \cos(2\pi f_2 t + \varphi_2) \tag{2.21}$$

where V_1 and V_2 are the voltage amplitudes of the two oscillation modes, f_1 and f_2 are the frequencies of the two-tone signals, φ_1 and φ_2 are the initial phases of the two oscillation modes, respectively. The output optical signal from the MZM is calculated as

$$E_{\text{out}} = E_0 \exp(j2\pi f_c t) \cos\left(\frac{\pi}{2V_\pi} V_{in}(t)\right) \tag{2.22}$$

where E_0 and f_c are the optical field amplitude and the carrier frequency of the optical light wave source, respectively. V_π is the half-wave voltage of the MZM. After detected by the PD, the recovered microwave signal is given by

$$V_{\text{PD}}(t) \propto \cos\left(\frac{\pi V_1}{V_\pi}\cos(2\pi f_1 t + \varphi_1) + \frac{\pi V_2}{V_\pi}\cos(2\pi f_2 t + \varphi_2)\right) \tag{2.23}$$

When an external signal with a frequency of $f_{\text{inj}} = f_2 - f_1$ is injected to the feedback loop of the OEO, the microwave signal feedback to the RF port of the MZM is written as

$$V_{\text{out}}(t) \propto \left\{ \begin{array}{l} V_{\text{inj}} J_1\left(\frac{\pi V_1}{V_\pi}\right) J_0\left(\frac{\pi V_2}{V_\pi}\right) \cos\left(2\pi(f_1 + f_{\text{inj}})t + \varphi_1 + \varphi_{\text{inj}}\right) + \\ V_{\text{inj}} J_0\left(\frac{\pi V_1}{V_\pi}\right) J_1\left(\frac{\pi V_2}{V_\pi}\right) \cos\left(2\pi(f_2 - f_{\text{inj}})t + \varphi_2 - \varphi_{\text{inj}}\right) \end{array} \right\} \tag{2.24}$$

where J_n is the n-th order Bessel function of the first kind. V_{inj} and φ_{inj} are the voltage and the initial phase of the injection signal, respectively. From Eq. (2.23), it can be seen that, the phase of the generated dual-tone microwave signals at f_1 and f_2 is locked to $\varphi_2 - \varphi_{\text{inj}}$ and $\varphi_1 + \varphi_{\text{inj}}$, respectively, which results in two mutually coherent, phase-locked microwave outputs.

By injecting one or more reference microwave tones or optically modulated seeds into the loop, selected oscillation frequencies can be forced to lock to the injected signals via injection-locking mechanisms. This not only suppresses unwanted spurious modes but also stabilizes the relative phases and amplitudes of the targeted frequencies, enabling stable dual-frequency or multi-tone operation. Such injection-based stabilization is particularly effective when the injected tones possess high spectral purity, since the loop naturally inherits their

phase stability and frequency accuracy.

CHAPTER 3 PARITY-TIME SYMMETRIC SINGLE-LONGITUDINAL-MODE FIBER RING LASER USING A SINGLE PHYSICAL LOOP[1]

3.1 Introduction

This chapter presents a SLM fiber ring laser in which PT-assisted mode selection is realized within a single physical loop [94]. The core idea is to exploit a polarization-dependent Sagnac loop to create two equivalent counter-propagating loops that share the same physical path length, so that the usual geometric mismatch problem of dual-loop PT-symmetric lasers is eliminated, and stability is enhanced. Practically, introducing PT symmetry in long fiber cavities is attractive because the long cavity supports a narrow Schawlow–Townes linewidth yet suffers from dense longitudinal modes (small FSR) that complicate single-mode selection. Conventional remedies—ultra-narrow filters (e.g., PS-FBGs) or dual/multi-loop Vernier designs—either impose strict component requirements or increase complexity and limit tunability. The proposed single-loop PT laser avoids these issues by performing mode selection through PT symmetry breaking while keeping the cavity long for linewidth reduction. Experimentally, we realize SLM lasing with a wavelength tuning range of 1530–1565 nm, a minimum linewidth of 390 Hz, and an SMSR of 41.9 dB. These results validate that a single physical loop can host an effective two-loop PT system and deliver high spectral purity with a compact configuration.

[1] This Chapter has been previously published in **Z. Dai**, Z. Fan, P. Li, and J. Yao, "Widely wavelength-tunable parity-time symmetric single-longitudinal-mode fiber ring laser with a single physical loop," *J. Lightw. Technol.*, vol. 39, no. 7, pp. 2151-2157, Apr. 2021.

3.2 Operation principle

The configuration of the proposed PT-symmetric SLM fiber ring laser is shown in Fig. 3.1(a). The cavity comprises a long section of single-mode fiber (SMF), which provides a large photon lifetime to support linewidth narrowing, an erbium-doped fiber amplifier (EDFA) as the gain medium, and an F-P filter is used as the tunable optical bandpass filter (TOBF) that defines the lasing wavelength tunable range. A polarization-dependent Sagnac loop, consisting of a polarization beam splitter (PBS) and two polarization controllers (PC1 and PC2), is embedded in the main ring to realize PT symmetry within a single physical loop.

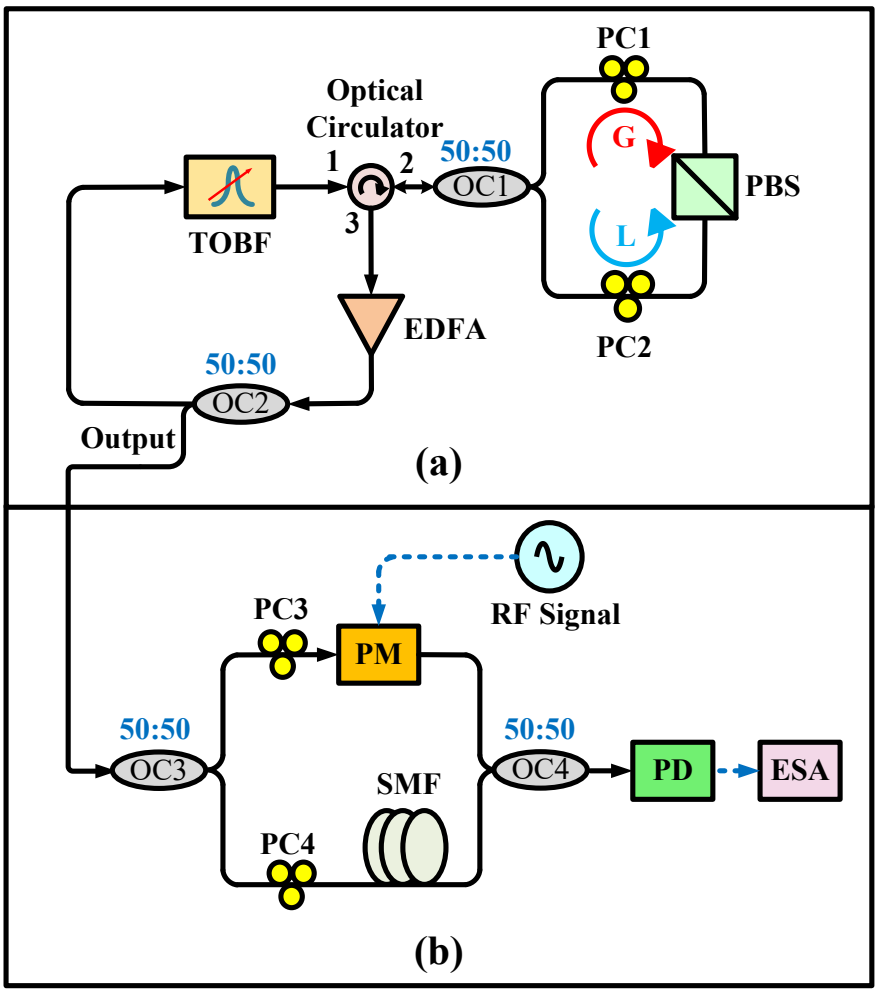

Fig. 3.1 (a) Schematic of the PT-symmetric fiber ring laser with a single physical loop (b) Frequency-shifted

self-heterodyne interferometer for evaluating the performance of the proposed PT-symmetric fiber ring laser. OC: optical coupler; PC: polarization controller; PBS: polarization beam splitter; TOBF: tunable optical bandpass filter; EDFA: erbium-doped fiber amplifier; PM: phase modulator; RF Signal: radio frequency signal; SMF: single-mode fiber; PD: photodetector; ESA: electrical spectrum analyzer.

When the optical signal from the EDFA enters the Sagnac loop, it is split into clockwise (CW) and counter-clockwise (CCW) components circulating within the same fiber loop. These two counter-propagating waves are equivalent to two sub-loops with identical physical length. Assuming that θ_1 and θ_2 are the polarization angles from the fully transmitted axis of the PBS from CW and CCW directions. These two angles can be separately tuned by two PCs in the Sagnac loop, then the amplitudes of the light waves after passing through the PBS are $A_n\cos\theta_1$ and $B_n\cos\theta_2$, where A_n and B_n are the mode amplitudes of the CW and CCW waves. Thus, by adjusting PC1 and PC2, the relative optical powers in the CW and CCW paths can be controlled, which can be regarded as artificially introducing two different level loss. Such that one loop experiences net gain and the other net loss, establishing the balanced gain/loss distribution required for PT symmetry.

Besides the gain/loss coefficients, the coupling coefficient κ plays a key role in the PT-symmetric systems. In the proposed PT-symmetric fiber ring laser, the two counter-propagating waves are coupled at the optical coupler (OC1), and the coupling coefficient is given by:

$$\kappa = \frac{Kz}{l} \tag{3.1}$$

where K is the coupling coefficient of OC1, z is the coupling length, and l is the ring cavity

length.

Then the coupled differential equations of the proposed laser are given by:

$$\frac{d}{dt}\begin{bmatrix}A_n\\B_n\end{bmatrix}=\begin{bmatrix}-i\omega_n+g_{A_n} & i\kappa\\ i\kappa & -i\omega_n+g_{B_n}\end{bmatrix}\begin{bmatrix}A_n\\B_n\end{bmatrix} \tag{3.2}$$

where g_{A_n} and g_{B_n} represent the net gain and loss coefficients of the two coupled loops for the n-th mode. Thus, the eigenfrequencies are calculated to be

$$\omega_n{}^{(1,2)}=\omega_n+i\left(\frac{g_{A_n}+g_{B_n}}{2}\right)\pm\sqrt{\kappa^2-\left(\frac{g_{A_n}-g_{B_n}}{2}\right)^2} \tag{3.3}$$

A PT-symmetric system requires the net gain and loss are identical in magnitude, which means, $g_{A_n}=-g_{B_n}=g_n$. Eq. (3.3) is simplified by

$$\omega_n{}^{(1,2)}=\omega_n\pm\sqrt{\kappa^2-g_n{}^2} \tag{3.4}$$

When $\kappa<g_n$, $\sqrt{\kappa^2-g_n{}^2}$ become imaginary, which means a conjugate pair of modes with one experiencing amplification and the other decay is located in the PT broken region, while other modes remain neutral, leading to SLM lasing.

In the analysis, the longitudinal mode exhibiting the maximum net gain is referred to as the primary mode, or the 0-th longitudinal mode. In a conventional laser system, SLM operation is achieved by ensuring that the gain of this primary mode surpasses the lasing threshold, while the gains of all other modes remain below threshold, as illustrated in Fig. 3.2(a). The gain contrast between the primary mode and the second highest mode is expressed by

$$g_{\max}=g_0-g_1 \tag{3.5}$$

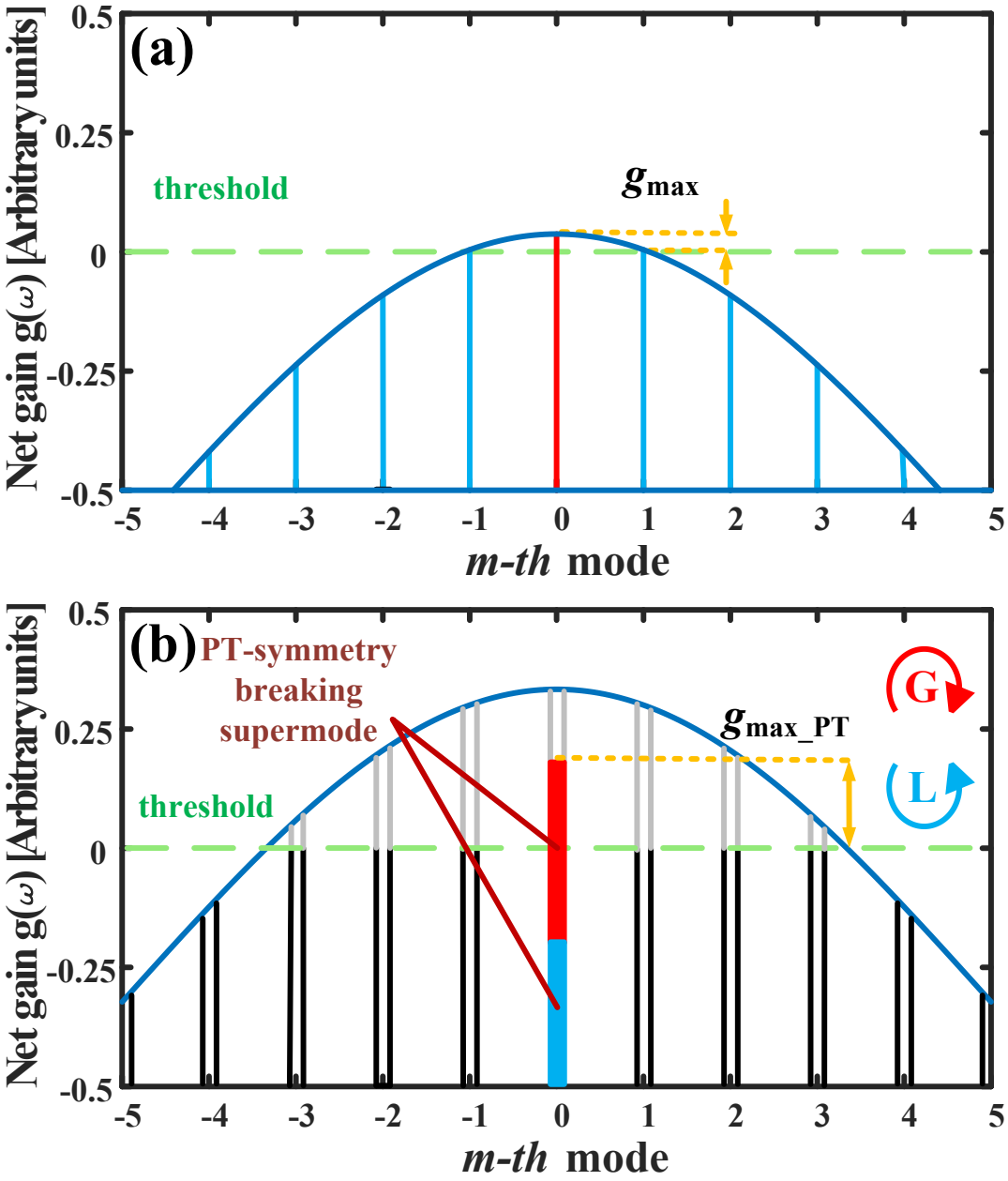

Fig. 3.2 Gain contrasts of (a) a conventional single-loop fiber ring laser, and (b) the proposed PT-symmetric fiber ring laser.

In the condition of PT-symmetric breaking, as shown in Fig. 3.2(b), the gain difference of these two modes is given by

$$g_{\text{PT-max}} = \sqrt{{g_0}^2 - {g_1}^2} \tag{3.6}$$

To quantify the improvement in mode selection based on PT symmetry, we calculate the gain contrast ratio, which is defined as the ratio between the gain difference between a PT-symmetric laser source and a conventional laser source, given by

$$G = \sqrt{\frac{g_0/g_1 + 1}{g_0/g_1 - 1}} \tag{3.7}$$

As can be seen, the smaller the gain difference between the primary mode and the second highest mode, the more significant the contribution of the PT-symmetric mode-selection mechanism to ensuring stable SLM lasing.

3.3 Experimental results

The experimental performance of the proposed PT-symmetric fiber ring laser is experimentally evaluated using the setup illustrated in Fig. 3.1(a). The EDFA (NORTEL FA17UFAC119C28) provides an optical gain of 30 dB with a saturation output power of 16 dBm. An F-P filter (OZ Optics) is incorporated into the loop to serve as the TOBF, providing a 3-dB bandwidth of 0.41 nm and a tuning range of 1530–1565 nm. Fig. 3.3 shows the transmission spectral of the TOBF when its central wavelength is set to 1550 nm. The overall cavity length of the fiber ring is 80.08 m, corresponding to an FSR of 2.55 MHz. Within the passband of the TOBF, more than 20000 longitudinal modes exist, making SLM operation infeasible without introducing PT symmetry. In this setup, the TOBF provides coarse wavelength selection to enable tunability across the C-band. The PCs are using three-paddle fiber controllers, each consisting of a half-wave plate positioned between two quarter-wave plates. PT symmetry is established by finely adjusting the half-wave plates of PC1 and PC2 to balance the gain and loss between the two equivalent loops, while any phase mismatch

induced by OC1 or fiber bending is compensated by tuning the quarter-wave plates. Because the two loops are coupled via OC1 with a fixed coupling ratio, the EDFA gain is maintained sufficiently high to guarantee operation in the PT-broken phase. The laser output is monitored using an optical spectrum analyzer (OSA, ANDO AQ6317B) with a spectral resolution of 0.01 nm.

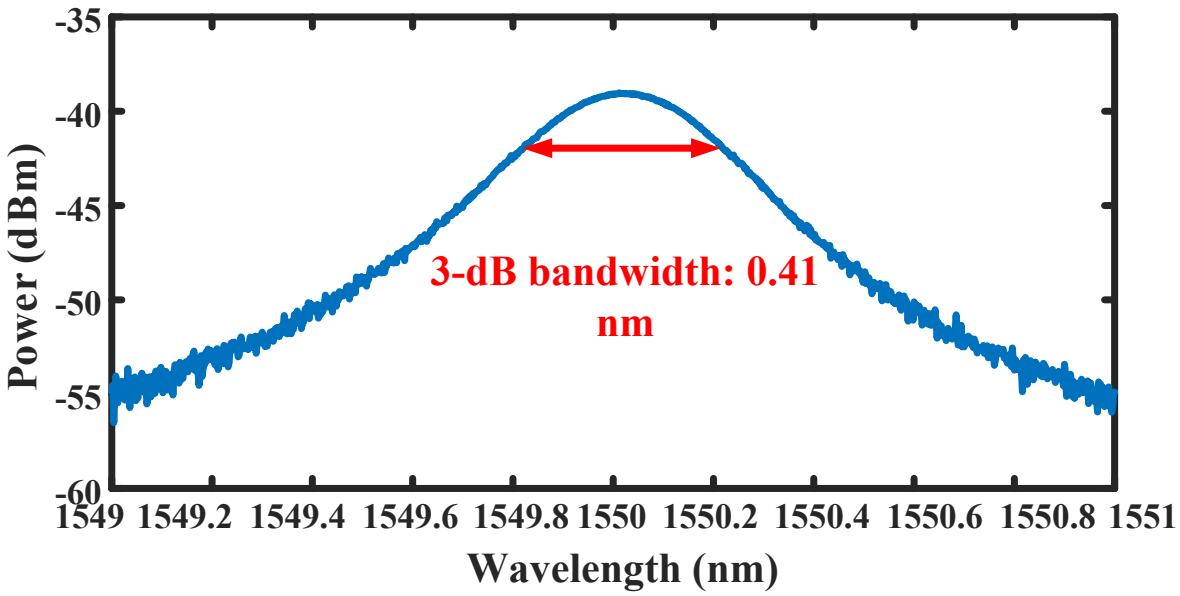

Fig. 3.3 The optical spectral response of the Fabry-Perot (F-P) filter at a center wavelength of 1550 nm

Fig. 3.4(a) shows the optical spectrum of the laser, indicating a lasing wavelength centered at 1550 nm. The measured optical signal-to-noise ratio (OSNR) reaches 41.9 dB, confirming the high spectral quality of the generated output. A zoom-in view of the spectrum is presented in Fig. 3.4(b). However, due to the limited resolution of the OSA, it is not possible to directly verify whether the laser resonant strictly in a SLM, nor can the linewidth of the output be accurately determined with this instrument.

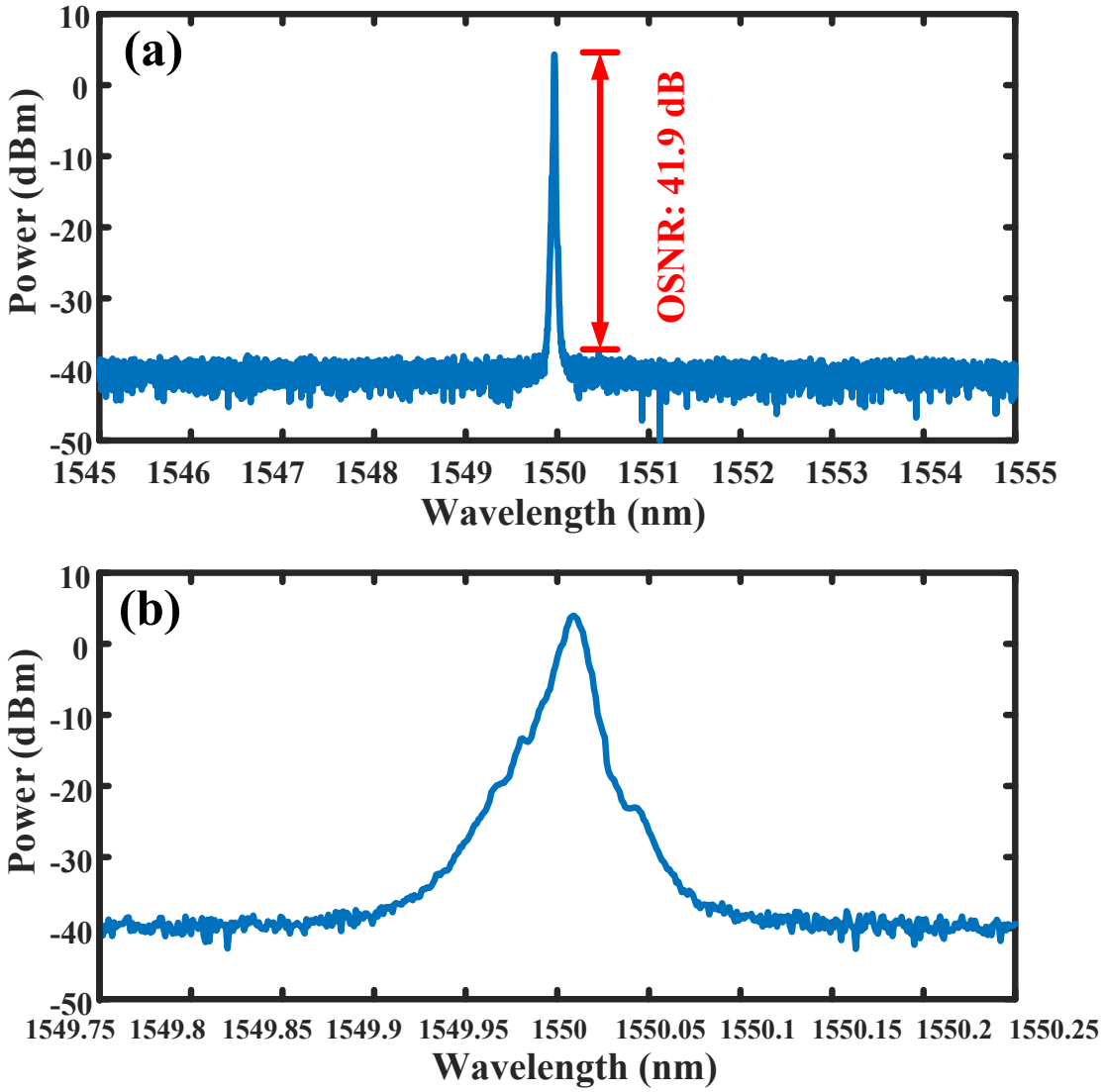

Fig. 3.4 (a) The optical spectrum of the generated light wave at the center wavelength of 1550 nm measured by an OSA, and (b) its zoom-in view with a span of 0.5 nm.

To achieve high-resolution spectral characterization, the shifted self-heterodyne technique [95] is employed. The measurement configuration is shown in Fig. 3.1(b). A 1 GHz microwave signal is applied to a PM, producing a frequency shift of 1 GHz in the upper arm so that the resulting beat signal appears at 1 GHz rather than near direct current (DC), thereby allowing a clearer observation. In the setup, the 1 GHz reference signal is generated by a microwave signal generator (Agilent E8254A) and applied to the PM (JDSU Model-10023874). A 10-km

section of SMF serves as the delay line in the lower arm. The combined signals are detected by a high-speed PD (New Focus 10058B) with a 3-dB bandwidth of 20 GHz, and the electrical spectrum is recorded using an electrical spectrum analyzer (ESA, Agilent E4448A).

Fig. 3.5(a) illustrates the electrical spectrum at the output of the PD when the gain and loss of the two loops are not balanced. Under this condition, PT symmetry is not satisfied and the laser operates in a multimode state, as evidenced by the multiple RF beat signals. A zoom-in view in Fig. 3.5(b) reveals an FSR of 2.55 MHz. When PC1 and PC2 are adjusted such that the gain and loss in the two loops are balanced and further exceed the coupling coefficient, the system enters the PT-broken region. Under this condition, SLM lasing is obtained. Fig. 3.5(c) clearly shows a single beat frequency at 1 GHz, confirming SLM operation, while the zoom-in spectrum in Fig. 3.5(d) demonstrates strong suppression of side modes.

For comparison, the performance of a conventional fiber ring laser with a single loop is also evaluated. In this case, the Sagnac loop is removed, and the EDFA is directly connected to the TOBF. The measured electrical spectrum at the PD output is shown in Fig. 3.5(e). Multiple RF beat signals are observed, originating from the beating of several longitudinal modes within the cavity. Because the cavity length of this conventional design is shorter than that of the PT-symmetric configuration, the corresponding FSR is larger, measured at 3 MHz, as illustrated by comparing Figs. 3.5(b) and (f).

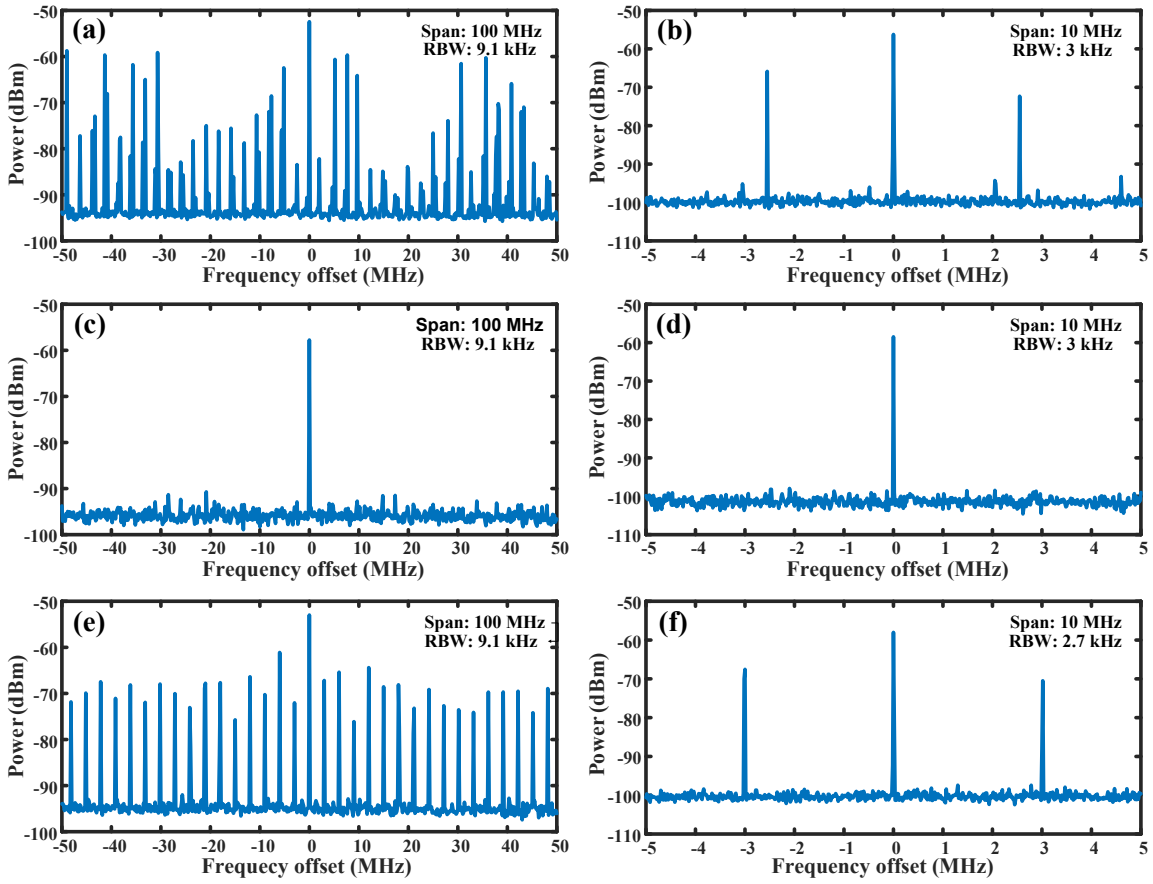

Fig. 3.5 The measured spectra of the RF beat signals at the output of the PD (a) without PT symmetry and (b) its zoom-in view, (c) with PT symmetry and (d) its zoom-in view. (e) The measured spectrum for a conventional single-loop fiber ring laser and (f) its zoom-in view.

The PT-symmetric laser is then operated in single-mode emission, and the linewidth of the generated light is measured. Fig. 3.6 demonstrates the electrical spectrum at the PD output. The 20-dB linewidth is measured to be 7.8 kHz, which corresponds to a 3-dB linewidth of approximately 390 Hz. It should be emphasized that, in theory, several thousand kilometers of fiber are required to completely remove the coherence between the two optical waves from the upper and lower arms to obtain a truly accurate sub-kHz linewidth measurement. In this experiment, only a 10-km fiber is used, which partially reduces the coherence but does not entirely eliminate the interference, leading to broadening of the self-heterodyne spectrum.

Moreover, additional broadening due to $1/f$ frequency noise [96] is unavoidable. Consequently, the measured linewidth is narrower than the actual linewidth.

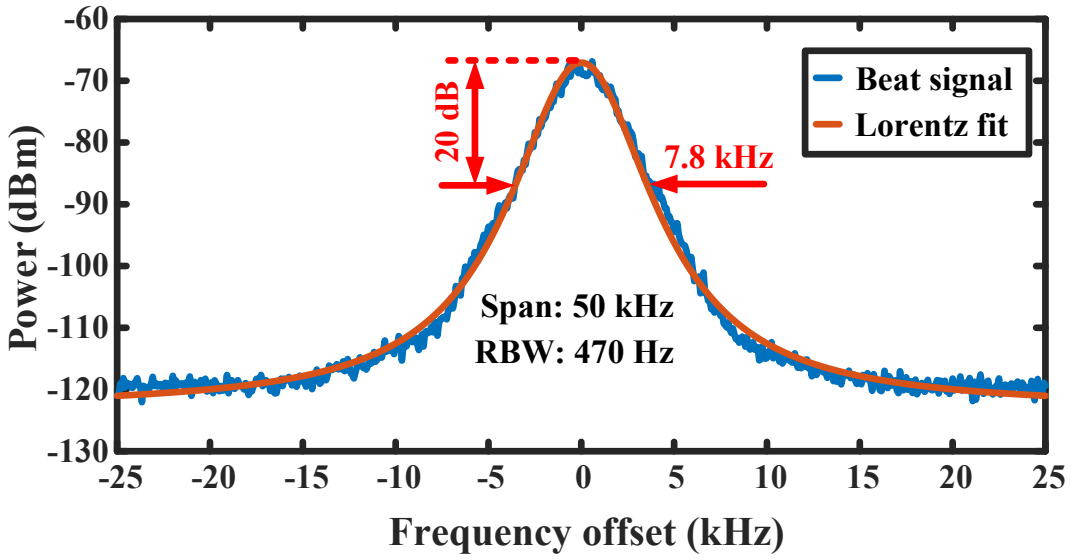

Fig. 3.6 The electrical spectrum at the output of the PD when the fiber ring laser is operating in the single mode. The 20-dB linewidth is 7.8 kHz.

The wavelength tunability of the proposed PT-symmetric fiber ring laser is also evaluated. In this experiment, the center wavelength of the TOBF is manually adjusted from 1530 nm to 1565 nm. As a result, the laser generates a SLM output that covers the entire C-band with a tuning span of 35 nm. Fig. 3.7(a) presents representative optical spectra at different tuning positions, while Fig. 3.7(b) illustrates continuous tuning between 1548 nm and 1552 nm achieved by smoothly adjusting the TOBF. The tuning range can be further extended if the EDFA employed in the cavity provides a broader gain bandwidth. This large tunability, achieved without relying on an ultra-narrowband wavelength-selective filter, highlights a key advantage of utilizing PT symmetry. It greatly simplifies the system design and significantly reduces implementation cost while maintaining stable SLM operation.

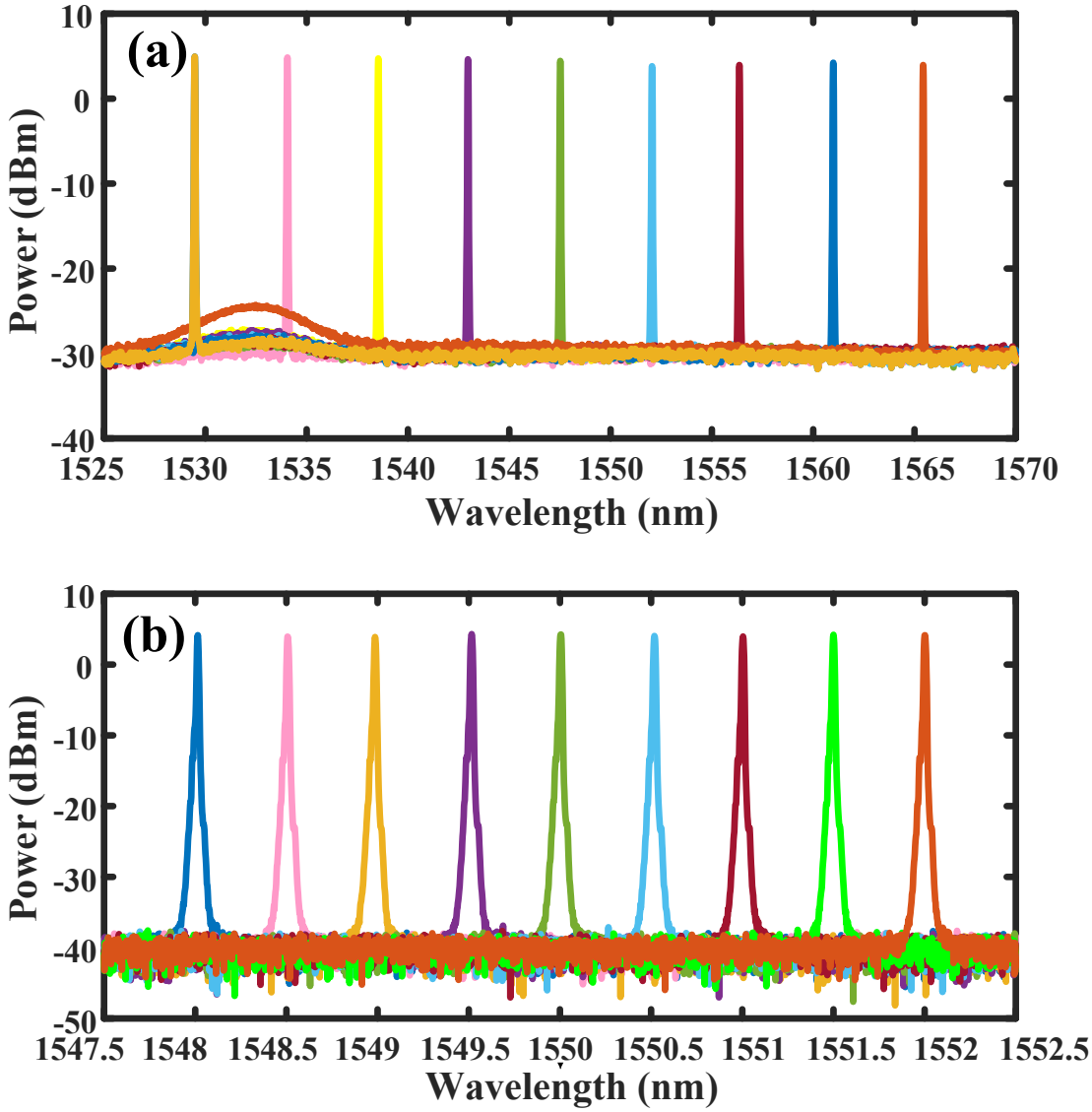

Fig. 3.7 The tuning of the wavelength of the fiber ring laser. (a) Measured wavelength-tunable range covering the entire C-band and (b) continuous wavelength tuning by tuning the TOBF in a 4 nm range.

3.4 Conclusion

We have realized a widely tunable, ultra-narrow-linewidth SLM fiber ring laser in which PT-symmetry assisted mode selection is implemented using one physical loop. The Sagnac loop construct furnishes two equivalent, length-identical loops with controllable gain and loss, while a simple TOBF sets the operating wavelength. The proposed laser provides a

wavelength tunability of 1530–1565 nm, a minimum linewidth of 390 Hz, and 41.9 dB SMSR, demonstrating that PT-symmetry breaking can enforce single-mode operation in long fiber cavities without resorting to ultra-narrow optical filters or complex multi-loop geometries.

CHAPTER 4 PARITY-TIME SYMMETRIC OPTO-ELECTRONIC OSCILLATOR USING A SINGLE PHYSICAL LOOP[2]

4.1 Introduction

OEOs are among the most promising architectures for generating spectrally pure, low-phase-noise microwave signals, owing to the use of long optical fiber delay lines that provide extremely high-quality factors. However, such long cavities inherently lead to densely spaced RF modes with small FSRs, making stable single-mode oscillation challenging. Conventional mode-selection techniques, including high-quality electronic BPFs, dual-loop Vernier configurations, and wavelength-multiplexed schemes, can partially address this issue, but often at the cost of increased system complexity, higher insertion loss, or reduced tunability.

The concept of PT symmetry offers an elegant alternative. By balancing gain and loss in coupled loops, PT symmetry allows a single oscillation mode to be selectively amplified while all others remain neutral. Early PT-symmetric OEO demonstrations were realized using two physically separated loops with identical lengths [32,33,97]. However, such configurations are sensitive to fabrication tolerances and environmental perturbations, as perfect geometrical identity is difficult to maintain. This mismatch degrades stability and limits practical implementation.

[2] This Chapter has been previously published in **Z. Dai**, Z. Fan, P. Li, and J. Yao, "Frequency-tunable parity-time-symmetric optoelectronic oscillator using a polarization-dependent Sagnac loop," *J. Lightw. Technol.*, vol. 38, no. 19, pp. 5327-5332, Oct. 2020.

In this chapter, we present the first demonstration of a PT-symmetric OEO realized in a single physical loop [98]. The key innovation is the use of a polarization-dependent Sagnac loop to form two counter-propagating feedback paths that are inherently identical in length. By introducing controlled gain and loss into these two equivalent loops, PT symmetry and symmetry breaking can be established within a single physical fiber loop. This configuration significantly simplifies the system architecture, improves stability, and enables single-mode microwave oscillation without relying on ultra-narrowband filters.

4.2 Operation principle

Fig. 4.1 illustrates the configuration of the proposed tunable PT-symmetric OEO. A continuous-wave beam from a tunable laser source (TLS) first passes through PC1 before entering the PM. PC1 is adjusted to align the polarization state of the optical carrier with the principal axis of the PM, thereby minimizing polarization-dependent insertion loss. The phase-modulated optical signal propagates through a long length of SMF before reaching a Sagnac loop. The Sagnac loop incorporates a PBS together with PC2 and PC3, and the incident optical signal is split into two paths that propagate along the CW and CCW directions of the Sagnac loop, thereby creating two mutually coupled feedback loops with identical length. By tuning PC2 and PC3, one loop can be adjusted to experience net gain while the other loss, thus matching the PT-symmetric condition. The recombined optical fields from the two paths interfere at an OC and are subsequently filtered by a PS-FBG. The PS-FBG functions as an MPF, utilizing PM–IM conversion to perform coarse frequency selection. The filtered signal is then amplified by an EDFA and converted to the electrical domain by a high-speed PD. The detected microwave signal is further boosted by an EA and

split into two branches: one is sent the PM to close the feedback loop, while the other is monitored by an ESA for performance evaluation.

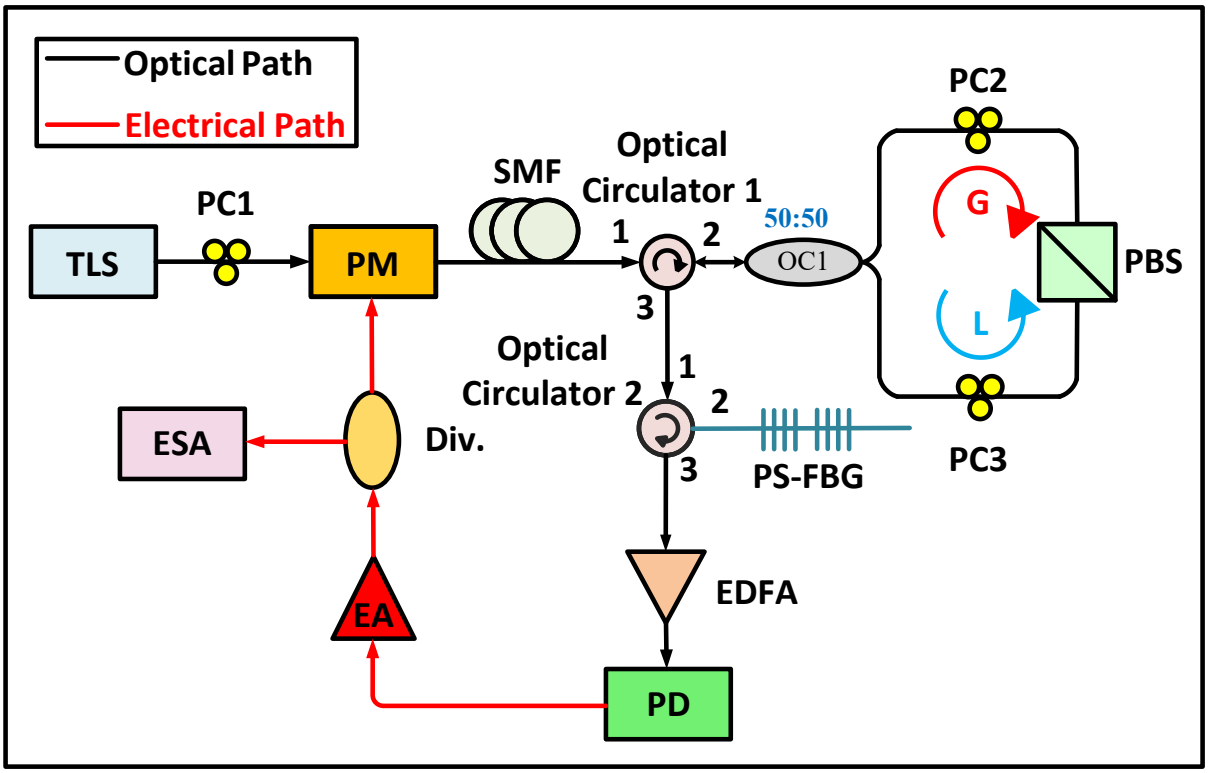

Fig. 4.1 Schematic diagram of the PT-symmetric OEO with a single physical loop. TLS: tunable laser source; PC: polarization controller; PM: phase modulator; SMF: single mode fiber; Cir.: circulator; OC: optical coupler; PBS: polarization beam splitter; PS-FBG: phase-shifted fiber Bragg grating; EDFA: erbium-doped fiber amplifier; PD: photodetector; EA: electrical amplifier; Div.: divider; ESA: electrical spectrum analyzer.

The non-Hermitian Hamiltonian of the proposed PT-symmetric OEO is given by:

$$H = \begin{bmatrix} -i\omega_n + \gamma & i\kappa \\ i\kappa & -i\omega_n - \gamma \end{bmatrix} \tag{4.1}$$

where ω_n is the oscillation frequency determined by the feedback loop round-trip delay, γ represents the gain-loss coefficient introduced by the polarization control in the Sagnac loop, and κ denotes the coupling coefficient. The eigenfrequencies of this non-Hermitian system

are given by

$$\omega_n{}^{(1,2)} = \omega_n \pm \sqrt{\kappa^2 - \gamma^2} \tag{4.2}$$

When $\gamma < \kappa$, the system remains in the unbroken PT-symmetric regime and both eigenmodes are real, leading to mode frequency splitting; when $\gamma = \kappa$, the system reaches EP, illustrating that the frequencies of the eigenmodes coalesce; when $\gamma > \kappa$, the PT symmetry is broken, and one eigenmode undergoes amplification while the other is attenuated. In this broken PT phase, only the amplifying mode satisfies the oscillation condition, thereby enforcing single-mode microwave oscillation.

To rigorously quantify the improvement achieved under PT-symmetric conditions compared with the conventional configuration, we introduce a gain-contrast enhancement factor G, expressed as

$$G = \frac{g_{\text{PT\_max}}}{g_{\text{max}}} = \sqrt{\frac{g_0/g_1 + 1}{g_0/g_1 - 1}} \tag{4.3}$$

As illustrated in Fig. 4.2, a significant enhancement of the gain contrast is observed, which facilitates more efficient selection of the primary mode and ensures stable single-mode oscillation.

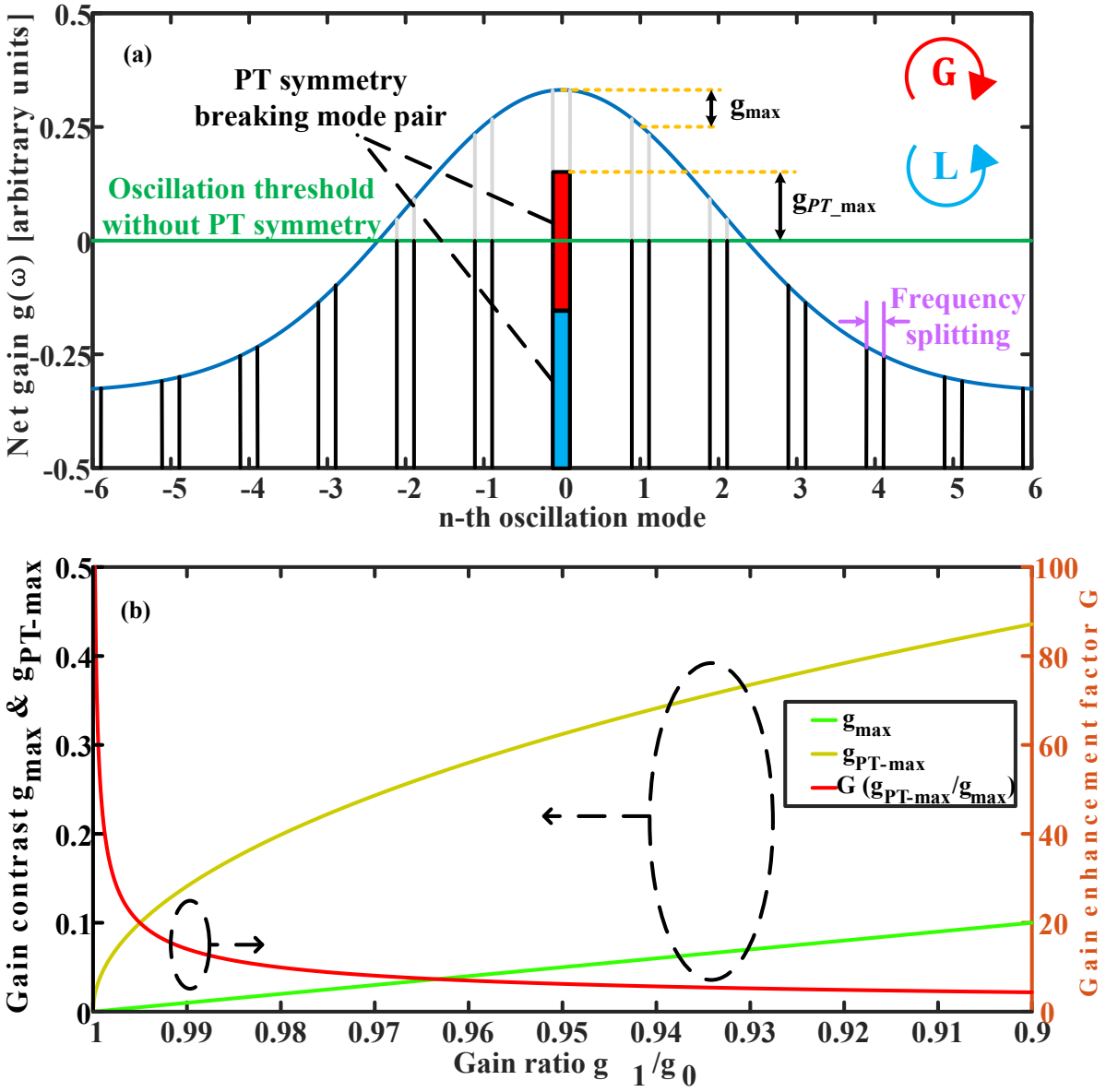

Fig. 4.2 Mode selection due to PT symmetry in a PT-symmetric OEO. (a) The mechanism of mode selection under PT symmetry broken condition. (b) The gain contrast enhancement when using PT-symmetric breaking.

4.3 Experimental results

The experimental performance of the proposed PT-symmetric OEO is evaluated using the setup illustrated in Fig. 4.1. A continuous-wave optical carrier generated by a TLS (Yokogawa AQ2201) is injected into a PM (JDSU) with a 3-dB bandwidth of 20 GHz. Optical amplification is provided by an EDFA (FiberPrime EDFA-C-14-S-FA), which

provides up to 30 dB gain with a saturated output power of 16 dBm. The modulated light is detected by a high-speed PD (Optilab LR-12-A-M) having a 3-dB bandwidth of 12 GHz and a responsivity of 0.85 A/W at 1550 nm. Two cascaded EAs (MultiLink MTC5515-751) are employed to ensure sufficient loop gain. The generated microwave signal is analyzed by an ESA (Agilent E4448A), while its phase noise performance is characterized with a signal analyzer (Agilent E5052B).

The measured electrical spectra of the oscillation are shown in Fig. 4.3(a)–(f). When the PT-symmetric condition is not satisfied, multimode oscillation is observed, as illustrated in Fig. 4.3(a). By carefully adjusting PC2 and PC3, the gain and loss in the two counter-propagating paths are balanced, fulfilling the PT-symmetry requirement. When the gain/loss coefficient exceeds the coupling coefficient, the system enters the PT-broken region, and stable single-mode oscillation is established. Under this condition, a microwave signal at 6 GHz is obtained, as displayed in Fig. 4.3(b)–(d) with different spans and resolution bandwidths (RBWs). The side modes are strongly suppressed, and an SMSR of 47 dB is measured, as shown in Fig. 4.3(d). Figure 4.3(f) further demonstrates the frequency-tuning capability of the system, which is continuously adjustable across a range of 2–12 GHz.

As described in the operation principle section, coarse frequency selection is provided by the MPF, realized through the PS-FBG. The notch of the PS-FBG is translated into the passband of the MPF by PM-IM conversion. Frequency tuning is achieved by adjusting the TLS wavelength, which shifts the MPF's central frequency. The frequency response of the MBF is characterized with a vector network analyzer (VNA, Agilent E8364A), as shown in Figs. 4.4(a) and (b). As can be seen in Fig. 4.4(b), the 3-dB bandwidth of the MPF is measured to

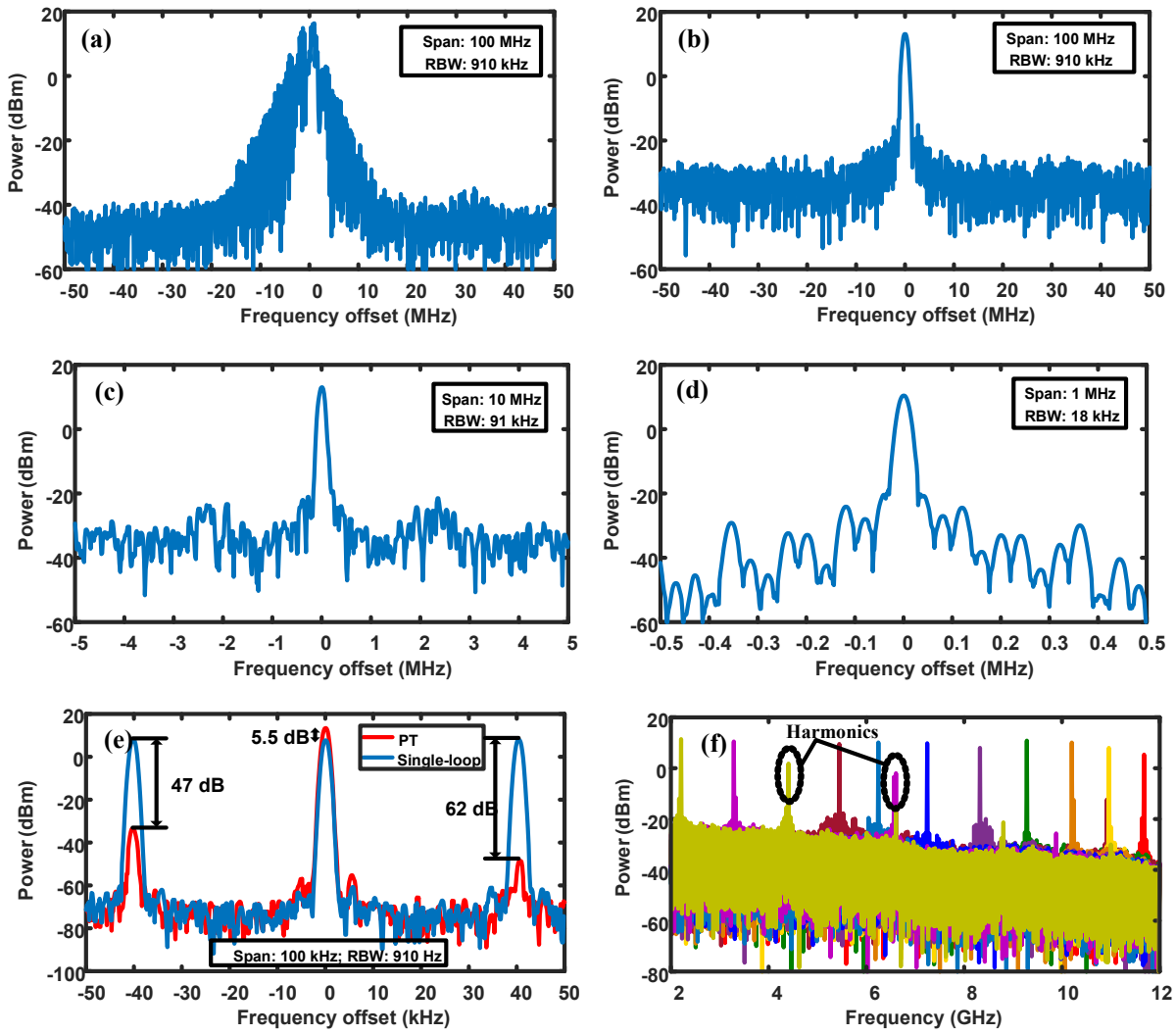

Fig. 4.3 The electrical spectra of the microwave signals generated by the PT-symmetric OEO with a loop length of 5 km. The spectra are measured at a central frequency of 6 GHz by an electrical spectrum analyzer. (a) Multi-mode oscillation measured with a span of 100 MHz and a resolution bandwidth (RBW) of 910 kHz; (b) Single-mode oscillation measured with a span of 100 MHz and an RBW of 910 kHz; (c) Single-mode oscillation measured with a span of 10 MHz and an RBW of 91 kHz; (d) Single-mode oscillation measured with a span of 1 MHz and an RBW of 18 kHz. (e) Single-mode oscillation measured with a span of 100 kHz and an RBW of 910 Hz. (f) Frequency tunability of the proposed PT-symmetric OEO with a tuning range from 2 to 12 GHz.

be approximately 260 MHz. This bandwidth corresponds to more than 6000 potential oscillation modes within the passband, highlighting that stable single-mode oscillation is

maintained as a direct consequence of PT-symmetry breaking.

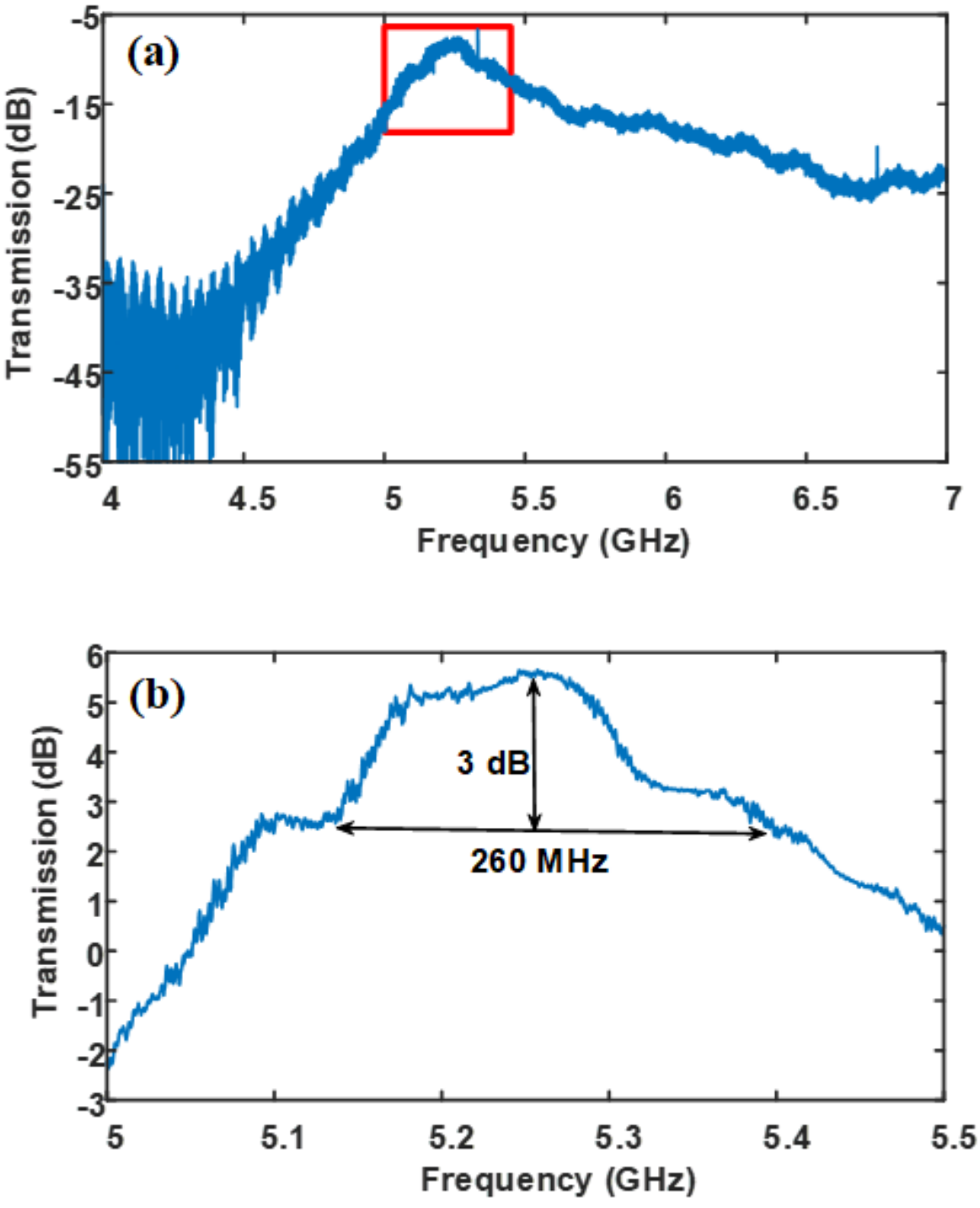

Fig. 4.4 (a) Measured transmission spectra of the MPBF and (b) Its zoom-in view.

In the experiment, the maximum realized frequency-tuning range is 10 GHz. This range is

primarily constrained by the bandwidth of the PM, PD, and EAs used in the loop. Employing devices with broader bandwidths can further expand the achievable tuning range. The phase-noise characteristics are also evaluated using a microwave signal analyzer (Agilent E5052B) in conjunction with a down-converter (Agilent E5053A). As shown in Fig. 4.5, the measured phase noise reaches −128 dBc/Hz at a 10-kHz offset. Additional peaks emerge beginning at approximately 40 kHz, corresponding to the FSR of the 5-km OEO loop, which is 40 kHz. Phase noise can be further reduced by extending the loop length to increase the quality of the loop. Since PT symmetry intrinsically ensures single-mode oscillation, no additional narrowband filtering is required, making the overall system design simpler.

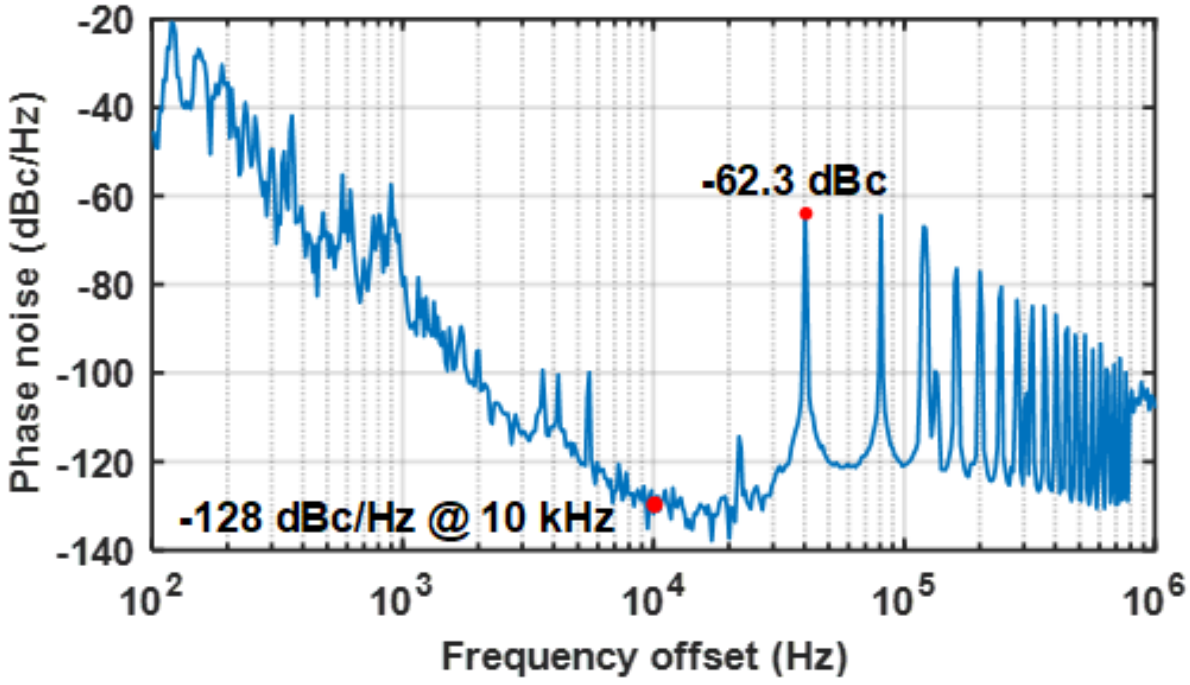

Fig. 4.5 Phase noise measurement at the frequency of 6 GHz. The phase noise level is −128 dBc/Hz at a frequency offset of 10 kHz.

4.4 Conclusion

This chapter has demonstrated a single physical loop PT-symmetric OEO, implemented using

a polarization-dependent Sagnac loop. By creating two equivalent counter-propagating feedback loops within a single fiber ring, the architecture ensures intrinsic length identity and avoids mismatch issues that plague dual-loop configurations. Theoretical analysis and experiments confirm that PT symmetry breaking provide an effective mechanism for mode selection.

Experimentally, the OEO achieved single-mode oscillation tunable from 2 to 12 GHz, with an SMSR of 47 dB and a phase noise of –128 dBc/Hz at 10 kHz offset. These results highlight that PT symmetry can eliminate the need for ultra-narrowband filters in long-loop OEOs, offering a compact, stable, and high-performance platform for microwave signal generation.

This work establishes a new design principle for OEOs, demonstrating that PT symmetry can be realized in the simplest possible geometry—a single physical loop. The concepts developed here form the foundation for the next chapter, where PT symmetry will be combined with rational dual-loop architectures and the Vernier effect to further improve sidemode suppression and operational stability.

CHAPTER 5 A DUAL-LOOP PARITY-TIME SYMMETRIC LASER WITH A RATIONAL LOOP LENGTH RATIO[3]

5.1 Introduction

PT-symmetric lasers exploit balanced gain and loss in coupled resonators to enable effective single-mode operation. Conventional implementations typically rely on two resonant loops or cavities of identical length to ensure matched resonances frequencies. However, achieving strict length identity is difficult in practice, particularly when using discrete fiber-based components, which leads to degraded performance and reduced mode selectivity.

In parallel, the Vernier effect has been widely adopted in dual-loop fiber lasers to enhance mode selection. By employing two loops of different lengths with a rational length ratio, the effective FSR becomes much larger than that of either individual loop, thereby reducing the density of competing modes. Here, the term "rational length ratio" refers to the condition where the lengths of the two loops satisfy a rational relationship, since compared to arbitrary length ratios, rational ratios provide predictable and controllable mode alignment. Yet, Vernier-only designs cannot guarantee absolute single-mode operation when multiple resonances fall within the gain bandwidth.

In this chapter, we propose and experimentally demonstrate a dual-loop PT-symmetric fiber laser with a rational loop-length ratio [99]. The key idea is that when the lengths of the two coupled loops follow a rational ratio, a subset of resonant modes in the long loop coincide in

[3] This Chapter has been previously published in **Z. Dai**, Z. Wang, and J. Yao, "A dual-loop parity-time symmetric system with a rational loop length ratio," *Opt. Lett.*, vol. 48, no. 1, pp. 143-146, Jan. 2023.

frequency with resonant modes of the short loop. PT symmetry can then be established selectively at these matched resonances. The resulting architecture combines PT-symmetry assisted mode selection with the Vernier effect, drastically improving the SMSR while maintaining narrow linewidth performance.

5.2 Operation principle

The demonstration of the proposed dual-loop PT-symmetric SLM fiber ring laser is shown in Fig. 5.1. The long loop, hereafter referred to as the gain loop, incorporates an EDFA that provides optical gain, a 4.8-km segment of SMF to extend the cavity length, PC1 for state-of-polarization adjustment, OC1 to facilitate power splitting, and an optical circulator combined with a uniform fiber Bragg grating (UFBG). In parallel, the short loop, defined as the loss loop, contains an optical isolator and a variable attenuator to introduce controllable loss. Both loops share the same EDFA and UFBG elements, ensuring compactness and mutual interaction between the two cavities. The laser output is extracted from the gain loop via OC2. The power coupling between these two loops is realized at the UFBG. Specifically, the forward-propagating light in the short loop couples with the partially reflected signal from the long loop, establishing mutual coupling between the gain and loss loops. The effective coupling coefficient is not fixed; instead, it can be tuned by rotating PC1 in the long loop, which alters the polarization state and thereby changes the overlap efficiency of the reflected and transmitted fields at the UFBG. In addition to serving as the coupling interface, the UFBG simultaneously functions as an optical BPF, defining the operating wavelength of the laser and suppressing unwanted modes outside its reflection window.

For a dual-loop resonant configuration, the longitudinal modes of the dual cavity are determined by the resonance conditions of both loops. Let the round-trip time of the two loops be denoted as τ_1 and τ_2 (τ_1 for the long loop and τ_2 for the short loop). The oscillation

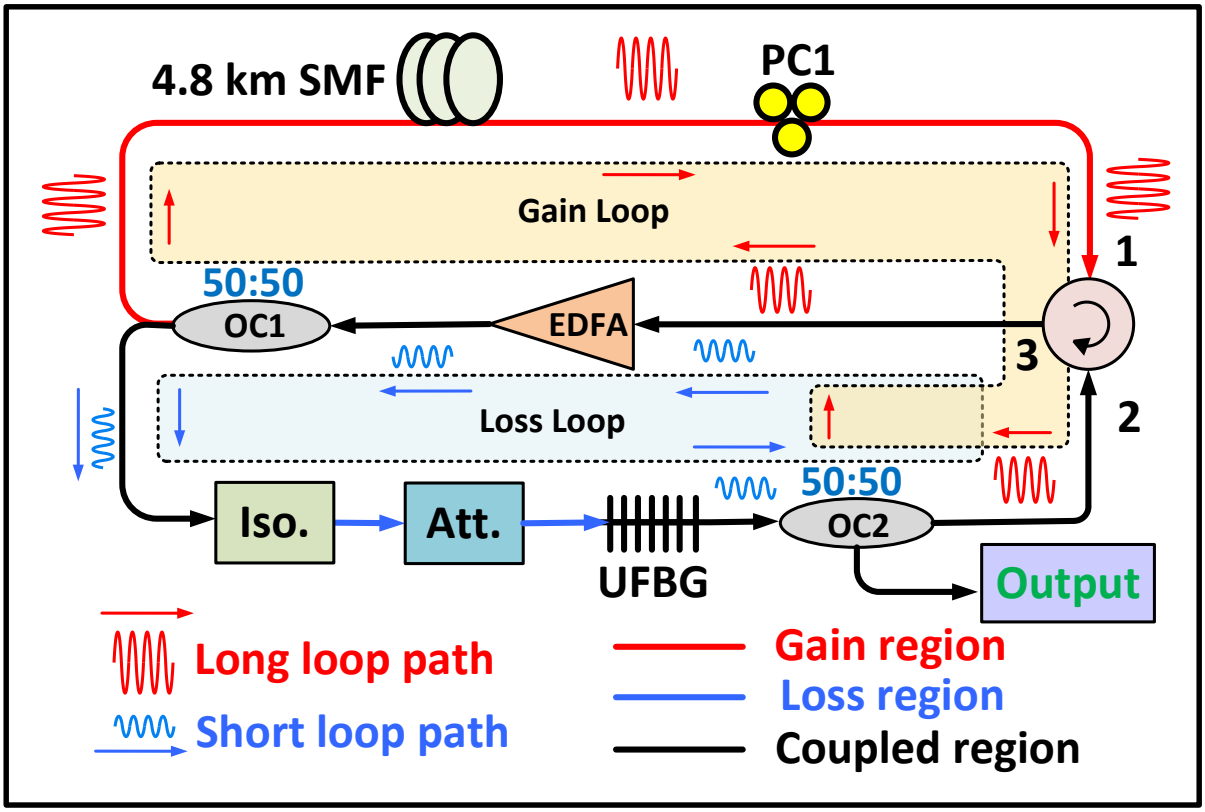

Fig. 5.1 Schematic diagram of a PT-symmetric fiber ring laser with non-identical loop lengths. SMF: single-mode fiber; PC: polarization controller; OC: optical coupler; EDFA: erbium-doped fiber amplifier; Iso.: isolator; Att.: attenuator; UFBG: uniform fiber Bragg grating.

frequencies of the composite system must simultaneously satisfy the resonance requirements of both loops, which can be expressed as

$$f = \frac{N}{\tau_1} = \frac{M}{\tau_2} \ (N > M) \tag{5.1}$$

where N and M are integers represent the N-th and M-th modes propagating in the long and short loops. Since $\tau_1 = N\tau_2/M$, the loop length ratio is calculated to be N/M. Thus, the

effective mode spacing or FSR of the dual-loop configuration is given by $\Delta f = N/[\gcd(N,M)\tau_1]$, where $\gcd(N,M)$ is the greatest common divisor of N and M. The enlargement of the effective FSR is dictated by the length of the shorter loop, a phenomenon commonly referred to as the Vernier effect.

In a conventional PT-symmetric system, the length of two coupled loops needs to be precisely identical to ensure the same intrinsic resonant frequencies, which imposes additional challenges on successful implementation. However, if the loop lengths are not identical, but have a rational loop length ratio, some of the resonant modes in the two loops can still be located at the same frequencies, which meets one of the necessary conditions for PT symmetry. Assume that two resonators are coupled and the loop length ratio becomes N/M, the resonant modes located at the same frequencies will be mutually coupled, and the differential coupled mode equations are expressed as:

$$\frac{d}{dt}\begin{bmatrix}A_p\\B_q\end{bmatrix} = \begin{bmatrix}-i\omega_p + \gamma_{A_p} & i\kappa\cos(\theta)\\ i\kappa\cos(\theta) & -i\omega_q + \gamma_{B_q}\end{bmatrix}\begin{bmatrix}A_p\\B_q\end{bmatrix} \tag{5.2}$$

where A_p and B_q are the amplitudes of p-th mode propagating in the long loop and q-th mode propagating in the short loop having the same frequency, which means $\omega_c = \omega_p = \omega_q = 2\pi p/\tau_1 = 2\pi p/\tau_2$. p and q must satisfy the relationship of $p = n \cdot N/\gcd(N,M)$ and $q = n \cdot M/\gcd(N,M)$, where n is a positive integer. κ represents the coupling coefficient of the UFBG, and θ denotes the angle between the linear polarization stats of these two loops. To satisfy PT-symmetric condition, the gain of the pth mode and the loss of the qth mode are tuned to be $\gamma = \gamma_{A_p} = -\gamma_{B_q}$. Thus, the eigenvalue of the proposed system is given by

$$\omega_c{}^{(1,2)} = \omega_c \pm \sqrt{\kappa\cos(\theta)^2 - \gamma^2} \tag{5.3}$$

When the round-trip time of the long loop is much greater than that of the short loop ($\tau_1 \gg \tau_2$), a single resonance of the short loop encompasses a cluster of closely spaced resonances from the long loop, as illustrated in Fig. 5.2. Under such conditions, the resonance in the short loop becomes simultaneously coupled to multiple neighboring resonances of the long loop. Since these long-loop modes lie very close in frequency, the coupling strength between the short-loop mode and its adjacent long-loop modes can be approximated as nearly identical.

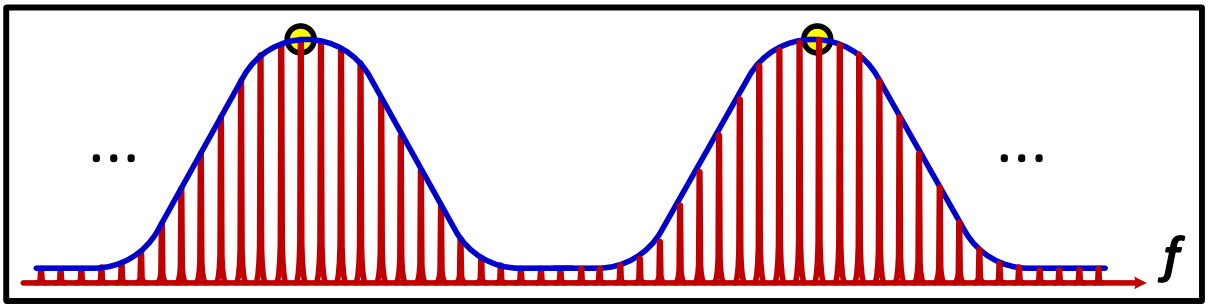

Fig. 5.2 Relationship between the resonant modes of the long (red) and the short (blue) loops.

Because of the Vernier effect, however, not all coupled modes contribute equally. The long-loop mode that aligns most closely in frequency with the short-loop resonance experiences the strongest constructive interaction and thus attains the largest effective gain. As a result, this specific pair of modes will be the first to undergo PT-symmetry breaking. Consequently, the overall mode spacing of the coupled system is governed primarily by the short loop, and the effective free spectral range is given by

$$\Delta f = \frac{2\pi}{\tau_2} \tag{5.4}$$

As indicated by Eq. (5.3), once $\gamma > \kappa\cos(\theta)$, the system transitions into the broken PT-symmetric region, resulting in one mode experiencing amplification and the other

experiencing attenuation, both centered around the frequency ω_c, while other modes remain neutral. The preferential growth of the amplifying mode enables effective mode selection, thereby supporting SLM lasing at ω_c.

In contrast to PT-symmetric laser configurations employing two loops of identical length, the use of an asymmetric dual-loop architecture significantly reduces the number of resonant modes within the cavity. This spectral sparsity simplifies the process of mode selection, thereby facilitating stable single-mode operation while preserving a narrow linewidth at the lasing wavelength. Moreover, the introduction of loop asymmetry contributes to an improvement in the SMSR, further enhancing the spectral purity of the laser output.

5.3 Experimental results

The experimental evaluation of the asymmetric dual-loop PT-symmetric fiber ring laser is carried out using the setup shown in Fig. 5.1. Mutual coupling between the two loops is realized by a UFBG designed to provide partial reflection. The measured transmission and reflection spectra of the UFBG, obtained using an optical vector analyzer (OVA, LUNA 5000), are presented in Fig. 5.3(a). The UFBG has a Bragg wavelength of 1555.4 nm, a bandwidth of 0.08 nm, and a reflection coefficient of 75%. By setting the cavity length ratio of the two loops to 200/3, the effective FSR of the system is 2.8 MHz. When both loops are closed and the gain and loss are balanced, the laser satisfies the PT-symmetric condition. Once the gain coefficient exceeds the coupling coefficient, the system enters the PT-broken phase and SLM lasing occurs. Fig. 5.3(b) shows the optical spectrum measured by an OSA (ANDO AQ6317B), revealing stable lasing at 1555.88 nm. The stability of the system is

measure and the results are shown in Fig. 5.4(a) and (b). As can be seen, the wavelength fluctuations and power fluctuations within one hour are within 3 pm and 0.12 dB, respectively.

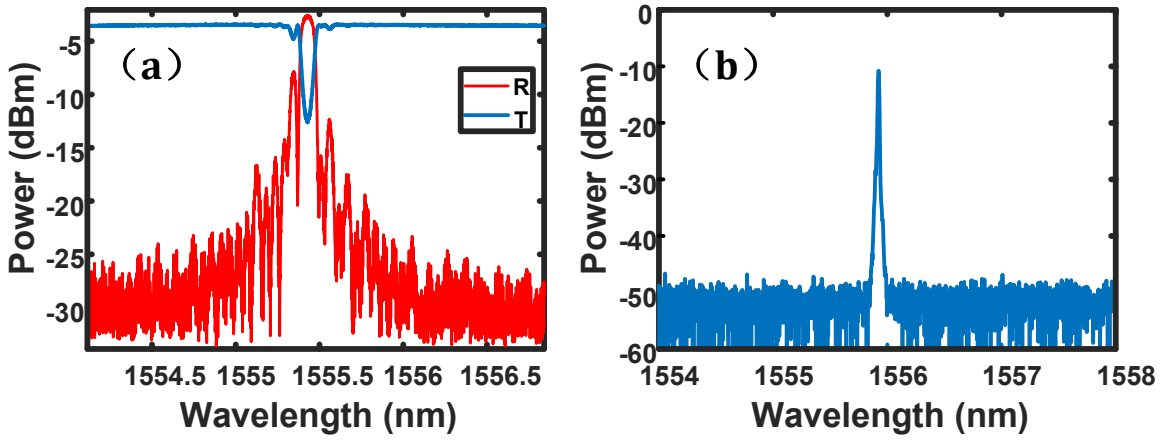

Fig. 5.3 (a) Transmission (blue) and reflection (red) spectra of the UFBG. (b) Measured optical spectrum of the generated light wave by using the UFBG in the dual-ring fiber ring laser.

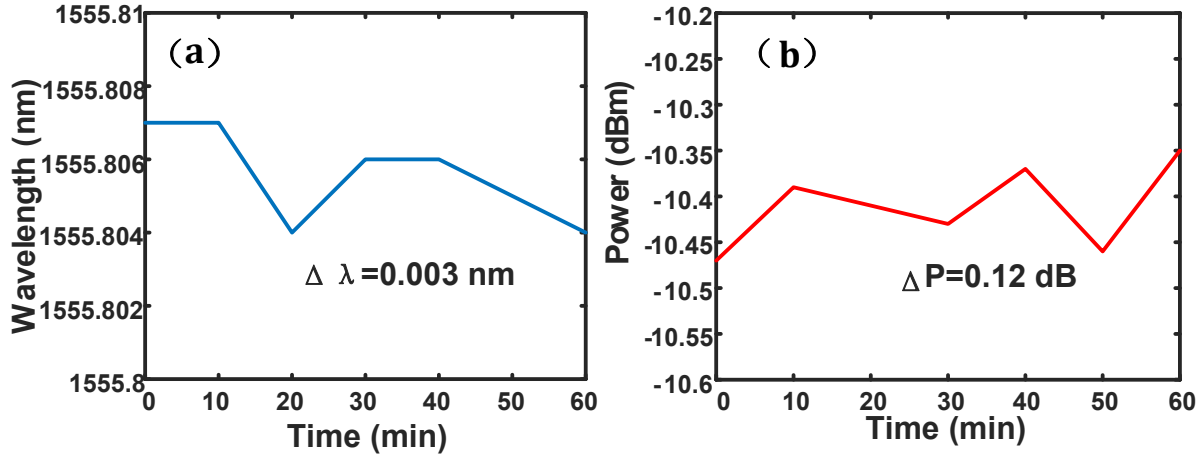

Fig. 5.4 (a) The wavelength fluctuations and (b) the power fluctuations of the dual-loop PT-symmetric fiber ring laser in an hour.

Because the effective FSR of 2.8 MHz is still much smaller than the 0.08-nm bandwidth of the UFBG, multimode operation occurs in the absence of PT symmetry. The limited resolution of the OSA also makes it insufficient to directly verify single-mode lasing. To

confirm single-mode operation enabled by PT symmetry, a frequency-shifted self-heterodyne measurement system is implemented, as illustrated in Fig. 5.5. The setup consists of a PM (JDSU), a 10-km SMF delay line, two OCs (OC3 and OC4), and a high-speed PD (Optilab LR-12-A-M). A 1-GHz microwave signal is applied to the PM to shift the frequency of the beat note away from DC, allowing accurate linewidth characterization.

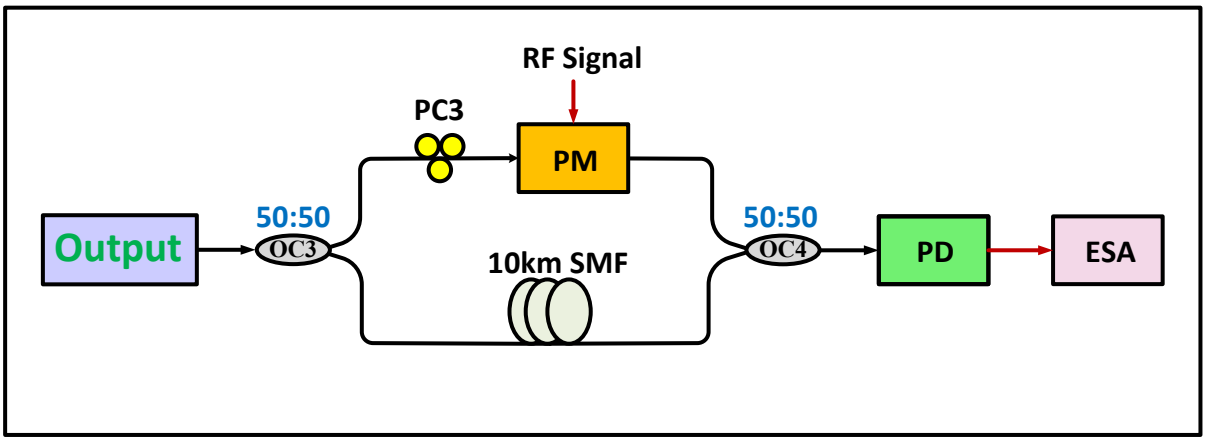

Fig. 5.5 Schematic diagram of the frequency-shifted self-heterodyne system. PM: phase modulator, PD: photodetector; ESA: electrical spectrum analyzer.

To evaluate the role of each loop individually, the short loop is first opened by disconnecting its isolator. The configuration then reduces to a single-loop fiber ring laser with a long cavity length of 4.86 km, corresponding to an FSR of 42 kHz. Since this spacing is far smaller than the UFBG bandwidth, the laser operates in multimode. Fig. 5.6(a) and (b) show the corresponding RF beat signals measured by an ESA (Agilent E4448A). A zoomed-in view in Fig. 5.6(b) confirms an FSR of approximately 42 kHz, with no evidence of single-mode lasing. When the long loop is disconnected by removing port 1 of the optical circulator, the short loop operates independently with a cavity length of 73 m and an FSR of 2.8 MHz. Again, because the FSR is narrower than the UFBG bandwidth, multimode oscillation

persists. Fig. 5.6(c) and (d) demonstrate the measured RF beat spectra, showing no indication of SLM lasing. These results confirm that single-mode operation cannot be achieved by adjusting the loop length alone.

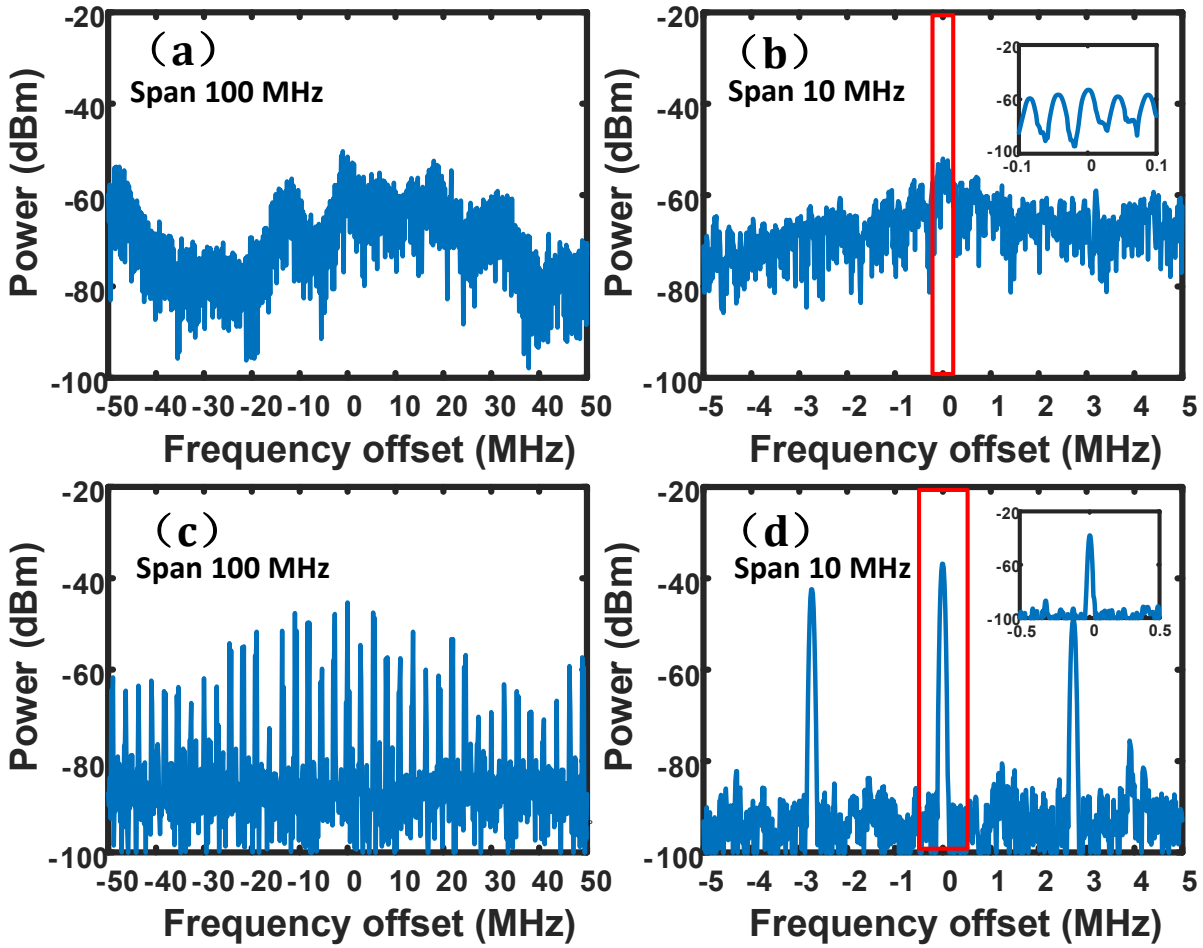

Fig. 5.6 Electrical spectra of the fiber ring laser with only the long loop closed measured at a span of (a)100 MHz and (b) 10 MHz. The electrical spectra of the fiber ring laser with only the short loop closed measured at a span of (c) 100 MHz and (d) 10 MHz.

When both loops are closed and the gain in each loop is set higher than the loss, the system operates as a dual-gain fiber ring laser. Due to the Vernier effect, the effective FSR becomes 2.8 MHz, equal to that of the short loop. The RF beat signals measured under this condition are shown in Fig. 5.7(a) and (b). The spectra clearly indicate multimode operation, although

the number of resonant modes is significantly reduced compared to the long-loop case. A zoom-in view of the fundamental resonance in Fig. 5.7(b) reveals two weak sidemodes, corresponding to residual long-loop resonances falling within the linewidth of the short-loop resonance. This demonstrates that although the Vernier effect reduces mode density, multimode operation still occurs when PT symmetry is not applied.

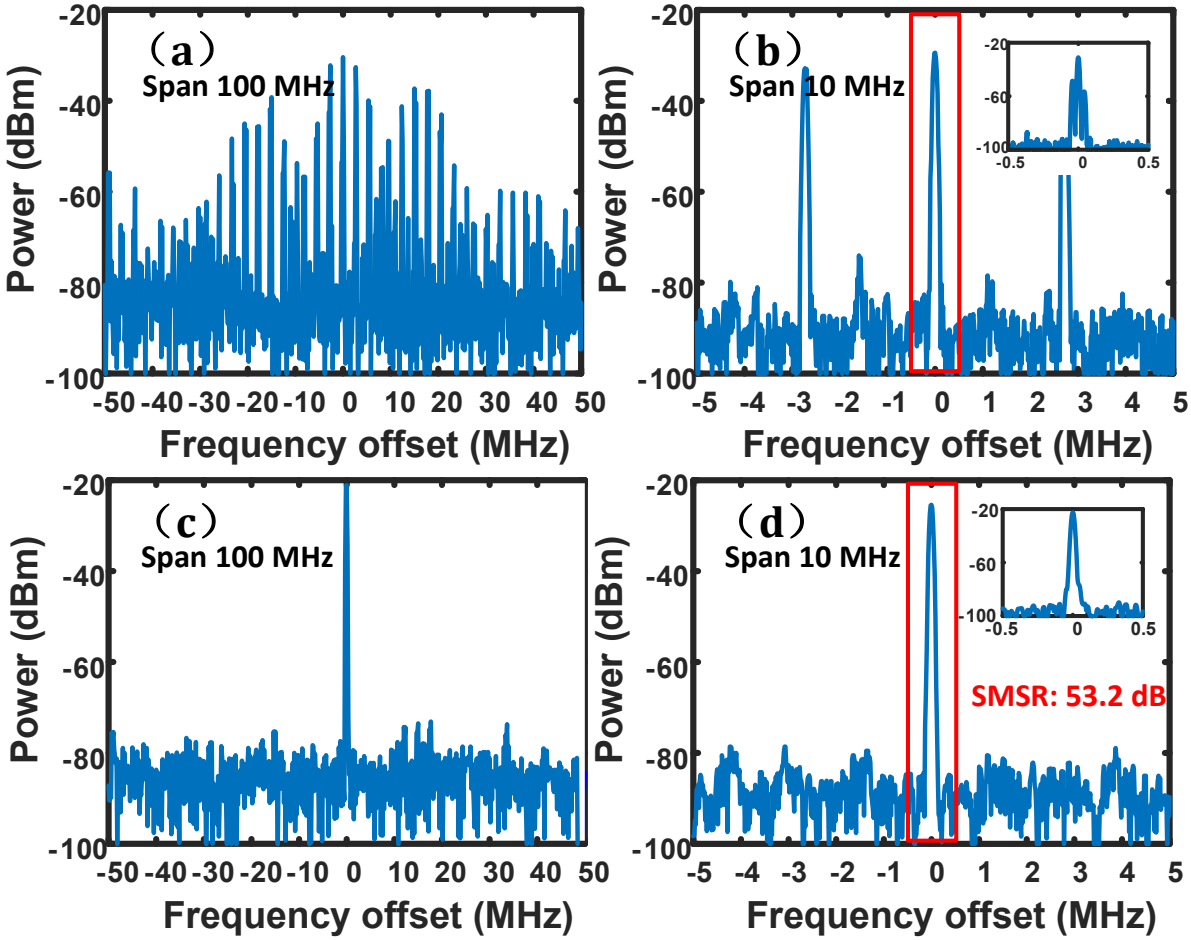

Fig. 5.7 Electrical spectra of the dual-loop fiber ring laser with each of the loops having a gain that is greater than the loss, measured at a span of (a) 100 MHz and (b) 10 MHz. The electrical spectra of the dual-loop fiber ring laser when the broken PT symmetry condition is satisfied, measured at a span of (c) 100 MHz and (d) 10 MHz.

SLM lasing is realized only when PT symmetry is introduced. By adjusting the PCs to

balance the gain and loss of the two loops, and ensuring that the gain/loss coefficient exceeds the coupling coefficient, the system enters the PT-broken region. The corresponding electrical spectra are shown in Fig. 5.7(c) and (d). A microwave signal at 1 GHz is observed with other modes strongly suppressed, confirming SLM operation. The SMSR reaches 53.2 dB, a substantial improvement attributed to the dual-loop architecture. Notably, the sidemodes observed in Fig. 5.7(b) are no longer present in Fig. 5.7(d), illustrating that PT symmetry further enhances mode selection.

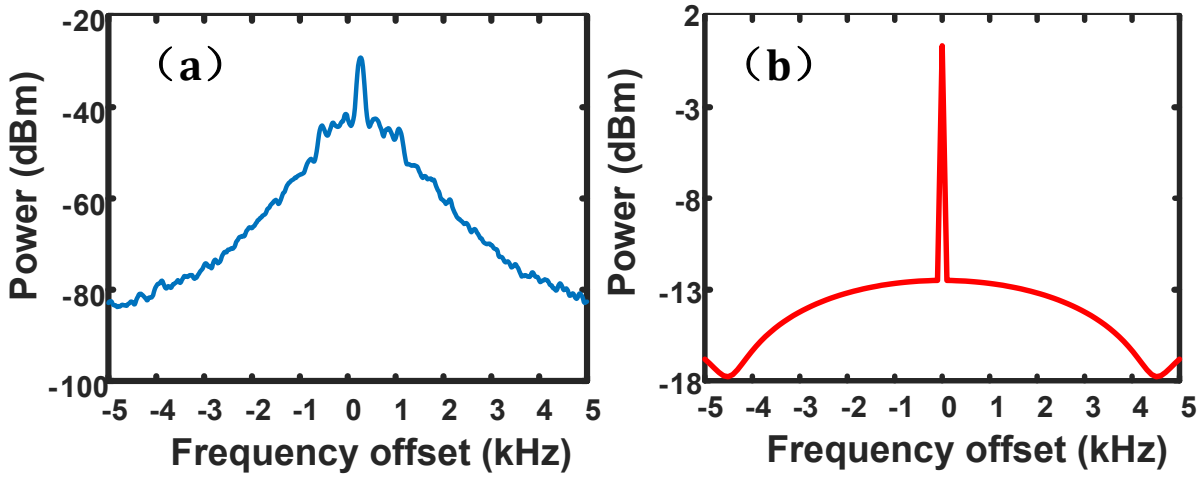

Fig. 5.8 (a) Electrical spectrum at the output of the frequency-shifted self-heterodyne system when the fiber ring laser is operating in single longitudinal mode. (b) Simulated power spectrum of the self-heterodyne signal.

In addition, the extended cavity length ensures linewidth narrowing according to the Schawlow–Townes relation. This effect is verified experimentally using the frequency-shifted self-heterodyne system. Fig. 5.8(a) shows the measured electrical spectrum, while Fig. 5.8(b) presents a simulated power spectrum of the self-heterodyne signal based on the analysis in [100]. A comparison of the two spectra confirms that the 3-dB linewidth of the proposed dual-loop PT-symmetric fiber ring laser is at the sub-kHz level. It should be noted, however,

that the 10-km delay fiber used in the self-heterodyne setup is not long enough to completely destroy the coherence between the two arms. As a result, residual interference broadens the measured spectrum, meaning the experimentally determined linewidth is narrower than the actual value. For a fully accurate measurement, a delay fiber of several thousand kilometers would be required.

5.4 Conclusion

This chapter has demonstrated a dual-loop PT-symmetric fiber laser with a rational loop-length ratio, experimentally realized using coupled fiber loops of 4.8 km and 73 m. By leveraging the Vernier effect and PT symmetry simultaneously, the system achieves SLM lasing at 1555.88 nm with an SMSR of 53.2 dB and a sub-kHz linewidth.

Compared with the single-loop PT-symmetric laser presented in Chapter 3, this design provides stronger sidemode suppression and improved mode stability by combining PT symmetry broken assisted mode selection with Vernier effect enhanced resonance sparsity. The approach introduces a general design principle for PT-symmetric lasers with non-identical loops, offering a flexible framework for high-performance laser architectures.

CHAPTER 6 A DUAL-LOOP PARITY-TIME SYMMETRIC OPTOELECTRONIC OSCILLATOR WITH A RATIONAL LOOP LENGTH RATIO[4]

6.1 Introduction

OEOs provide a powerful means for generating spectrally pure and tunable microwave signals by exploiting the long coherence time of photons in optical fiber delay lines. However, long cavities inevitably lead to dense oscillation spectra with closely spaced longitudinal modes, making single-mode oscillation a central challenge. Dual-loop OEOs employing the Vernier effect have been widely investigated to enlarge the effective FSR, thereby reducing the number of competing modes. While this method improves mode selection, multimode oscillations often persist when the effective FSR is still smaller than the passband of the filter.

PT symmetry introduces an additional intrinsic mode-selection mechanism, whereby balanced gain and loss between coupled loops enforce single-mode oscillation without the need for extremely narrow RF filters. Earlier PT-OEOs based on identical dual loops or single-loop with Sagnac loop configurations successfully demonstrated single-mode selection. Nevertheless, identical dual loops are difficult to realize stably with discrete components, and Sagnac-loop based designs, though compact, lack the probability of further enhancement of the SMSR.

[4] This Chapter has been previously published in **Z. Dai** and J. Yao, "A frequency-tunable parity-time symmetric optoelectronic oscillator with two coupled loops having a rational loop length ratio," *J. Lightw. Technol.*, vol. 42, no. 24, pp. 8577-8581, Dec. 2024.

In this chapter, we propose and experimentally demonstrate a dual-loop PT-symmetric OEO with a rational loop-length ratio [101]. By combining the Vernier effect with PT symmetry, this architecture achieves stable frequency-tunable single-mode oscillation with improved SMSR and enhanced stability.

6.2 Operation principle

The schematic diagram of the dual-loop PT-symmetric OEO with a rational loop-length ratio is shown in Fig. 6.1. A continuous-wave optical carrier emitted by a TLS is adjusted by PC1 to align with the principal axis of the PM, thereby minimizing polarization-dependent loss. The modulated optical signal passes through a PS-FBG, which serves as an MPF by PM–IM conversion for coarse mode selection. The reflected component from the PS-FBG is thern launched into a PBS through PC2. By adjusting PC2, the optical power ratio at the two output ports of the PBS can be tailored such that the stronger optical signal propagates through the long path, consisting of 4.8 km of SMF, while the weaker optical signal propagates through the short path of 240 m SMF. PC3 is incorporated into the long loop to allow fine adjustment of the optical power in that path, enabling precise control of the gain/loss balance. The two optical signals, after experiencing different delays, are recombined at a polarization beam combiner (PBC), amplified by an EDFA, and then converted into the electrical domain by a high-speed PD, producing a microwave signal. This electrical signal is further amplified by an EA and fed back to the PM, thus implementing the OEO feedback loop.

For frequency tuning, an MPF implemented by the TLS, the PM, the PS-FBG, and the PD, is employed to provide coarse mode selection with its center frequency controlled by tuning the

wavelength of the TLS. It is important to emphasize that adopting a PBS and PBC for power splitting and recombination, rather than conventional optical couplers, effectively suppresses

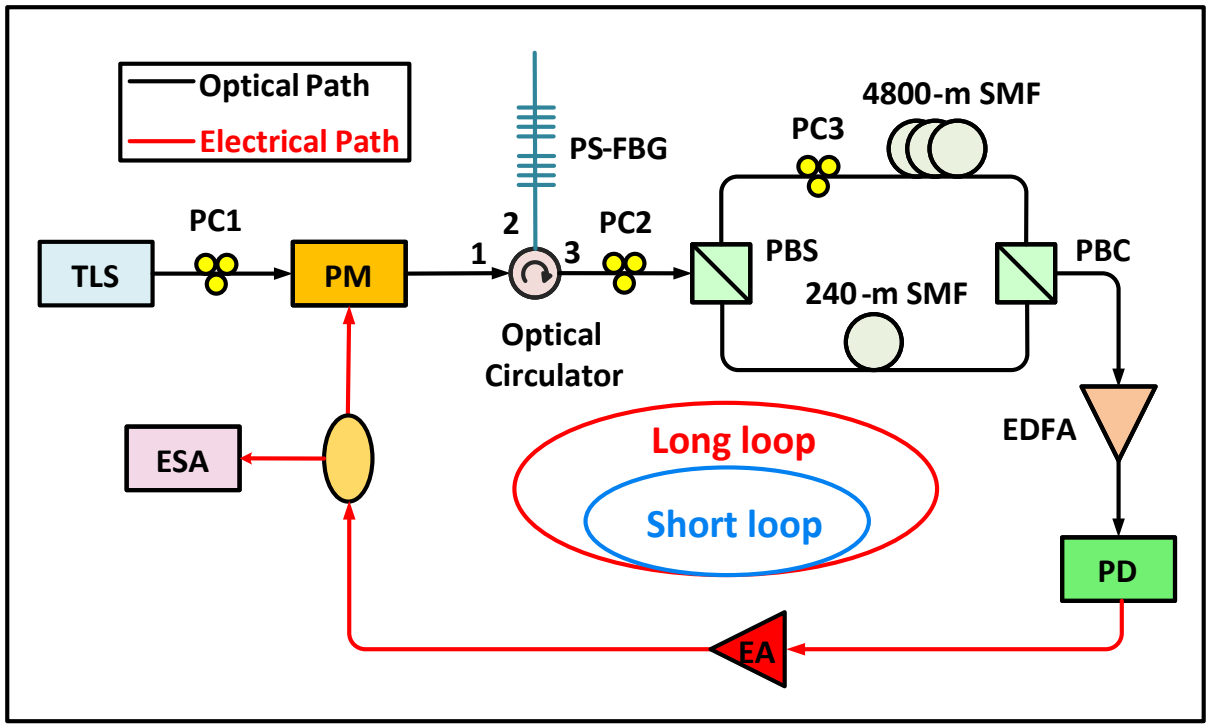

Fig. 6.1 Schematic diagram of the dual-loop PT-symmetric OEO with non-identical loop lengths. TLS: Tunable laser source; PC: Polarization controller; PM: Phase modulator; PS-FBG: Phase-shifted fiber Bragg grating; PBS: Polarization beam splitter; SMF: Single-mode fiber; PBC: Polarization beam combiner; EDFA: Erbium-doped fiber amplifier; PD: Photodetector; EA: Electrical amplifier; Div.: Divider; ESA: Electrical spectrum analyzer.

unwanted interference effects. This design enhances the operational stability of the OEO, preventing the degradation in performance that typically arises from optical interference.

Similar to the principle analysis in Character 5, when the length of the long loop is much longer than that of the short loop ($\tau_1 \gg \tau_2$), the effective FSR is determined by the short loop ($\Delta\omega = 2\pi/\tau_2$). The pairs of modes in the dual-loop located at the same frequencies are

mutually coupled, while other modes are suppressed by the Vernier effect.

The open-loop gain of the proposed dual-loop OEO is determined by combining the frequency responses of both the optical and electrical domain, and can be expressed as

$$g(\omega) = g_o(\omega) g_e(\omega) \tag{6.1}$$

where g_o represents the microwave net gain contributed by the optical components, while g_e denotes the gain provided by the electrical components. In the proposed dual-loop OEO, the overall optical frequency response is composed of two main factors: the transfer function of the MPF [102] and the dispersion-induced power penalty [103]. This combined optical response can be expressed as

$$g_o(\omega) = G_0 A J_1\left(\frac{V_e}{V_\pi}\right)\left[\sqrt{r\left(\frac{c}{n_0\lambda} + \omega\right)} - \sqrt{r\left(\frac{c}{n_0\lambda} - \omega\right)}\right] \times \cos\left(\frac{D_1 L_1 \lambda^2 \omega^2}{4\pi c} + \frac{\pi}{2}\right) \tag{6.2}$$

where G_0 denotes the optical gain provided by the EDFA, while A is a constant determined jointly by the fiber attenuation and the responsivity of the PD. The term J_1 represents the first-order Bessel function of the first kind, V_e is the voltage of the driving signal, and V_π corresponds to the half-wave voltage of the PM. The function $r(\omega)$ describes the power reflection coefficient of the PS-FBG. In addition, c is the velocity of light in vacuum, n_0 is the effective refractive index of the SMF, and λ is the wavelength of the optical carrier. The parameters D_1 and L_1 denote the chromatic dispersion parameter and the fiber length of the long loop, respectively.

Since the dispersion-induced power penalty varies only slightly within the operational bandwidth of the MPF (typically below 1 GHz), it can be approximated as a constant,

denoted by δ. Likewise, the electrical net gain is assumed to remain constant within this frequency range ($g_e(\omega) = g_e$). Accordingly, Eq. (6.1) can be simplified and rewritten as

$$g(\omega) = G_0 A J_1\left(\frac{V_e}{V_\pi}\right)\left[\sqrt{r\left(\frac{c}{n_0\lambda} + \omega\right)} - \sqrt{r\left(\frac{c}{n_0\lambda} - \omega\right)}\right]\delta g_e \tag{6.3}$$

Considering that the mode spacing $\Delta\omega$ is relatively small and the open-loop gain varies slowly with frequency, the primary oscillation mode ω_m can be approximated as lying at the center of the MPF passband. The nearest competing mode, represented ω_n, is typically located adjacent to the primary mode, such that $\Delta\omega = |\omega_m - \omega_n|$. During the PM–IM conversion process, it is assumed that the lower sideband is completely suppressed by the notch of the PS-FBG. Under this condition, the following relationship holds $\sqrt{r\left(\frac{c}{n_0\lambda} + \omega_m\right)} - \sqrt{r\left(\frac{c}{n_0\lambda} - \omega_n\right)} = 1$. Based on this relation, the gain difference between the primary mode and the adjacent secondary mode induced by the Vernier effect can be expressed as

$$\Delta g_{\mathrm{V}} = g(\omega_m) - g(\omega_n) = \chi\left[\sqrt{r\left(\frac{c}{n_0\lambda} - \omega_n\right)} - \sqrt{r\left(\frac{c}{n_0\lambda} - \omega_m\right)}\right] \tag{6.4}$$

where $\chi = G_0 A J_1\left(\frac{V_e}{V_\pi}\right)\delta g_e$.

Furthermore, the gain difference can be further increased when the dual-loop OEO operates in the PT-symmetric broken regime. To satisfy the PT-symmetric condition, t the effective gain and loss of the coupled primary modes in the two loops must be carefully balanced, thus, the gain difference of PT symmetry is given by:

$$\Delta g_{\mathrm{PT}} = \sqrt{g^2(\omega_m) - g^2(\omega_n)} = \chi \sqrt{2\left(\sqrt{r\left(\frac{c}{n_0\lambda} - \omega_n\right)} - \sqrt{r\left(\frac{c}{n_0\lambda} - \omega_m\right)}\right)} \tag{6.5}$$

Given that the values of $\sqrt{r\left(\frac{c}{n_0\lambda} - \omega_m\right)}$ and $\sqrt{r\left(\frac{c}{n_0\lambda} - \omega_n\right)}$ are both smaller than unity and approach zero, we can have $\Delta g_{\mathrm{PT}} \gg \Delta g_{\mathrm{V}}$. It can be observed that the introduction of PT symmetry markedly enlarges the gain difference between the primary mode and the nearest secondary mode, thereby indicating that the sidemodes are more effectively suppressed. With reduced competition from adjacent modes, the stability of single-mode oscillation is consequently enhanced.

Fig. 6.2 illustrates the combined influence of the Vernier effect and PT-symmetry breaking on mode selection. In particular, Fig. 6.2(a) and (b) display the resonant modes in the long loop and short loop, respectively. The red curves represent the open-loop frequency response of the OEO, while the green dashed lines indicate the oscillation threshold. As shown in Fig. 6.2(c), the Vernier effect strongly suppresses a portion of the long-loop modes. Moreover, Fig. 6.2(d) demonstrates that the gain difference between the primary mode and the secondary mode is further enlarged once PT symmetry is broken.

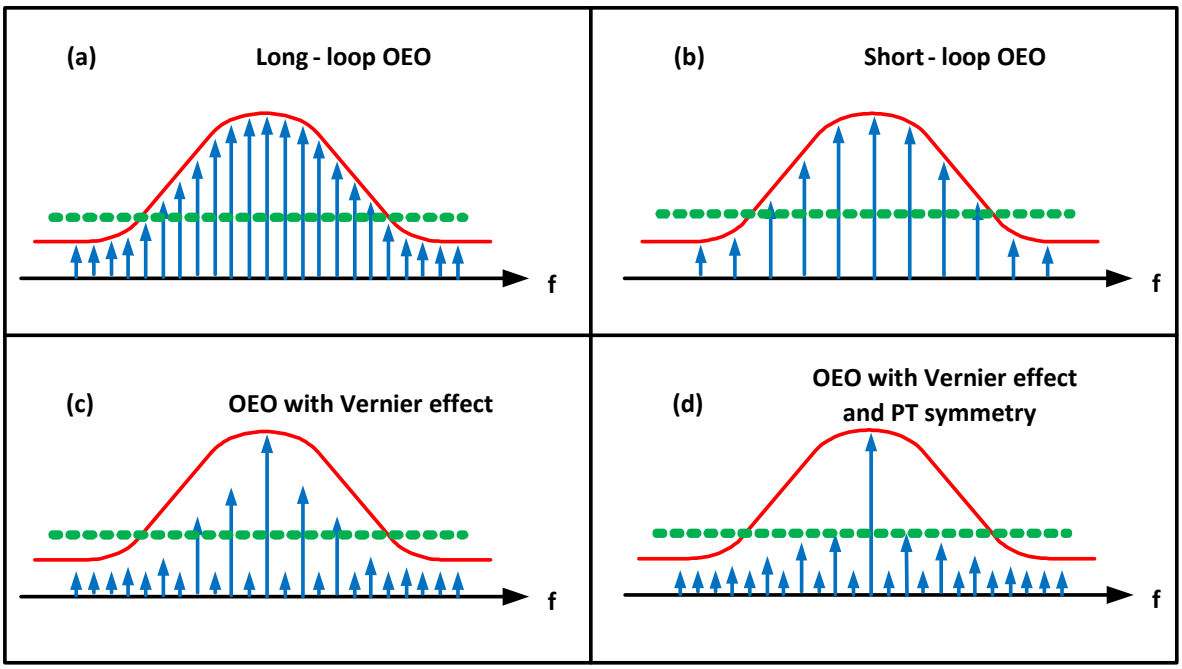

Fig. 6.2 The eigenmodes of (a) a single long-loop OEO, (b) a single short-loop OEO, (c) a dual-loop OEO with the Vernier effect, and (d) a dual-loop OEO with the joint of the Vernier effect and the PT symmetry.

6.3 Experimental results

The experimental validation of the proposed dual-loop PT-symmetric OEO with a rational loop-length ratio is carried out using the setup illustrated in Fig. 6.1 A continuous-wave optical carrier from a TLS (Yokogawa AQ2201) is sent through PC1 into a PM (JDSU) with a 3-dB bandwidth of 20 GHz. The PS-FBG exhibits a notch filter centered at 1545.79 nm with an FWHM of 3.1 pm, corresponding to a MPF bandwidth of approximately 390 MHz. Optical amplification is provided by an EDFA (FiberPrime EDFA-C-14-S-FA), which provides up to 30 dB gain with a saturated output power of 16 dBm. The modulated signal is detected by a high-speed PD (Optilab LR-12-A-M) with a 3-dB bandwidth of 12 GHz, and further amplified by two cascaded EAs (MultiLink MTC5515) providing more than 40 dB of small-signal gain. The generated microwave signal is analyzed with an ESA (Agilent

E4448A), while its phase-noise characteristics are measured using a signal analyzer (Agilent E5052B).

The microwave spectra obtained under different configurations are shown in Fig. 6.3. When PC2 is tuned to evenly split the optical power into the two arms of the PBS, the system can be tested with only one loop closed. With the upper arm disconnected, only the short loop remains active. As shown in Fig. 6.3(a), multimode oscillation occurs with an FSR of 850 kHz, corresponding to the 240-m loop length. Conversely, when the lower arm is disconnected, only the long loop is active. In this case, multimode oscillation with a mode spacing of 42.5 kHz is observed in Fig. 6.3(b), consistent with the 4800-m loop length. When both loops are closed and contribute gain, the oscillator functions as a conventional dual-loop OEO. Under this condition, mode selection is determined solely by the Vernier effect. As shown in Fig. 6.3(c), single-mode oscillation at 6 GHz with an SMSR of 36.8 dB is obtained. However, because the MPF bandwidth of 390 MHz accommodates more than 400 cavity modes, the oscillation remains unstable, and mode hopping is observed due to mode competition.

PC2 is then adjusted so that the short loop experiences a net loss while the long loop maintains gain. Under these conditions, PT symmetry is not satisfied since the gain and loss are not balanced, and the oscillator reverts to multimode operation, as illustrated in Fig. 6.3(d). Because the short loop does not contribute gain, the Vernier effect is weakened, and the joint effect of the two loops is significantly reduced. To realize PT-symmetric operation, both PC2 and PC3 are tuned so that the gain and loss are balanced, and the net gain exceeds the coupling coefficient. The system then enters the PT-broken phase. In this region, the

combination of the Vernier effect and PT symmetry ensures stable single-mode oscillation. As shown in Fig. 6.3(e) and (f), the oscillator generates a 6-GHz signal with an SMSR of 40.7 dB, higher than that achieved with the Vernier effect alone. The stability of the oscillator is confirmed by monitoring power fluctuations and mode hopping over 20 minutes, during which the output power variation remains within 0.6 dB and no mode hopping is observed. To further validate the joint role of the Vernier effect and PT symmetry, control experiments are performed. When the short loop is disconnected, multimode oscillation reappears, while disconnecting the long loop suppresses oscillation entirely due to net loss. When both loops are reconnected under the PT-broken condition, stable single-mode oscillation is restored.

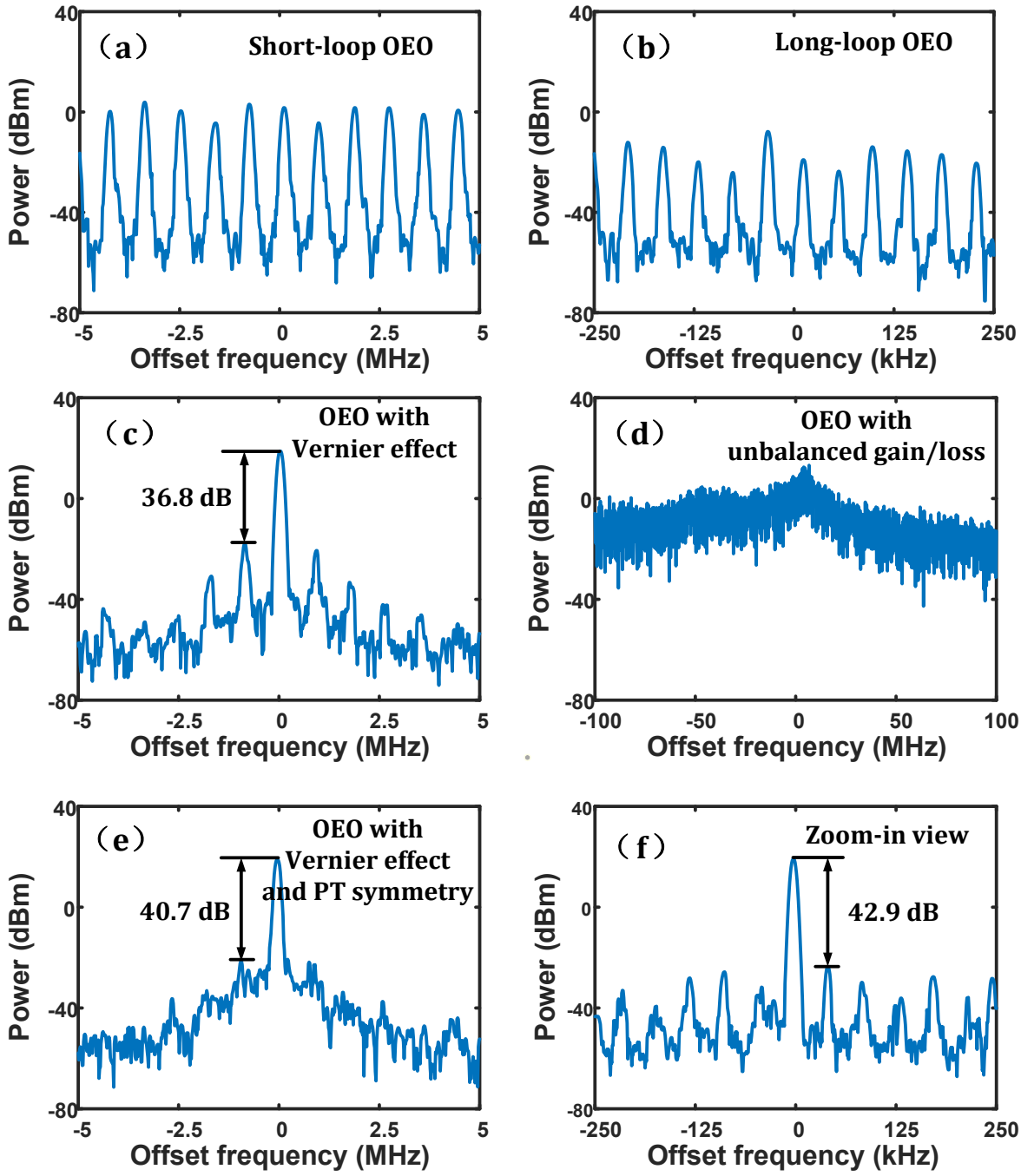

Fig. 6.3 The electrical spectra of the microwave signals generated by the PT-symmetric OEO. The spectra are measured at a central frequency of 6 GHz by an electrical spectrum analyzer. (a) Multi-mode oscillation in the short loop measured with a span of 10 MHz; (b) multi-mode oscillation in the long loop measured with a span of 500 kHz; (c) single-mode oscillation in the dual-loop based on the Vernier effect measured with a span of 10 MHz; (d) multi-mode oscillation in the dual-loop when PT symmetry condition is not matched, measured with a

span of 200 MHz; (e) single-mode oscillation in the dual-loop based on the joint of the Vernier effect and the PT symmetry measured with a span of 10 MHz, and (f) a zoom-in view with a span of 500 kHz

The tunability and phase-noise characteristics of the oscillator are also evaluated. Frequency tuning is achieved by adjusting the center frequency of the MPF, which is controlled by tuning the TLS wavelength. As shown in Fig. 6.4(a), the oscillator maintains stable single-mode operation across a tuning range of 2–12 GHz. The phase-noise performance of a 6-GHz oscillation is presented in Fig. 6.4(b). The measured phase noise reaches −114 dBc/Hz at a 10-kHz frequency offset. Additional resonant peaks appear at offset frequencies about 42.5 kHz, corresponding to the effective FSR of the coupled dual loops. These spurious tones remain below −80 dBc/Hz, confirming that the dominant oscillation mode is effectively selected.

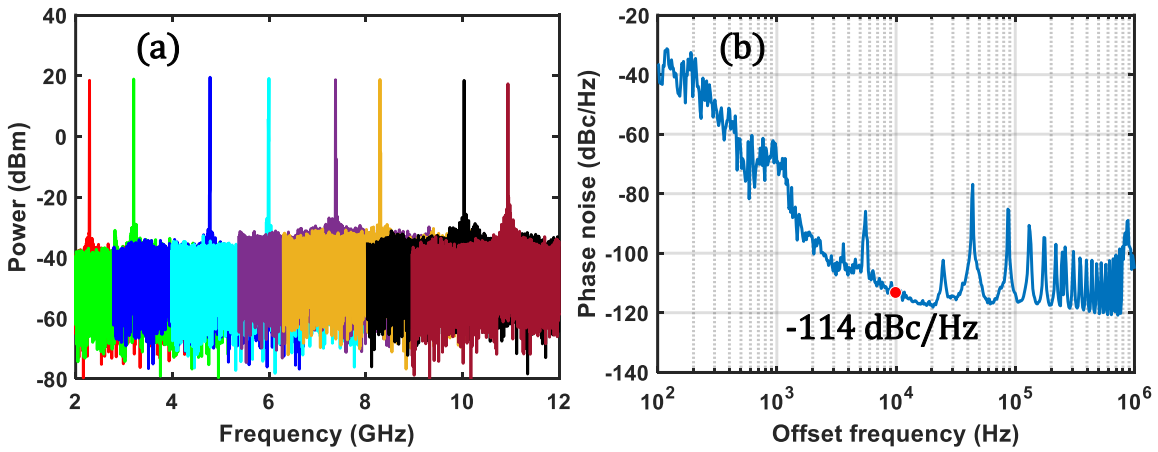

Fig. 6.4 (a) Frequency tunability of the proposed OEO with a tuning range from 2 to 12 GHz; (b) phase noise measurement of the generated microwave signal at 6 GHz. The phase noise level is −114 dBc/Hz at an offset frequency of 10 kHz.

6.4 Conclusion

This chapter has reported a dual-loop PT-symmetric OEO with a rational loop-length ratio, in which the Vernier effect and PT symmetry jointly enable efficient and stable mode selection. By employing loop lengths of 4.8 km and 240 m, a rational ratio condition was established, enlarging the effective FSR and easing mode competition. Mode selection by PT symmetry broken further suppressed residual sidemodes, resulting in a stable frequency-tunable oscillation from 2 to 12 GHz, with an SMSR of 40.7 dB, and a phase noise of –114 dBc/Hz at 10 kHz offset.

Compared with the single-loop PT-OEO in Chapter 4, this design provides superior sidemode suppression and stability, while preserving frequency tunability across a wide range. The combination of PT symmetry and Vernier effect thus establishes a general framework for high-performance OEOs, paving the way for integrated OEOs with compactness.

CHAPTER 7 A DUAL-FREQUENCY PARITY-TIME SYMMETRIC OPTO-ELECTRONIC OSCILLATOR

7.1 Introduction

Dual-frequency microwave sources represent essential building blocks for a variety of applications, including coherent radar systems, photonic-assisted millimeter-wave generation, high-resolution ranging, and multi-channel communication platforms. For these applications, it is not only desirable to generate two microwave tones with well-defined and tunable frequency spacing, but also critical to ensure that both tones maintain single-mode purity and exhibit excellent long-term frequency stability. OEOs, enabled using long, low-loss optical fiber delay lines, naturally offer relatively low phase noise performance. However, conventional OEOs inherently support a dense set of modes because the long cavity delay reduces the FSR to the order of tens of kilohertz. When configured to oscillate at two distinct frequencies, such systems often experience severe multimode competition and frequent mode switching, which degrade the purity and stability of dual-frequency oscillation.

To address these challenges, this chapter introduces and experimentally demonstrates a dual-frequency PT-symmetric OEO. The combination of PT symmetry and injection locking offers an efficient solution to achieve dual-frequency operation in which both oscillation tones are single-mode and mutually phase-stabilized. The core concept is to use a dual-wavelength-sliced ASE source that passes through a large-dispersion optical element, thereby forming two independent oscillation channels in the microwave photonic domain. A PT-symmetric

mode selection mechanism is then applied to eliminate unwanted modes surrounding each channel and ensure single-mode dominance. Subsequently, an external injection signal equal to the frequency difference between the two oscillation channels is introduced to lock their relative phase. By integrating these two mechanisms, we implement a tunable dual-frequency OEO capable of maintaining high spectral purity and stable frequency spacing.

7.2 Operation principle

The schematic diagram of the proposed dual-frequency PT-symmetric OEO is shown in Fig. 7.1. An ASE source generated by an EDFA serves as a broadband optical input and is passed through a PBS to produce a linearly polarized state. For a z-cut $LiNbO_3$ MZM, both the ordinary and extraordinary optical modes are supported, but with different modulation efficiencies. By adjusting PC1, the polarization state of the light sent to the MZM is precisely controlled, and the modulated optical signal at the output of the MZM is given by

$$\begin{bmatrix} E_x \\ E_z \end{bmatrix} = \sqrt{P} \begin{bmatrix} \sin\theta \exp(j2\pi f_c t) \cos\left(\frac{\pi}{V_\pi^{\mathrm{TE}}} V_{\mathrm{in}}(t)\right) \\ \cos\theta \exp(j2\pi f_c t) \cos\left(\frac{\pi}{V_\pi^{\mathrm{TM}}} V_{\mathrm{in}}(t)\right) \end{bmatrix} \tag{7.1}$$

where P is the power of the optical carrier, θ is the polarization angle respected to the z-axis, V_π^{TE} and V_π^{TM} are the half-wave voltages of the MZM for the TE and TM modes, respectively. $V_{\mathrm{in}}(t)$ represents the microwave signal injected into the RF port of the MZM. As can be seen, the optical power splitting ratio between the two orthogonally polarized optical signals can be arbitrarily tuned, illustrating that the gain/loss ratio can be separately controlled to satisfy the PT symmetry condition.

After transmission through a long segment of SMF and amplification by an EDFA, the

modulated optical signal is then spectrally re-shaped by a wave shaper implementing two cosine-shaped profiles, and subsequently detected by a PD to form a dual-passband MPF. The electrical signals are amplified and fed back to the MZM together with an external injection signal whose frequency equals the difference between the center of two tones, thereby closing the OEO loop.

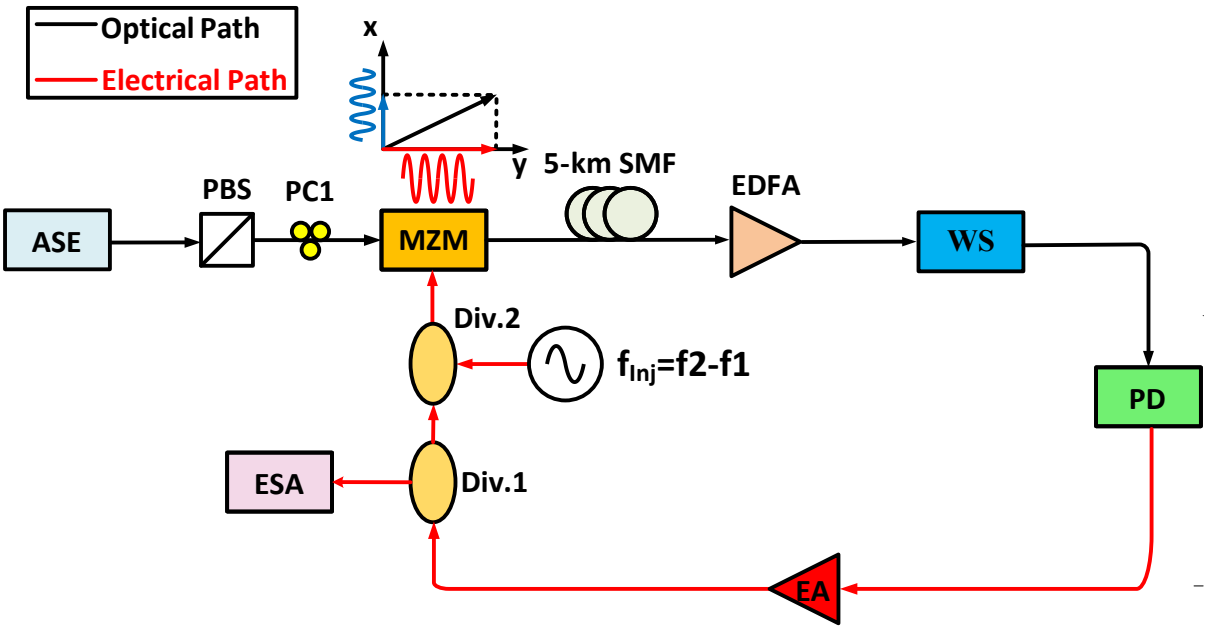

Fig. 7.1 Schematic diagram of a tunable dual-frequency PT-symmetric OEO. ASE: amplified spontaneous emission source; PBS: Polarization beam splitter; PC: Polarization controller; MZM: Mach-Zehnder modulator; SMF: Single-mode fiber; EDFA: Erbium-doped fiber amplifier; WS: Wave shaper; PD: Photodetector; EA: Electrical amplifier; Div.: Divider; ESA: Electrical spectrum analyzer.

The key component in our proposed OEO to realize dual-frequency oscillation is the reconfigurable dual-passband MPF implemented with the ASE source, the wave shaper, and the PD. When the ASE spectrum is shaped by a programmable optical filter (wave shaper) with a cosine function profile, given by

$$S(\lambda) = \frac{1}{2} + \frac{1}{2}\cos\left(2\pi\frac{\lambda - \lambda_0}{\Delta\lambda}\right) \tag{7.2}$$

where λ_0 represents the center wavelength of the ASE spectrum, and $\Delta\lambda$ denotes the slicing period of the optical filter, each period of the shaped spectrum acts as an individual tap in the filter impulse response. Due to the dispersion of the long-length SMF, these taps experience distinct group delays, and the relative delay between two adjacent taps can be expressed as

$$\Delta\tau = DL\Delta\lambda \tag{7.3}$$

where D and L are the group velocity dispersion parameter and the length of the SMF, respectively. This wavelength-dependent delay leads to the formation of an MPF within the system, whose center frequency is determined by

$$f_c = \frac{1}{\Delta\tau} = \frac{1}{DL\Delta\lambda} \tag{7.4}$$

Therefore, by adjusting the spectral slicing period, and thus $\Delta\lambda$, the center frequency of the MPF can be flexibly tuned. To realize a dual-passband MPF, an additional cosine component is introduced, and the optical spectrum shaping profile is written as

$$S(\lambda) = \frac{1}{2} + \frac{1}{4}\left[V_1\cos\left(2\pi\frac{\lambda - \lambda_0}{\Delta\lambda_1}\right) + V_2\cos\left(2\pi\frac{\lambda - \lambda_0}{\Delta\lambda_2}\right)\right] \tag{7.5}$$

where V_1 and V_2 are the parameters ranging from 0 to 1, to control the amplitudes of the cosine-shaped spectra, thus, adjusting the peak value of the corresponding passband, respectively. By controlling the spectral slicing period and the V parameters, a balanced dual-band MPF is achieved.

To further suppress the strong mode competition between two oscillation tones within the same feedback loop, a mutual injection locking method is applied. As shown in Fig. 7.1, an

external RF signal with frequency f_{inj}, chosen to match the difference between the two oscillation modes, is fed into the loop via the MZM. As a result, the free-running oscillation at f_1 (lower frequency) produces a phase-coherent component at $f_1 + f_{\text{inj}} = f_2$; conversely, the oscillation at f_2 (higher frequency) gives rise to a synchronized replica at $f_2 - f_{\text{inj}} = f_1$. These reciprocal interactions effectively lock the two tones to each other. Once the locking condition is satisfied, the OEO maintains a stable dual-frequency state in which both modes remain phase-aligned and immune to conventional mode competition.

However, owing to the long-length SMF, the FSR is small, and the single-mode oscillation in each tone cannot be guaranteed. As mentioned at the beginning of the principle analysis, the gain/loss of the orthogonally polarized optical signals are tuned to be balanced and exceeds the coupling coefficient to make the system located at the PT symmetry broken region, thus, both f_1 and f_2 can be forced into single-mode oscillation, and these two frequency signals are stabilized by the injection locking.

7.3 Experimental results

The performance of the proposed dual-frequency PT-symmetric OEO is evaluated based on the setup illustrated in Fig. 7.1. An ASE source generated by an EDFA (NORTEL FA17UFAC119C28) is first passed through a PBS to ensure a well-defined linear polarization. The linearly polarized light is then launched into PC1, where its polarization state is adjusted to match the PT symmetry condition. After polarization alignment, the optical signal is applied to an MZM (JDSU, model:10021840), which is biased at the quadrature point. The modulated optical signal then propagates through a 5-km SMF to introduce a long time delay,

and is subsequently amplified by a second EDFA (NORTEL FA17UFAC119C20). The amplified optical spectrum is then spectrally sliced by a programmable optical filter (Finisar WaveShaper 4000S) with a filter wavelength range from 1540 nm to 1560 nm. The V parameters are set to be $V_1 = 0.95$ and $V_2 = 1$, and the slicing periods are chosen as $\Delta\lambda_1 = 1.6\,nm$ and $\Delta\lambda_2 = 1.4\,nm$, respectively. The resulting sliced optical spectrum measured by an OSA (ANDO AQ6317B) is shown in Fig. 7.2. The sliced optical signal is then converted to an electrical signal at a high-speed PD (Optilab LR-12-A-M) with a 3-dB bandwidth of 12 GHz. Three cascades EAs with a bandwidth from 4 GHz to 15 GHz are used to provide sufficient electrical gain in the OEO loop. The generated microwave signal is analyzed by an ESA (Agilent E4448A), and is then fed back to the MZM together with an external injection locking signal generated by a signal generator (Agilent E8254A) to close the OEO loop.

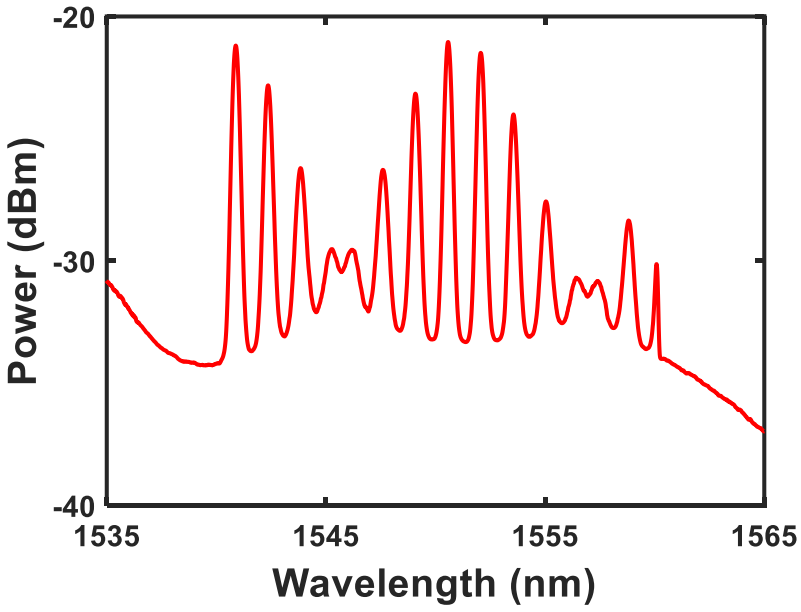

Fig. 7.2 Measured optical spectrum of the sliced broadband source.

Since the key to achieving dual-frequency oscillation lies in creating a well-balanced dual-

passband MPF, the frequency response of the MPF is evaluated. To do so, the loop of the OEO is opened at the output port of the last EA, and the frequency response is measured using a vector network analyzer (Keysight N5224A). Fig. 7.3 illustrates the measured frequency response of the dual-band MPF. Two passbands centered at 8.15 GHz and 9.35 GHz with a same peak level are observed, each with a 3-dB bandwidth of approximately 500 MHz. Accordingly, the external injection-locking signal is set to 1.2 GHz, matching the frequency spacing between the two passbands.

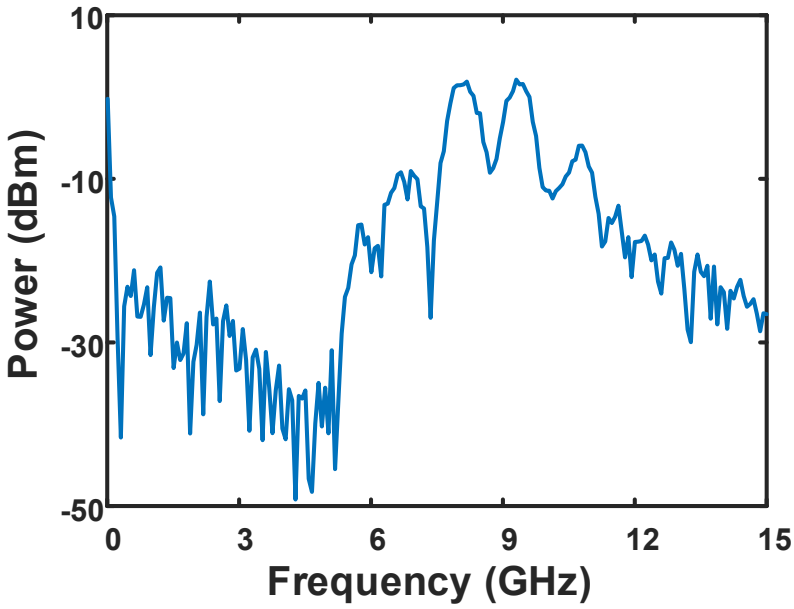

Fig. 7.3 Measured frequency response of the dual-band MPF.

Once the loop is closed, oscillation naturally occurs at the centers of the two MPF passbands. Fig. 7.4(a) shows the electrical spectrum without injection locking, where strong multi-mode oscillation is observed in both passbands. When the 1.2-GHz external signal is injected into the loop, most unwanted modes are suppressed and few-mode oscillation is achieved in two tones, shown in Fig. 7.4(b), indicating that injection locking can effectively suppress most of the unwanted modes. However, injection locking alone cannot guarantee single-mode

operation. To address this limitation, PC1 is finely tuned to control the gain/loss coefficient of the two orthogonally polarized optical signals to make the proposed OEO operate at PT broken region. Under this condition, single-mode oscillation is achieved in both tones, as illustrated in Fig. 7.4(c).

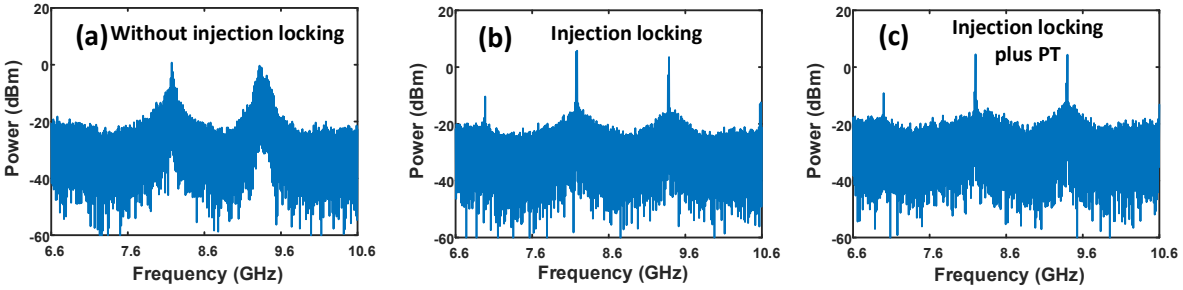

Fig. 7.4 The electrical spectra of the microwave signals generated by the proposed dual-tone PT-symmetric OEO. (a) Multi-mode oscillation in the dual-band without injection locking; (b) few-mode oscillation in the dual-band with injection locking; (c) single-mode oscillation in the dual-band with combination of injection locking and PT symmetry.

To further evaluate the generated signals in each tone, we provide the zoom-in view of the electrical spectra at each MPF passband, demonstrated in Fig. 7.5. As illustrated in Fig. 7.5 (a) and (e), when only injection locking method is applied, few-mode oscillations occur at the center frequencies of 8.15 GHz and 9.35 GHz, respectively. From their zoom-in view in Fig. 7.5 (c) and (g), we can obtain that the FSR of the proposed OEO is 44 kHz, and the mode competition is still strong in each tone. By tuning PC1 to make the OEO operate at the PT broken region, single-mode oscillation is achieved in each tone, shown in Fig. 7.5 (b) and (f). Fig. 7.5 (d) and (h) illustrate that the SMSR is improved to 17.2 dB at 8.15 GHz and 22.3 dB at 9.35 GHz, confirming that single-mode oscillation in the dual-tone OEO is induced by PT-

symmetry breaking.

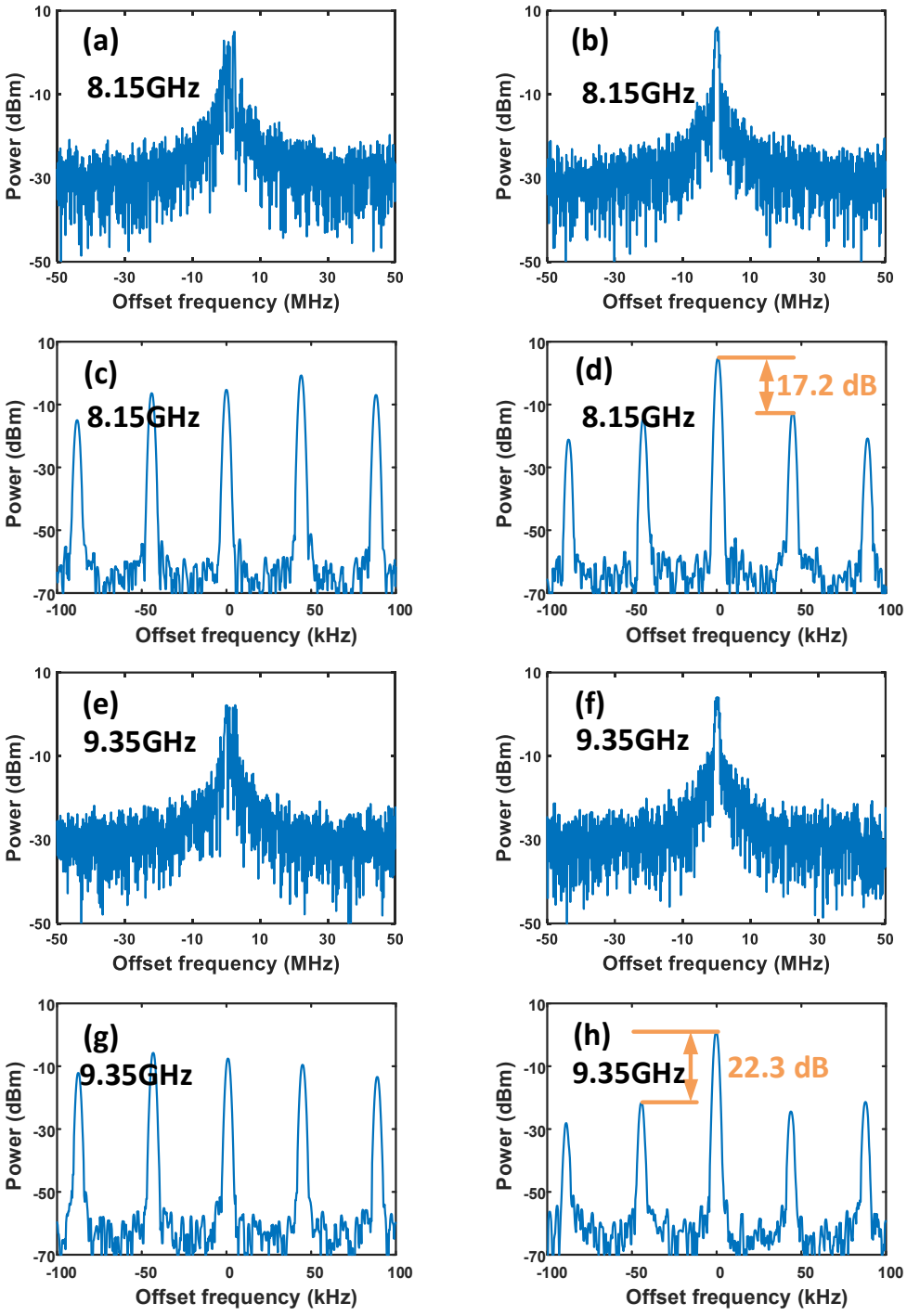

Fig. 7.5 The electrical spectra of the generated microwave signals in each tone. (a) and (e) are the multi-mode oscillations only with injection locking measured with a span of 100 MHz at 8.15 GHz and 9.35 GHz, respectively; (c) and (g) are the corresponding zoom-in view measured with a span of 200 kHz; (b) and (f) are

the single-mode oscillation based on the joint of the injection locking and the PT symmetry at 8.15 GHz and 9.35 GHz, respectively, measured with a span of 100 MHz; (d) and (h) are the corresponding zoom-in view measured with a span of 200 kHz.

7.4 Conclusion

This chapter presented a tunable dual-frequency PT-symmetric optoelectronic oscillator capable of generating two spectrally pure and mutually stabilized microwave tones. By integrating PT-symmetric gain/loss control with frequency-difference injection locking, the proposed system effectively suppresses all competing modes in each oscillation band and simultaneously enforces a stable phase relationship between the two generated signals.

The experimental implementation demonstrated two single-mode oscillation tones at 8.15 GHz and 9.35 GHz, with measured SMSRs of 17.2 dB and 22.3 dB, respectively. These results confirm that PT-symmetric gain/loss engineering provides a powerful mechanism for eliminating the dense competitive side modes inherent to long-delay OEOs. The successful activation of injection locking further ensures that the frequency spacing between the two oscillation bands remains constant, producing a coherent dual-frequency output with excellent long-term stability. To the best of our knowledge, this is the first time generating multiple single-mode frequencies in a PT-symmetric system. Previous studies of PT-symmetric OEOs primarily focused on single-frequency operation; the extension to a multi-frequency regime introduces a new degree of control enabled by PT symmetry in microwave photonics.

Beyond the specific implementation reported here, the demonstrated architecture provides a

platform for advanced multi-tone microwave photonic sources. This capability opens new opportunities for dual-frequency and multi-tone radar systems, dual-comb microwave photonics, and photonic-assisted sensing architectures that require highly stable multi-frequency sources.

CHAPTER 8 SUMMARY AND FUTURE RESEARCH

8.1 Summary

This thesis has addressed the long-standing challenge of achieving stable single-frequency operation in lasers and OEOs by exploiting the framework of PT symmetry. Conventional lasers and OEOs based on long cavities benefit from narrow linewidths and low phase noise, but their dense mode spectra inevitably lead to severe mode competition, multimode oscillation, and degraded stability. Traditional approaches to mode selection, such as narrowband optical filters, multi-loop configurations, or injection locking, have provided partial solutions but introduce compromises in complexity, insertion loss, tunability, or environmental robustness. PT symmetry offers an intrinsically different approach: by balancing gain and loss, it enables non-Hermitian mode selection in which one mode is amplified while its conjugate is suppressed. Building on this principle, the thesis has proposed and experimentally demonstrated four novel architectures—a single-loop PT fiber laser, a single-loop PT-OEO, a rational dual-loop PT fiber laser, and a rational dual-loop PT-OEO—that collectively advance the state of the art in photonics and microwave photonics.

The single-loop PT fiber laser represents the first realization of PT symmetry within a single cavity, achieved by engineering counter-propagating modes in the polarization-dependent Sagnac loop to emulate gain/loss dynamics. This design eliminates the need for two physically identical loops, reducing system complexity and improving stability against environmental change, while experiments confirmed that it delivers stable SLM operation

with high sidemode suppression and narrow linewidth. Extending this concept to microwave photonics, the single-loop PT-OEO introduced in this work is the first of its kind to achieve single-mode microwave oscillation without relying on ultra-narrowband RF filters. By embedding PT symmetry broken, stable operation over a broad frequency range from 2 to 12 GHz was achieved with excellent phase noise performance, validating that PT symmetry can provide both effective single-mode selection and low-phase-noise characteristics critical for radar and communication systems. These results establish that PT symmetry is not confined to optical resonators but can be effectively applied in hybrid opto-electronic systems.

The thesis further advanced PT-enabled architectures by combining them with the Vernier effect, leading to dual-loop PT fiber laser and PT-OEO with rational loop length ratio. In these systems, two loops of rationally related lengths produce an enlarged effective FSR, reducing mode density, while PT symmetry enforces selective amplification of a single dominant mode. Experimental demonstrations showed that the dual-loop PT fiber laser with rational loop length ratio achieve extremely high SMSR and narrow linewidths, outperforming conventional Vernier effect-only designs. Similarly, the dual-loop PT-OEO demonstrated stable single-mode oscillation and superior phase noise performance across a wide tuning range without requiring external filtering. These dual-loop PT designs illustrate the synergistic benefits of combining non-Hermitian physics with established mode-control techniques, providing stability and simplicity that surpass traditional methods.

To expand the PT symmetry-based architectures to achieve multi-frequency oscillation, a tunable dual-frequency PT-symmetric OEO is proposed and experimentally demonstrated. A sliced ASE source propagates through a large-dispersion optical element to form two well-

balanced MPF channels. PT symmetry suppresses multimode competition within each individual channel, ensuring clean single-mode generation at both target frequencies. Subsequently, an external RF injection signal stabilizes the relative phase and frequency spacing between the two oscillation branches, eliminating mutual mode competition and enabling highly stable dual-frequency operation. Experiments showed that two oscillation tones at 8.15 GHz and 9.35 GHz were simultaneously generated with SMSRs of 17.2 dB and 22.3 dB, respectively. This architecture establishes a new method for realizing dual-frequency, and potentially multi-frequency, OEOs with enhanced stability and spectral purity.

In conclusion, the five architectures developed in this thesis illustrate the versatility of PT symmetry as a unifying framework for mode selection across both optical and microwave domains. Unlike conventional approaches, PT-based designs achieve effective mode control within the system dynamics, avoiding reliance on delicate filters or external references. By systematically progressing from single-loop to dual-loop structures, and from fiber lasers to OEOs, the research demonstrates a coherent strategy that translates theoretical predictions into practical devices. The results highlight not only improved performance metrics such as SMSR, linewidth, and phase noise, but also enhanced scalability. Overall, this thesis establishes PT symmetry as a practical design principle for high-performance lasers and OEOs, transforming it from a theoretical novelty into a tool for engineering functional photonic and optoelectronic systems with clear pathways toward real applications.

8.2 Future research

While the work presented in this thesis has demonstrated that PT symmetry can provide an

outstanding mechanism for mode selection in both fiber lasers and OEOs, it also opens several ways for future research that extend beyond the specific designs demonstrated here. The four architectures in this thesis represent a new paradigm for simplifying PT-symmetric system design, enhancing stability, and overcoming long-standing challenges associated with dense mode spectra in long cavities. As with all emerging approaches, further exploration is needed to fully exploit the potential of PT symmetry in photonics and microwave photonics.

One of the most promising directions is the integration of PT-symmetric architectures into photonic integrated circuits. While this thesis has focused on fiber-based implementations, integrated photonics platforms such as silicon, SiN, and InP offer unique opportunities for miniaturization, mass production, and environmental stabilization. Embedding PT symmetry into integrated components could lead to compact single-mode lasers and chip-scale OEOs with ultralow phase noise. Recent progress in heterogeneous integration, where III–V gain materials are combined with low-loss passive platforms, suggests that electrically pumped PT-symmetric microring lasers and on-chip PT-OEOs are within reach. Realizing such systems would enable scalable deployment of PT-enabled devices in communication, sensing, and radar technologies, bridging the gap between laboratory demonstrations and industrial applications.

Future research should also explore the use of PT symmetry in sensing applications. As demonstrated in other optical platforms, systems operating at EPs display non-linear scaling laws that dramatically enhance sensitivity to small perturbations. Extending this concept to PT fiber lasers and PT-OEOs could lead to a new class of ultrasensitive sensors capable of detecting weak physical or environmental signals. For instance, PT fiber lasers could be

employed for high-resolution strain or temperature sensing, while PT-OEOs might be adapted for rotation sensing or magnetic field detection. The combination of narrow linewidth, high signal purity, and EP-enhanced sensitivity could unlock novel sensing modalities that outperform traditional photonic or electronic sensors.

REFERENCES

[1] J. J. Sakurai, Modern Quantum Mechanics, rev. ed. Reading, MA, USA: Addison-Wesley, Jan. 1994.

[2] C. M. Bender and S. Boettcher, "Real spectra in non-Hermitian Hamiltonians having PT symmetry," *Phys. Rev. Lett.*, vol. 80, no. 24, pp. 5243–5246, June 1998.

[3] C. M. Bender, S. Boettcher, and P. N. Meisinger, "PT-Symmetric Quantum Mechanics," *J. Math. Phys.*, vol. 40, no. 5, pp. 2201-2229, Sep. 1998.

[4] C. M. Bender, D. C. Brody, and H. F. Jones, "Must a Hamiltonian be Hermitian?," *Am. J. Phys.*, vol. 71, no. 11, pp. 1095–1102, Nov. 2003.

[5] Z. Ahmed, "Real and complex discrete eigenvalues in an exactly solvable one-dimensional complex PT-invariant potential," *Phys. Lett. A*, vol. 282, no. 6, pp. 343-348, Apr. 2001.

[6] G. Lévai and M. Znojil, "Systematic search for PT-symmetric potentials with real energy spectra," *J. Phys. A: Math. Gen.*, vol. 33, no. 40, pp. 7165–7180, Oct. 2000.

[7] M. Müller and I. Rotter, "Exceptional points in open quantum systems," *J. Phys. A: Math. Theor.*, vol. 41, no. 24, pp. 244018, June 2008.

[8] A. Guo, G. J. Salamo, D. Duchesne, R. Morandotti, M. Volatier-Ravat, V. Aimez, G. A. Siviloglou, and D. N. Christodoulides, "Observation of PT-symmetry breaking in complex optical potentials," *Phys. Rev. Lett.*, vol. 103, no. 9, pp. 093902, Aug. 2009.

[9] C. E. Rüter, K. G. Makris, R. El-Ganainy, D. N. Christodoulides, M. Segev, and D. Kip,

"Observation of parity–time symmetry in optics," *Nat. Phys.*, vol. 6, pp. 192–195, Mar. 2010.

[10] S. Klaiman, U. Günther, and N. Moiseyev, "Visualization of branch points in PT-symmetric waveguides," *Phys. Rev. Lett.*, vol. 101, no. 8, pp. 080402, Aug. 2008.

[11] L. Feng, Z. J. Wong, R.M. Ma, Y. Wang, and X. Zhang, "Single-mode laser by parity-time symmetry breaking," *Science*, vol. 346, no. 6212, pp. 972–975, Nov. 2014.

[12] H. Hodaei, M.A. Miri, M. Heinrich, D. N. Christodoulides, and M. Khajavikhan, "Parity-time–symmetric microring lasers," *Science*, vol. 346, no. 6212, pp. 975–978, Nov. 2014.

[13] W. Chen, Ş. Kaya Özdemir, G. Zhao, J. Wiersig, and L. Yang, "Exceptional points enhance sensing in an optical microcavity," *Nature*, vol. 548, pp. 192–196, Aug. 2017.

[14] H. Hodaei, A. U. Hassan, S. Wittek, H. Garcia-Gracia, R. El-Ganainy, D. N. Christodoulides, and M. Khajavikhan, "Enhanced sensitivity at higher-order exceptional points," *Nature*, vol. 548, pp. 187–191, Aug. 2017.

[15] J. Wiersig, "Enhancing the sensitivity of frequency and energy splitting detection by using exceptional points: Application to microcavity sensors for single-particle detection," *Phys. Rev. Lett.*, vol. 112, no. 20, pp. 203901, May 2014.

[16] Y. Wang, S. Li, S. Kiravittaya, X. Wu, and Y. Mei, "Mode-splitting based optofluidic sensing at exceptional points in tubular microcavities," *Opt. Commun.*, vol. 446, pp. 128–133, Apr. 2019.

[17] M. J. Grant and M. J. F. Digonnet, “Enhanced rotation sensing and exceptional points in a parity–time-symmetric coupled-ring gyroscope,” *Opt. Lett.*, vol. 45, pp. 6538–6541, Nov. 2020.

[18] Z. Li, C. S. Prasad, X. Wang, D. Zhang, and G. V. Naik, “Sensing beyond the exceptional point for high detectivity,” *ACS Photonics*, vol. 11, no. 8, pp. 2954–2960, Aug. 2024

[19] M. Wimmer, A. Regensburger, M.-A. Miri, C. Bersch, D. N. Christodoulides, and U. Peschel, “Observation of optical solitons in PT-symmetric lattices,” *Nat. Commun.*, vol. 6, art. 7782, July 2015.

[20] X. Bian, Y. Zhang, Z. Zhai, H. Yu, F. Zuo, G. Chen, and C. Jiang, “Enhanced four-wave mixing in PT-symmetric optomechanical systems,” *Opt. Express*, vol. 28, no. 7, pp. 9049–9061, Mar. 2020.

[21] Z. Niu, Y. Jiang, J. Wen, C. Zhang, S. Du, and I. Novikova, “Four-wave mixing with anti-parity-time symmetry in hot ^{85}Rb vapor,” *Appl. Phys. Lett.*, vol. 124, no. 4, Art. no. 044005, Jan. 2024.

[22] H. Zhao, X. Qiao, T. Wu, B. Midya, S. Longhi, and L. Feng, “Non-Hermitian topological light steering,” *Science*, vol. 365, no. 6458, pp. 1163–1166, Sep. 2019.

[23] M. Parto, W. Hayenga, B. Midya, K. Makris, R. El-Ganainy, and M. Khajavikhan, “Non-Hermitian and topological photonics: optics at an exceptional point,” *Nanophotonics*, vol. 10, no. 1, pp. 403–423, Jan. 2021.

[24] Z. Lin, H. Ramezani, T. Eichelkraut, T. Kottos, H. Cao, and D. N. Christodoulides, "Unidirectional invisibility induced by PT-symmetric periodic structures," *Phys. Rev. Lett.*, vol. 106, no. 21, pp. 213901, May 2011.

[25] S. Zheng, W. Yu, and W. Zhang, "Design and optimization of a passive PT-symmetric grating with asymmetric reflection and diffraction," *Opt. Express*, vol. 30, no. 16, pp. 29340–29351, Aug. 2022.

[26] W. Liu, M. Li, R. S. Guzzon, E. J. Norberg, J. S. Parker, M. Lu, L. A. Coldren & J. Yao, "An integrated parity-time symmetric wavelength-tunable single-mode microring laser," *Nat. Commun.*, vol. 8, Article 15389, May 2017.

[27] L. Chang, X. Jiang, S. Hua, C. Yang, J. Wen, L. Jiang, G. Li, G. Wang, and M. Xiao, "Parity–time symmetry and variable optical isolation in active–passive-coupled microresonators," *Nat. Photonics*, vol. 8, no. 7, pp. 524–529, Jul. 2014.

[28] X. Zhou, Y. Liu, H. Lu, and C. Sun, "PT symmetry breaking and nonlinear optical isolation in coupled microcavities," *Opt. Express*, vol. 24, no. 7, pp. 6916–6930, Apr. 2016.

[29] B. Zhang, N. Chen, X. Lu, Y. Hu, Z. Yang, X. Zhang, and J. Xu, "Bandwidth tunable optical bandpass filter based on parity-time symmetry," *Micromachines*, vol. 13, no. 1, art. no. 89, Jan. 2022

[30] R. Pradip, V. S. A. Varri, L. McRae, F. Brückerhoff-Plückelmann, D. Wendland, A. P. Ovvyan, S. Taheriniya, W. Pernice, and S. Ferrari, "Fast thermo-optic switching through parity-time symmetry breaking on silicon nitride," *Opt. Express*, vol. 33, no. 17,

pp. 36100–36109, Aug. 2025.

[31] R. Fleury, D. Sounas, and A. Alù, “An invisible acoustic sensor based on parity-time symmetry,” *Nat. Commun.*, vol. 6, p. 5905, Jan. 2015.

[32] J. Zhang and J. Yao, “Parity–time–symmetric optoelectronic oscillator,” *Sci. Adv.*, vol. 4, no. 6, Art. no. eaar6782, June 2018.

[33] Y. Liu, T. Hao, W. Li, J. Capmany, N. Zhu, and M. Li, “Observation of parity–time symmetry in microwave photonics,” *Light Sci. Appl.*, vol. 7, Art. no. 38, Jul. 2018.

[34] A. Einstein, “On the quantum theory of radiation,” *Physikalische Zeitschrift*, vol. 18, pp. 121–128, 1917.

[35] T. H. Maiman, “Stimulated optical radiation in ruby,” *Nature*, vol. 187, pp. 493–494, Aug. 1960.

[36] A. Javan, J. V. Bennett, and D. R. Herriott, “Population inversion and continuous optical maser oscillation in a gas discharge containing a He–Ne mixture,” *Phys. Rev. Lett.*, vol. 6, no. 3, pp. 106–110, Feb. 1961.

[37] C. K. N. Patel, “Continuous-wave laser action on vibrational-rotational transitions of CO_2,” *Phys. Rev.*, vol. 136, no. 5A, pp. A1187–A1193, Nov. 1964.

[38] W. T. Silfvast, Laser Fundamentals, 2nd ed. Cambridge, U.K.: Cambridge Univ. Press, Mar. 2004, Ch. 5.

[39] H. Kogelnik and C. V. Shank, “Coupled-wave theory of distributed feedback lasers,” *J. Appl. Phys.*, vol. 43, no. 5, pp. 2327–2335, May 1972.

[40] H. I. Ralph and C. H. Henry, “Theory of the linewidth of semiconductor lasers,” *IEEE J. Quantum Electron.*, vol. 18, no. 2, pp. 259–264, Feb. 1982.

[41] R. L. Fork, B. I. Greene, and C. V. Shank, “Generation of optical pulses shorter than 0.1 psec by colliding pulse mode locking,” *Appl. Phys. Lett.*, vol. 38, no. 9, pp. 671–672, May 1981.

[42] D. E. Spence, P. N. Kean, and W. Sibbett, “60-fsec pulse generation from a self-mode-locked Ti:sapphire laser,” *Opt. Lett.*, vol. 16, no. 1, pp. 42–44, Jan. 1991.

[43] E. Snitzer, H. Po, F. Hakimi, R. Tumminelli, and B. C. McCollum, “Double-clad, offset core Nd fiber laser,” in Proc. Optical Fiber Sensors Conf., OSA Tech. Dig. Series, vol. 2, pp. 10–12, Jan. 1988.

[44] T. W. Hänsch, “Nobel Lecture: Passion for precision,” *Rev. Mod. Phys.*, vol. 78, no. 4, pp. 1297–1309, Nov. 2006.

[45] S. T. Cundiff and J. Ye, “Colloquium: Femtosecond optical frequency combs,” *Rev. Mod. Phys.*, vol. 75, no. 1, pp. 325–342, Mar. 2003.

[46] U. Keller, “Recent developments in compact ultrafast lasers,” *Nature*, vol. 424, no. 6950, pp. 831–838, Aug. 2003.

[47] J. Capmany and D. Novak, “Microwave photonics combines two worlds,” *Nat. Photonics*, vol. 1, pp. 319–330, June 2007.

[48] D. J. Richardson, J. Nilsson, and W. A. Clarkson, “High power fiber lasers: current status and future perspectives,” *J. Opt. Soc. Am. B*, vol. 27, no. 11, pp. B63–B92, Nov.

2010.

[49] A. H. Zewail, “Femtochemistry: Atomic-scale dynamics of the chemical bond,” *J. Phys. Chem. A*, vol. 104, no. 24, pp. 5660–5694, June 2000.

[50] M. D. Duncan, J. Reintjes, and T. J. Manuccia, “Scanning coherent anti-Stokes Raman microscope,” *Opt. Lett.*, vol. 7, no. 8, pp. 350–352, Aug. 1982.

[51] H. Soda, Y. Kotaki, H. Sudo, H. Ishikawa, and H. Imai, “GaInAsP/InP surface emitting injection lasers,” *Jpn. J. Appl. Phys.*, vol. 18, no. 12, pp. 2329–2330, Dec. 1979.

[52] O. Mikami, K. Akimoto, and C. Kinoshita, “1.55 μm GaInAsP/InP distributed feedback lasers,” *Jpn. J. Appl. Phys.*, vol. 20, no. 4, pp. L488–L490, Apr. 1981.

[53] J. T. Kringlebotn, J.-L. Archambault, L. Reekie, and D. N. Payne, “Er^{3+}:Yb^{3+}-codoped fiber distributed-feedback laser,” *Opt. Lett.*, vol. 19, no. 24, pp. 2101–2103, Dec. 1994.

[54] C.-H. Yeh, T.-T. Huang, H.-C. Chien, C.-H. Ko, and S. Chi, “Tunable S-band erbium-doped triple-ring laser with single-longitudinal-mode operation,” *Opt. Express*, vol. 15, no. 2, pp. 382–386, Jan. 2007.

[55] C. H. Henry, N. A. Olsson, and N. K. Dutta, “Locking range and stability of injection-locked 1.54 μm InGaAsP semiconductor lasers,” *IEEE J. Quantum Electron.*, vol. QE-21, no. 8, pp. 1152–1156, Aug. 1985.

[56] K. Petermann, “External optical feedback phenomena in semiconductor lasers,” *IEEE J. Sel. Top. Quantum Electron.*, vol. 1, no. 2, pp. 480–489, June 1995.

[57] G. Roelkens, L. Liu, D. Liang, R. Jones, A. Fang, B. Koch, and J. Bowers, “III–

V/silicon photonics for on-chip and intra-chip optical interconnects," *Laser Photon. Rev.*, vol. 4, no. 6, pp. 751–779, Nov. 2010.

[58] C. Xiang, J. Guo, W. Jin, J. D. Peters, W. Xie, L. Chang, B. Shen, H. Wang, Q.-F. Yang, L. Wu, D. Kinghorn, M. Paniccia, K. J. Vahala, P. A. Morton, and J. E. Bowers, "High-performance lasers for fully integrated silicon nitride photonics," *Nat. Commun.*, vol. 12, Art. no. 6329, Oct. 2021.

[59] X. S. Yao and L. Maleki, "Optoelectronic oscillator for photonic systems," *IEEE J. Quantum Electron.*, vol. 32, no. 7, pp. 1141–1149, July 1996.

[60] X. S. Yao and L. Maleki, "Optoelectronic microwave oscillator," *J. Opt. Soc. Am. B*, vol. 13, no. 8, pp. 1725–1735, Aug. 1996.

[61] J. Yao, "Microwave photonics," *J. Lightw. Technol.*, vol. 27, no. 3, pp. 314–335, Feb. 2009.

[62] J. Yao, "Optoelectronic oscillators for high speed and high resolution optical sensing," *J. Lightw. Technol.*, vol. 35, no. 16, pp. 3489–3497, Aug. 2017.

[63] X. S. Yao and L. Maleki, "Multiloop optoelectronic oscillator," *IEEE J. Quantum Electron.*, vol. 36, no. 1, pp. 79–84, Jan. 2000.

[64] W. Li and J. P. Yao, "An optically tunable frequency-multiplying optoelectronic oscillator," *IEEE Photon. Technol. Lett.*, vol. 24, no. 10, pp. 812-814, May 2012.

[65] W. Li, M. Li, and J. P. Yao, "A narrow-passband and frequency-tunable micro-wave photonic filter based on phase-modulation to intensity-modulation conversion using a

phase-shifted fiber Bragg grating," *IEEE Trans. Microw. Theory Tech.*, vol. 60, no. 5, pp. 1287-1296, May 2012.

[66] I. Ozdur, M. Akbulut, N. Hoghooghi, D. Mandridis, M. U. Piracha, and P. J. Delfyett, "Optoelectronic loop design with 1000 finesse Fabry–Perot etalon," *Opt. Lett.*, vol. 35, no. 6, pp. 799–801, Mar. 2010.

[67] K. Saleh, R. Henriet, S. Diallo, G. Lin, R. Martinenghi, I. V. Balakireva, P. Salzenstein, A. Coillet, and Y. K. Chembo, "Phase noise performance comparison between optoelectronic oscillators based on optical delay lines and whispering gallery mode resonators," *Opt. Express*, vol. 22, no. 26, pp. 32158–32173, Dec. 2014.

[68] P.-H. Merrer, K. Saleh, O. Llopis, S. Berneschi, F. Cosi, and G. Nunzi Conti, "Characterization technique of optical whispering gallery mode resonators in the microwave frequency domain for optoelectronic oscillators," *Appl. Opt.*, vol. 51, no. 20, pp. 4742–4748, July 2012.

[69] A. B. Matsko, L. Maleki, A. A. Savchenkov, and V. S. Ilchenko, "Whispering-gallery mode based optoelectronic microwave oscillator," *Opt. Lett.*, vol. 31, no. 9, pp. 1313–1315, May 2006.

[70] G. Zhang, T. Hao, Q. Cen, M. Li, N. Shi, W. Li, X. Xiao, N. Qi, J. Dong, Y. Dai, N. Zhu, and M. Li, "Hybrid-integrated wideband tunable optoelectronic oscillator," *Opt. Express*, vol. 31, no. 10, pp. 16929–16938, May 2023.

[71] J. Tang, Z. Chen, Q. Li, X. Wang, L. Su, T. Hua, F. Xia, and Y. Li, "Integrated optoelectronic oscillator," *Opt. Express*, vol. 26, no. 9, pp. 12257–12266, May 2018.

[72] S. Haykin and K. R. Chowdhury, “Cognitive radar: a way of the future,” *IEEE Signal Process. Mag.*, vol. 23, no. 1, pp. 30–40, Jan. 2006.

[73] F. Scotti, F. Laghezza, P. Ghelfi, and A. Bogoni, “Multi-band software defined coherent radar based on a single photonic transceiver,” *IEEE Trans. Microwave Theory Tech.*, vol. 63, no. 2, pp. 546–552, Feb. 2015.

[74] T. H. Brandao, F. Scotti, H. R. D. Filgueiras, A. A. de Castro Alves, D. Onori, S. Melo, A. Bogoni, and A. C. Sodre, “Coherent dual-band radar system based on a unique antenna and a photonics-based transceiver,” *IET Radar Sonar Nav.*, vol. 13, no. 4, pp. 505–511, Jan. 2019.

[75] F. Laghezza, F. Scotti, P. Ghelfi, and A. Bogoni, “Photonics-assisted multiband RF transceiver for wireless communications,” *J. Lightw. Technol.*, vol. 32, no. 16, pp. 2896–2904, Aug. 2014.

[76] S. Kiani, P. Rezaei, and M. Navaei, “Dual-sensing and dual-frequency microwave SRR sensor for liquid samples permittivity detection,” *Measurement,* vol. 160, pp. 107805, Aug. 2020.

[77] S. Kiani, P. Rezaei, and M. Fakhr, “Dual-frequency microwave resonant sensor to detect noninvasive glucose-level changes through the fingertip,” *IEEE Trans. Instrum. Meas.*, vol. 70, Art no. 6004608, pp. 1–8, Jan. 2021.

[78] H. A. Haus and W. Huang, “Coupled-mode theory,” *Proc. IEEE*, vol. 79, no. 10, pp. 1505–1518, Oct. 1991.

[79] A. Yariv and P. Yeh, Photonics: Optical Electronics in Modern Communications, 6th ed., Oxford Univ. Press, 2007.

[80] H. A. Haus, Waves and Fields in Optoelectronics, Englewood Cliffs, NJ, USA: Prentice-Hall, 1984.

[81] F. A Berezin, M Shubin. The Schrödinger Equation. Vol. 66. Springer Science & Business Media, 2012.

[82] R. El-Ganainy, K. G. Makris, M. Khajavikhan, Z. H. Musslimani, S. Rotter, and D. N. Christodoulides, "Parity–time symmetry and exceptional points in photonics," *Nat. Physics*, vol. 14, no. 1, pp. 11–19, Jan. 2018.

[83] Z. Liu and R. Slavík, "Optical injection locking: from principle to applications," *J. Lightw. Technol.*, vol. 38, no. 1, pp. 43-59, Jan. 2020.

[84] X. Zhang, K. Jia, S. Cheng, Y. Shi, S.-N. Zhu, and Z. Xie, "Narrow-linewidth self-injection locking 1 μm laser using a fiber Fabry–Pérot resonator," *J. Opt. Soc. Am. B*, vol. 42, no. 5, pp. 1160–1163, Apr. 2025.

[85] Z. Fan, Z. Dai, Q. Qiu, and J. P. Yao, "Parity-time symmetry in a single-loop photonic system," *J. Lightw. Technol.*, vol. 38, no. 15, pp. 3866-3873, Aug. 2020.

[86] G. P. Agrawal and N. K. Dutta, Semiconductor Lasers, 2nd ed. New York, NY, USA: Springer, 1993.

[87] A. L. Schawlow and C. H. Townes, "Infrared and optical masers," *Phys. Rev.*, vol. 112, no. 6, pp. 1940–1949, Dec. 1958.

[88] Z. Xie, S. Li, H. Yan, X. Xiao, X. Zheng, and B. Zhou, “Tunable dual frequency optoelectronic oscillator with low intermodulation based on dual-parallel Mach-Zehnder modulator,” *Opt. Express*, vol. 24, no. 26, pp. 30282–30288, Dec. 2016.

[89] B. Gao, F. Zhang, P. Zhou, and S. Pan, “A frequency-tunable two-tone RF signal generator by polarization multiplexed optoelectronic oscillator,” *IEEE Microwave Wireless Compon. Lett.*, vol. 27, no. 2, pp. 192–194, Feb. 2017.

[90] S. Liu, C. Du, L. Yang, M. Liu, Z. Tang, and S. Pan, “Coherent dual-frequency signal generation in an optoelectronic oscillator,” *Opt. Lett.*, vol. 48, no. 11, pp. 2921–2924, Jun. 2023.

[91] F. Kong, W. Li, and J. Yao, “Transverse load sensing based on a dual-frequency optoelectronic oscillator,” *Opt. Lett.*, vol. 38, no. 14, pp. 2611– 2613, Jul. 2013.

[92] P. Zhou and S. Pan, “A tunable multi-frequency optoelectronic oscillator based on stimulated Brillouin scattering,” 14th ICOCN, pp. 1-3, 2015, Nanjing, China.

[93] Y. Chen, Z. Fan, and Q. Qiu, “Theoretical and experimental study on stable oscillation of dual-frequency signals in an optoelectronic oscillator,” *Appl. Opt.*, vol. 63, no. 2, pp. 350–358, Jan. 2024.

[94] Z. Dai, Z. Fan, P. Li, and J. Yao, “Widely wavelength-tunable parity-time symmetric single-longitudinal-mode fiber ring laser with a single physical loop,” *J. Lightw. Technol.*, vol. 39, no. 7, pp. 2151-2157, Apr. 2021.

[95] T. Okoshi, K. Kikuchi, and A. Nakayama, “Novel method for high resolution

measurement of laser output spectrum," *Electron. Lett.*, vol. 16, no. 16, pp. 630–631, Jul. 1980.

[96] L. B. Mercer, "1/f frequency noise effects on self-heterodyne linewidth measurements," *J. Lightw. Technol.*, vol. 9, no. 4, pp. 485–493, Apr. 1991.

[97] Z. Fan, W. Zhang, Q. Qiu, and J. Yao, "Hybrid frequency-tunable parity-time-symmetric optoelectronic oscillator," *J. Lightw. Technol.*, vol. 38, no. 8, pp. 2127-2133, Apr. 2020.

[98] Z. Dai, Z. Fan, P. Li, and J. Yao, "Frequency-tunable parity-time-symmetric optoelectronic oscillator using a polarization-dependent Sagnac loop," *J. Lightw. Technol.*, vol. 38, no. 19, pp. 5327-5332, Oct. 2020.

[99] Z. Dai, Z. Wang, and J. Yao, "A dual-loop parity-time symmetric system with a rational loop length ratio," *Opt. Lett.*, vol. 48, no. 1, pp. 143-146, Jan. 2023.

[100] L. Richter, H. Mandelberg, M. Kruger, and P. McGrath, "Linewidth determination from self-heterodyne measurements with subcoherence delay times," *IEEE J. Quantum Electron.*, vol. 22, no. 11, pp. 2070–2074, Nov. 1986.

[101] Z. Dai and J. Yao, "A frequency-tunable parity-time symmetric optoelectronic oscillator with two coupled loops having a rational loop length ratio," *J. Lightw. Technol.*, vol. 42, no. 24, pp. 8577-8581, Dec. 2024.

[102] W. Li, M. Li, and J. Yao, "A narrow-passband and frequency-tunable microwave photonic filter based on phase-modulation to intensity-modulation conversion using a

phase-shifted fiber Bragg grating," *IEEE Trans. Microw. Theory Tech.*, vol. 60, no. 5, pp. 1287–1296, May 2012.

[103] W. Li and J. Yao, "An optically tunable optoelectronic oscillator," *J. Lightw. Technol.*, vol. 28, no. 18, pp. 2640–2645, Sep. 2010.

LIST OF PUBLICATIONS

Journal papers

[1] **Z. Dai**, Y. Guan and J. Yao, "Optical convolution processing based on an amplified fiber-optic recirculating loop," *J. Lightw. Technol.*, vol. 43, no. 21, pp. 9920-9926, Nov. 2025.

[2] L. Huang, **Z. Dai**, and J. Yao, "Modified Ito generalization of the Hermite polynomials for the linearization of radio over fiber links with increased numerical stability," *IEEE Trans. Microw. Theory Tech.*, vol. 73, no. 3, pp. 1752-1760, Mar. 2025.

[3] **Z. Dai** and J. Yao, "A frequency-tunable parity-time symmetric optoelectronic oscillator with two coupled loops having a rational loop length ratio," *J. Lightw. Technol.*, vol. 42, no. 24, pp. 8577-8581, Dec. 2024.

[4] J. Fu, **Z. Dai**, X. Han, and J. Yao, "Wavelength-Space parity-time symmetric optoelectronic oscillator using a chirped fiber Bragg grating," *IEEE Photon. Technol. Lett.*, vol. 36, no. 3, pp 187-190, Feb. 2024.

[5] P. Li, **Z. Dai**, L. Huang, and J. Yao, "Non-orthogonal multiple access in a radio over fiber link based on optical power allocation," *Opt. Lett.*, vol. 48, no. 23, pp. 6204-6207, Nov. 2023.

[6] **Z. Dai**, Z. Wang, and J. Yao, "A dual-loop parity-time symmetric system with a rational loop length ratio," *Opt. Lett.*, vol. 48, no. 1, pp. 143-146, Jan. 2023.

[7] **Z. Dai**, P. Li, and J. Yao, "Silicon photonic integrated Fano resonator with increased

slope rate for microwave signal processing," *J. Lightw. Technol.*, vol. 40, no. 20, pp. 6911-6918, Oct. 2022.

[8] P. Li, **Z. Dai**, L. Yan, and J. Yao, "A microwave photonic link with quadrupled capacity based on coherent detection and digital phase noise cancellation," *J. Lightw. Technol.*, vol. 40, no. 20, pp. 6845-6851, Oct. 2022.

[9] P. Li, **Z. Dai**, L. Yan, and J. Yao, "A microwave photonic link to transmit four microwave vector signals on a single optical carrier based on coherent detection and digital signal processing," *Opt. Express*, vol. 30, no. 5, pp. 6690-6699, Feb. 2022.

[10] P. Li, R. Xu, **Z. Dai**, Z. Lu, L. Yan, and J. Yao, "A high spectral efficiency radio over fiber link based on coherent detection and digital phase noise cancellation," *J. Lightw. Technol.*, vol. 39, no. 20, pp. 6443-6449, Oct. 2021.

[11] **Z. Dai**, Z. Fan, P. Li, and J. Yao, "Widely wavelength-tunable parity-time symmetric single-longitudinal-mode fiber ring laser with a single physical loop," *J. Lightw. Technol.*, vol. 39, no. 7, pp. 2151-2157, Apr. 2021.

[12] **Z. Dai**, Z. Fan, P. Li, and J. Yao, "Frequency-tunable parity-time-symmetric optoelectronic oscillator using a polarization-dependent Sagnac loop," *J. Lightw. Technol.*, vol. 38, no. 19, pp. 5327-5332, Oct. 2020.

[13] Z. Fan, **Z. Dai**, Q. Qiu, and J. Yao, "Parity-time symmetry in a single-loop photonic system," *J. Lightw. Technol.*, vol. 38, no. 15, pp. 3866-3873, Aug. 2020.

[14] P. Li, **Z. Dai**, Z. Fan, L. Yan, and J. Yao, "Parity-time symmetric frequency-tunable

optoelectronic oscillator with a single dual-polarization optical loop," *Opt. Lett.*, vol. 45, no. 11, pp. 3139-3142, Jun. 2020.

Conference papers

[1] **Z. Dai**, Y. Guan, and J. Yao, "Optical convolution processing based on an amplified fiber-optic recirculating loop," MWP 2024, 17-20 Sep. 2024, Pisa, Italy.

[2] P. Li, **Z. Dai**, L. Yan, and J. Yao, "Radio over fiber links with increased spectral efficiency based on coherent detection and digital processing," MWP 2021, 15-17 Nov. 2021, Pisa, Italy.

[3] **Z. Dai**, P. Li, and J. Yao, "SiP Fano resonator with increased slope rate for microwave signal processing," MWP 2021, 15-17 Nov. 2021, Pisa, Italy.

[4] Z, Fan, **Z. Dai**, W. Zhang, Q. Qiu, and J. Yao, "A single-loop PT-symmetric sub-kHz fiber laser based on an integrated microdisk resonator," OFC2020, 8-12 Mar. 2020, San Diego, USA.

[5] **Z. Dai**, Z. Fan, and J. Yao, "Wavelength-tunable PT-symmetric single-longitudinal-mode fiber laser with a single physical loop," OFC2020, 8-12 Mar. 2020, San Diego, USA.

[6] **Z. Dai**, Z. Fan, C. Li, and J. Yao, "Frequency-tunable parity-time-symmetric optoelectronic oscillator using a polarization-dependent Sagnac loop," OFC2020, 8-12 Mar. 2020, San Diego, USA.